Master's thesis

NTNU
Norwegian University of Science and Technology
Faculty of Medicine and Health Sciences
Department of Clinical and Molecular Medicine

Julie Tro Jerud

The role of *Fusobacterium nucleatum* and the Epstein-Barr virus encoded EBV-miR-BART10-3p in colorectal cancer

- focusing on the genes *CXCL8, CSF2*, *SAP18* and *CCND1*

Master's thesis in MSc Molecular Medicine
Supervisor: Robin Mjelle
May 2020

NTNU
Kunnskap for en bedre verden

Julie Tro Jerud

The role of *Fusobacterium nucleatum* and the Epstein-Barr virus encoded EBV-miR-BART10-3p in colorectal cancer

- focusing on the genes *CXCL8, CSF2*, *SAP18* and *CCND1*

Master's thesis in MSc Molecular Medicine
Supervisor: Robin Mjelle
May 2020

Norwegian University of Science and Technology
Faculty of Medicine and Health Sciences
Department of Clinical and Molecular Medicine

NTNU
Norwegian University of
Science and Technology

Acknowledgements

This master's thesis was conducted at the Department of Clinical and Molecular Medicine, Faculty of Medicine and Health Science, at the Norwegian University of Science and Technology (NTNU) in Trondheim.

First, I would like to thank my main supervisor researcher Robin Mjelle for his great support throughout the project, for the help and patience in the lab, and guidance throughout the writing of the thesis. I would also like to thank Per Arne Aas for always being available for questions and help at the lab. I would like to thank Bjørnar Sporsheim and Kjartan Wøllo Egeberg at the Cellular & Molecular Imaging Core Facility (CMIC) at NTNU for the training and teaching of microscopes Zeiss LSM 510 META confocal microscope and EVOS 1. And I would also like to thank my co-supervisors, Eva Hofsli and Pål Sætrom.

I would like to thank the research group "Systems Biology for Oncology" at St. Olavs Hospital HF and NTNU for the opportunity to work on the project and establishment of the cancer tissue originated spheroids (CTOSs) method. And a special appreciation to Evelina Folkesson for all the work she has put into the project by organization, writing of procedures and lab work, in addition to guidance with the CTOSs-part of the thesis. I wish the group the best with further experiments and research.

At last I would like to thank to my fellow student Vibeke Sognnes for cooperation on laboratory experiments, for lifting my mood and giving me motivation when nothing felt right. Without you, this process would have been much more difficult, and I am grateful I got to share this experience with you.

Abstract

Colorectal cancer (CRC) is the third most common cancer in the world, and the second leading cause of cancer deaths for both sexes combined. Development of CRC is a multistep process that involves both genetic and epigenetic alterations in tumor suppressor genes and oncogenes, that are required for cancer initiation and progression. The minority of CRC patients have familial (25%) or inherited (3%) form of CRC, while the majority (72%) occurs sporadically, suggesting that environmental factors are important for CRC development.

In recent years, there has been a rising awareness that the intestinal microbiota may be involved in the initiation, facilitation, and development of CRC. MicroRNAs from the infectious Epstein-Barr virus and the oral bacteria *Fusobacterium nucleatum* have been shown to be upregulated in CRC tissues compared to adjacent healthy tissue, indicating their role in the initiation and progression of CRC.

Here we show that *Fusobacterium nucleatum* internalize in the colorectal cell line DLD-1 visualized by LSM confocal microscopy and fluorescent staining, as well as upregulate the cytokines CXCL8 and CSF2 in co-culture with the cell lines DLD-1 and SW620. The gene expression of *CXCL8* and *CSF2*, as well as the cytokine release of CXCL8, were shown to increase with both incubation time and increased concentration of *F. nucleatum*, as detected by real-time qPCR and ELISA assay. CXCL8 and CSF2 are both involved in the immune responses and are shown to be associated with initiation and progression of CRC by creating an inflammatory microenvironment favorable for tumor progression.

The Epstein-Barr virus originated microRNA EBV-miR-BART10-3p is shown to directly target and downregulate the genes *SAP18* and *CCND1* in the CRC cell line SW620, by real-time qPCR and luciferase assay.

A cancer tissue originated spheroid (CTOS) method, based on the CTOSs method from Kondo et al. (2011) and Jeppesen et al. (2017) has been developed and established, including spheroid cultivation, splitting, freezing, and thawing. The CTOSs method gives a high yield of viable spheroids, which survive the process of being split, frozen and thawed.

Sammendrag

Kolorektal kreft er den tredje mest vanlige krefttypen i verden, og den nest ledende årsaken til dødsfall forårsaket av kreft for begge kjønn. Utviklingen av kolorektal kreft er en prosess som foregår gjennom flere trinn som involverer både genetiske og epigenetiske endringer i tumorsuppressorgener og onkogener, som er nødvendige for initiering og progresjon av kreft. Minoriteten av kolorektal kreft-pasienter har familiær eller arvelig form av kolorektal kreft, mens majoriteten av krefttilfellene oppstår sporadisk, noe som antyder at miljø og livsstil representerer risikofaktorer for kolorektal kreft.

Økt bevissthet omkring tarmmikrobiota sin rolle i initieringen, tilrettelegging og utvikling av kolorektal kreft har i senere år vokst frem. Epstein-Barr virus og den orale bakterien *Fusobacterium nucelatum* er påvist oppregulert i kolorektalt tumorvev sammenlignet med tilstøtende friskt vev, noe som fremhever deres rolle i initiering og progresjon av kolorektal kreft.

Fusobacterium nucleatum er blitt vist å infisere og internalisere i den kolorektale cellelinjen DLD-1, visualisert ved LSM-konfokal mikroskopi og fluorescens-farging, samt å oppregulere cytokinene CXCL8 og CSF2 i co-kultur i cellelinjene DLD-1 og SW620. Genekspresjonen til *CXCL8* og *CSF2* og protein sekresjonen av CXCL8, ble vist å øke både ved inkubasjonstid og økt konsentrasjon av *F. nucleatum*, ved hjelp av real-time qPCR og ELISA. CXCL8 og CSF2 er begge involvert i kroppen sin immunrespons, og er vist å være involvert i initieringen og progresjonen av kolorektal kreft ved å skape et inflammatorisk mikromiljø som er gunstig for tumorprogresjonen.

Vi viser at EBV-miR-BART10-3p binder og nedregulerer genene *SAP18* og *CCND1* i cellelinjen SW620 ved real-time qPCR og luciferase analyse.

En pasient-derivert sfæroide metode (CTOSs), basert på CTOSs-metoden fra Kondo et al. (2011) og Jeppesen et al. (2017) er blitt utviklet og etablert, i form av sfæroidedyrking, splitting, frysing og tining. CTOSs-metoden gir et høyt utbytte av levedyktige sfæroider, som overlever prosessen med splitting, frysing og tining.

Table of contents

Abbreviations

AKT	Protein kinase B
ASAP	Apoptosis- and splicing-associated protein
BART	BamHI A rightward transcripts
Bp	Base pair
BTRC	Beta-transducin repeat containing E3 ubiquitin protein ligase
cDNA	Complementary DNA
CD receptor	Cluster of differentiation-receptor
CRC	Colorectal cancer
CSF2	Colony Stimulating Factor 2
CTOS	Cancer tissue originated spheroids
CXCL8	C-X-C Motif Chemokine Ligand 8
DKK	Dickkopf Wnt signaling pathway inhibitor 1
EBV	Epstein-Barr virus
EBVaGC	Epstein-Barr virus-associated gastric carcinoma
ERK	Extracellular-signal-regulated-kinase
HLA	Human leukocyte antigen
HSPCs	Hematopoietic stem and progenitor cell
IL	Interleukin
JAK2	Janus kinase 2
LPS	Lipopolysaccharide
MAPK	Mitogen-activated protein kinase
MEK	Mitogen-activated protein kinase kinase
miRNA	MicroRNA
MOI	Multiplicity of infection

Mo-MDSCs	Monocytic Myeloid-Derived Suppressor cells
MPPS	Mitochondrial processing peptidase
mRNA	Messenger RNA
MYD88	MYD88 Innate immune signal transduction adaptor
NF-κB	Nuclear Factor kappa B
NK cells	Natural killer cells
NPC	Nasopharyngeal cancer
PCR	Polymerase chain reaction
PI3K	Phosphatidylinositol-3-kinase
RAF	Rapidly accelerated fibrosarcoma
RB	Retinoblastoma protein
RNA	Ribonucleic acid
RNPS1	RNA binding protein with serine rich domain 1
STAT	Signal transducer and activator of transcription
TAM	Tyro3, Axl and Mer receptor
TIGIT	T cell immunoreceptor with Ig and ITIM domains
TLR	Toll-like receptor
TNF-α	Tumor Necrosis Factor-Alpha
TP53	Tumor protein p53

List of figures

List of tables

List of supplementary protocols

1 Introduction

1.1 Colorectal cancer

Colorectal cancer (CRC) is the third most common cancer in the world, and the second leading cause of cancer deaths for both sexes combined (1). The incidence of CRC shows an increase in high developed regions compared to less developed regions (2), which may reflect an increase of exposure to risk factors, such as smoking, alcohol intake, physical inactivity, bodyweight and intake of red and processed meat (3). The mortality incidence rates also show an increase in medium-to-high ranked countries on the Human Development Index (HDI), because of modest or lack of symptoms at an early stage, giving many patients with advanced disease and metastasis at diagnosis (2). More focus on preventive measurements such as screening program and surveillance, as well as improvements in disease management, has resulted in reduced incidence and mortality in the highest HDI-ranked countries (2, 4).

Development of colorectal cancer is a multistep process that involves both genetic and epigenetic alterations in tumor suppressor genes and oncogenes, that are required for cancer initiation and progression (3). The colorectal carcinogenesis model presented by Vogelstein et al. (5) suggest that the earliest trigger event of colorectal carcinogenesis is inactivation of the APC (adenomatous polyposis coli) pathway. Mutations in tumor suppressor genes (*APC, SMAD2, SMAD4, TP53*), oncogenes (*KRAS, BRAF, Bcl2, PI3K*) and other genes, such as DNA mismatch repair (MMR), can lead to the transition from single crypt lesions to adenomatous polyps and final development of invasive malignant carcinomas (3, 6). This is known as the adenoma-carcinoma sequence (7). The minority of CRC patients have familial (25 %) or inherited (3 %) form of CRC, while the majority (72 %) occurs sporadically, suggesting that environmental factors represent as risk factors (3).

1.1.1 Diagnosis

Primary diagnosis of colorectal cancer is based on clinical findings by endoscopic examination and biopsy (8). Colonoscopy is the gold standard for diagnosis, as it has high diagnostic accuracy, can assess the location of the tumor, and enable simultaneous biopsy sampling and polyp removal. This gives histological confirmation of the diagnosis and material for molecular profiling (9). When positive CRC findings are made, CT-scan of

thorax, abdomen and pelvis is performed to evaluate the accurate localization, tumor extent and staging of the disease. For rectal cancer patients is MRI of the rectum and pelvis also recommended. Measurement of CEA (carcinoembryonic antigen) tumor marker levels is recommended for disease monitoring (8).

1.1.2 Classification and disease staging

The tumor-node-metastasis (TNM) classification system, defined by the American Joint Committee on Cancer (AJCC), is widely used and recommended classification system for colorectal cancer. The TMN system for CRC is based on the depth of invasion of the bowel wall (T), extent of regional lymph node involvement (N), and presence of distant metastatic disease (M) (3). The TMN staging can be based on clinical (c) findings, pathological- and microscopic (p) examination of primary tumor, lymph node metastasis and distant lesions, or by medical imaging diagnostics and clinical findings. The staging of tumor status is necessary for a more accurate determination of the extent of the disease and result of treatment intervention. TNM parameter groupings determines the stage groups (stage I-IV) where increasing stage corresponds to more advanced disease, e.g. invasion of submucosa (stage I) and metastasis (stage IV) (10). AJCC TNM cancer staging system and staging grouping is found in supplementary table S1 and S2.

1.1.3 Treatment

The Norwegian Cancer Registry reports that about 80 % of CRC patients undergo surgical resection of primary tumor as the primary modality of treatment (11). The main goal with surgical resection is to remove the tumor for curative intent, long-term survival and to reduce the risk of recurrence (11). The approach of appropriate treatment is based on the pathological assessment of tumor, stage of the disease and patients comorbidity (12). Often is surgery sufficient for management of early-stage disease (stage I-II), whereas advanced-stage disease (stage III-IV) typically require supplementary chemo- and/or radiotherapy (9).

Neoadjuvant (preoperative) chemoradiotherapy of rectal cancer is used to reduce tumor size and even stage, and to optimize the chances for a successful resection and minimize local recurrence (9). For patients with locally advanced disease, long-term radiotherapy in combination with chemotherapy and delayed surgery is recommended (8). Short-term

radiotherapy and immediate surgery are an alternative for the less advanced staged cancers. Short-term radiotherapy with delayed surgery is used for elderly patients and metastatic CRC, where it is important to start postoperative chemotherapy (8, 9). Postoperative (adjuvant) radiotherapy in combination with chemotherapy reduces the risk of micro-metastases after surgery and is recommended for patients with non-complete surgical restriction (micro/macroscopically non-radical restriction) or patients with infiltrating T4-tumors who had not received preoperative radiotherapy (8).

1.1.4 Early detection and screening

The median age for colorectal cancer is > 70 years for both men and women (9, 11, 13). Colorectal cancer may cause symptoms like bloody stool, change in bowel habits, abdominal pain, anemia and general fatigue (8, 9). Symptoms often occurs at a late stage when treatment efficiency is limited, and 20–30 % of newly diagnosed patients have metastatic disease (stage IV) at diagnosis (4). The prognosis is significantly better when disease is diagnosed at an earlier stage, as the 5-year survival rate declines from 90 % for patients diagnosed with early-stage disease (stage I–II), to 14 % for patients diagnosed with late-stage disease (III–IV) (14).

Colorectal cancer, on average, progresses for several years before becoming symptomatic and sporadic disease-progression from colorectal adenoma to CRC takes at least 5–10 years (9). Colorectal cancer mortality rates have decreased substantially over the past several decades, much to the implementation of screening programs, early detection of cancerous lesions and removal of precancerous polyps (9, 15). Fecal occult blood tests (FOTBs) and colonoscopy are the most widely used methods for CRC screening (6). FOTB is used to detect the presence of blood in feces, are easy to perform and non-invasive, but have a limited sensitivity and specificity (16). Colonoscopy is considered as the gold standard for detection of colorectal cancer and is weighed as the most specific and sensitive CRC detection method. However, sensitivity has shown to decrease for detection of polyps < 10 mm (15). Colonoscopy is an invasive and time-consuming screening method, as it requires trained personnel. It is also considered troublesome for patients since it requires complete bowel preparation and can be seen as uncomfortable (9, 15). In later years there have been major improvements in non-invasive screening. Tests like fecal immunochemical test (FITs), fecal DNA test, and several biomarkers are being investigated as alternatives to current screening methods (6, 9, 15, 16).

1.2 Virus and bacteria in colorectal cancer

In recent years, there has been a rising awareness that intestinal microbiota may be involved in the initiation, facilitation and development of colorectal cancer (17). Several reports have described virus and bacteria involvement with CRC and especially, Epstein-Barr virus (EBV) and *Fusobacterium nucleatum* (*F. nucleatum)* have been associated with CRC (18-22). Both EBV and *F. nucleatum* have been shown to evade immune invasion, induce inflammation, increase proliferation and tumor survival, and be a cause of metastasis (20, 21, 23-30).

Human viruses are strongly associated with cancer, as it in many cases is shown to be the cause of carcinogenesis, and especially the gut virome is shown to be associated with and potentially impact human cancer (31). Altered human virome composition and diversity have been identified in various diseases like periodontal disease, HIV, cystic fibrosis, urinary tract infection and inflammatory bowel disease (IBD) (31). There has been shown that oncogenic viruses induce and maintains persistent infection in the host and hides from the immune system, which is compatible with carcinogenic processes (32). In addition, utilize oncogenic viruses mechanisms in such manner that their genome is maintained in the host cells during proliferation, and this cell-immortalization is influenced either directly or indirectly by the oncogenic viruses (32). The viral miRNAs seem to have a leading role in viral persistence and propagation, modulating viral and host gene expression, which again leads to immune invisibility in infected cells and being the cause for carcinogenesis (33).

Directly mechanisms of viruses can be deregulated expression of cellular oncogenes or tumor suppressor genes, influenced by integration of viral genome into the host genome or the expression of viral oncogenes which inactivate major regulators of genome stability and cell cycle, leading to DNA damage and transformation of the host cell. Indirect mechanisms of host cell transformation can be tissue damage caused by immune cells and chronic inflammation or establishment of immunosuppression due to viral infection, resulting in inhibition of antitumor surveillance mechanisms (32).

The intestinal microbiota plays an essential role in regulating the intestinal homeostasis through its capacity to modulate various biological activities ranging from barrier, immunity and metabolic function (34). Microbial dysbiosis is associated with intestinal disorders like inflammatory bowel disease (IBD), irritable bowel syndrome (IBS), celiac disease and CRC (34, 35). It has been estimated that more than 20 % of the cancer burden worldwide is

attributable to known intestinal infectious agents (35). Growing evidence indicates that CRC arises from a stepwise disturbance of the composition of the gut microbiota, induced by food components or diet, in addition to genetic alterations in oncogenes and tumor suppressor genes (35). Some bacteria such as *Streptococcus gallolyticus, F. nucleatum, Escherichia coli, B. fragilis* and *E. fagecalis* have a high prevalence in CRC patients compared to the normal population, but no single species has been found to be universally present among all individuals with CRC and there is significant variation in microbial composition between individuals (35-37).

Different hypotheses explain the role of microbial unbalance in carcinogenesis. Some propose that microbial dysbiosis creates a functional imbalance that triggers continuous proinflammatory responses and epithelial cell transformation, leading to cancer (35, 38). Other propose a "driver-passenger theory" suggesting that intestinal bacteria triggers DNA damage in epithelial cells which contributes to cancer initiation and that in a second step, ongoing tumorigenesis alters the surrounding microenvironment, favoring proliferation of opportunistic bacteria (35, 39).

The human microbiota has been shown to colonize in mucosal biofilms, harboring both bacteria and virus (40, 41). These multispecies biofilm communities correlate with biological changes, like loss of E-cadherin, increased IL-6, activation of STAT3, increased polyamine synthesis and increased epithelial proliferation (40). Colon biofilms have been shown to be carcinogenic and the presence of bacterial biofilms is associated with CRC (40, 42). It is also suggested that the community position, health status of the host and organization of the microbiota at the mucosal surface contributes to tumorigenesis in CRC (42, 43).

Several reports have described *F. nucleatum* and EBVs involvement in colorectal cancer. Both *F. nucleatum* and EBV miRNAs are found to be elevated in tumor tissue when compared to adjacent normal tissue (17, 20, 26, 44-47). *F. nucleatum* has also been detected in stool from CRC patients (17, 20, 47). Mjelle et al. (44) have in a meta-analysis of small RNA sequencing data described *F. nucleatum* and EBV-miR-BART10-3p's as higher expressed in CRC tumor tissue, compared to normal tissue (44). They also describe that there was no correlation in tumor expression between EBV and *F. nucleatum* in tumor tissue, indicating that the presence of *F. nucleatum* and EBV in tumor tissue is independent (44).

1.3 Colorectal cancer and *Fusobacterium nucleatum*

1.3.1 *Fusobacterium nucleatum*

Fusobacterium nucleatum is a gram-negative anaerobic bacterium originating from the oral cavity, shown to have a role in several oral diseases, such as periodontitis and gingivitis (36, 48). Other diseases associated with *F. nucleatum* is Alzheimer's disease, brain abscess, cardiovascular disease, miscarriage, and inflammatory bowel disease (25). Recently, several papers have suggested that *F. nucleatum* plays a significant role in CRC (18-21), both in the emerging steps of colorectal cancer and as a causative and promotive agent (19, 49).

F. nucleatum has been detected in both CRC tissue and stool from CRC patients (17, 20, 47). The abundance of *F. nucleatum* is shown to gradually increase from normal tissue to adenomas and to adenocarcinomas in CRC, correlating with advanced disease (24, 47, 50). The amount *F. nucleatum* found in CRC tissues are also associated with worse diagnosis and shorter survival, indicating that it can be used as a prognostic and diagnostic marker (47, 51). It is also suggested that *F. nucleatum* prevalence in adenomas can function as the "second hit" in the "two-hit theory" for initiation of CRC, due to *APC* mutations already present in the cells (50).

1.3.2 *F. nucleatum* virulence factors promoting cancer

F. nucleatum elicits host proinflammatory response and possesses virulence characteristics that promote its adhesiveness to host epithelial cells and their ability to invade epithelial cells (50). *F. nucleatum* has been shown to increase proliferation (21, 23), promote chemoresistance (52), induce inflammation (25), suppress the host immune modulation (20, 25), and is related to poor prognosis (47) and metastasis (24). The fusobacterial proteins FadA, Fap2, RadD and lipopolysaccharide (LPS) are virulence factors *F. nucleatum* utilize to infect cells and elicit and avoid the human immune response (41, 47, 53).

The fusobacterial adhesin RadD conduct adherence by co-aggregation to other microbes and multispecies-biofilm formation (41, 48). The fusobacterial lectin, Fap2, bind to the polysaccharide, Gal-GalNAc, which is overexpressed by CRC adenocarcinomas and metastases, mediating fusobacterial enrichment and abundance in CRC (53). In addition, Fap2 binds to the TIGIT-receptor on immune cells, especially natural killer (NK) cells, inhibiting

tumor cell killing by immune cells (54). The Fap2 adhesin also mediates co-aggregation to neighboring bacteria and hemagglutination functions, contributing to the pathogenesis of colon cancer (53).

F. nucleatum induces inflammatory and oncogenic responses to stimulate growth of CRC cells by directly adhering to and invading colonic epithelial cells through the FadA surface protein, which interacts with E-cadherin and activates β-catenin and *Wnt* signaling (20, 21). This induces oncogenic gene expression and promotes growth of CRC cells (36). FadA protein exists in two forms, a secreted mature form (mFadA) and the non-secreted pre-FadA that is anchored to the membrane of *F. nucleatum* (55). Pre-FadA and mFadA forms the activity complex, FadAc, that modulates E-cadherin and activates β-catenin signaling (21). This activation leads to increased expression of transcription factors, oncogenes, *Wnt* genes, and inflammatory genes, as well as growth stimulation of CRC cells (21).

Fusobacterial lipopolysaccharide (LPS) engages the host cell Toll-like receptor (TLR)-4 in healthy colon tissue, resulting in induction of inflammatory cytokines and chemokines, giving macrophage infiltration, changes in genetics and epigenetics, miRNA regulation and tumor progression (23). Binding of LPS and TLR-4, signals to MYD88, activating NF-κB and increases the expression of miR-21, leading to an oncogenic cascade in CRC, including for instance increased growth and proliferation (23, 56). In colorectal cancer tissue, *F. nucleatum* and miR-21 levels were shown to both correlate with advanced stage disease and poor diagnosis (23, 44).

Adhering and invasion of *F. nucleatum* promotes expression and release of several inflammatory genes such as NF-κB and cytokines, including IL-6, IL-8, IL-18 and tumor necrosis factor-α (TNF-α), which promotes cell proliferation (20, 21). This again recruits tumor-infiltrating immune cells and generates a proinflammatory microenvironment, creating favorable circumstances for carcinoma progression (20). The fusobacterial metabolism produces amino acid products like formyl-methionyl-leucyl-phenylalanine and short chain fatty acids, that are myeloid cell chemo attractants (20). The products of the fusobacterial metabolism may make the tumor microenvironment more tumor-permissive over time by directly promoting tumor cell proliferation, blood vessel growth, or immune cell infiltration (20).

1.4 MicroRNA

MicroRNAs (miRNAs) are a class of approximately 22 nucleotides (nts) long non-coding RNAs transcribed from the genomes of all multicellular organisms and some viruses (57-59). MicroRNAs play a physiological and pathophysiological role in cell proliferation, differentiation, development, apoptosis and oncogenesis, by regulating protein expression in a post-transcriptional manner (57, 60). MicroRNAs were first discovered in the invertebrate model organism *Caenorhabditis elegans (C. elegans)* (61). Studying the genes *lin-4* and *let-7* in *C. elegans*, Victor Ambros and colleagues discovered that these genes produced non-coding RNAs of approximately 22 nts in length, instead of producing mRNAs, and that these small RNAs were essential for development of the worm by binding to complementary sites of the genes *lin-14* and *lin-41*, respectively (61-63).

Virally encoded miRNAs are subjects of rapid evolution and unlike the host miRNA target sites, the virally encoded miRNA target sites, are generally not evolutionary conserved across species (64). Because of this, viral miRNA, like most human miRNAs, rarely binds to their mRNA targets with perfect complementarity, but when this occurs it usually causes a specific, irreversible endonucleolytic cleavage event in the target transcript, causing regulation of mRNA transcription (65). Since viruses do not have the required miRNA processing proteins, viral miRNAs take advantage of and utilize the same processing machinery as host miRNAs. Similar as for host miRNAs, binding of viral miRNA to target genes can cause both direct and indirect effects on genes and pathways.

1.4.1 MicroRNA biogenesis

MicroRNAs are initially transcribed by RNA polymerase II to form a pri-miRNA precursor within the stem of an approximately 80 nts RNA hairpin (58, 66). The pri-miRNA precursor is then processed by the nuclear RNase III enzyme Drosha and double-stranded (ds) RNA binding protein DGCR8 to generate the pre-miRNA intermediate hairpin at approximately 60 nts (57). The cytoplasmic RNA II enzyme Dicer cleaves the pre-miRNA to an approximately 22 nts long RNA duplex (58). One of the strands of the duplex, referred to the mature miRNA, is loaded into the RNA-induced silencing complex (RISC) and serves as a guide for the Argonaute protein to bind partially complementary target sites, usually within the 3’UTR of mRNAs (67). The miRNA seed sequence, which consists of the nucleotides 2 to 7 from the

miRNA 5'end, is exposed during mRNA binding by RISC and plays a key role in target mRNA recognition (57, 67). It is predicted that each miRNA functionally interacts with over hundred mRNA targets and perfect base pairing of the miRNA seed sequence to the 3'UTR of an mRNA target is often, but not always required for effective RISC recruitment and miRNA mediated repression (57, 67). RISC binding results in either translation inhibition or mRNA degradation by partial destabilization of the target mRNA and recruitment of degradation proteins (64).

1.5 Epstein-Barr virus

The Epstein-Barr virus (EBV) belongs to the Herpesviridae family and is an enveloped virus with a DNA core surrounded by an icosahedral nucleocapsid and a tegument, as shown in figure 1.1 (68, 69). The EBV genome consists of a double-stranded DNA, with a length of approximately 172 kb (69). It is estimated that more than 90 % of the world's population have been infected with EBV by the age of 35 (68). EBV spreads through salivary transmission and establishes a lifelong, latent infection in memory B lymphocytes (26, 68). Epstein-Barr virus is best known for causing infectious mononucleosis and has been associated with several malignancies of epithelial and lymphocytic origin (69).

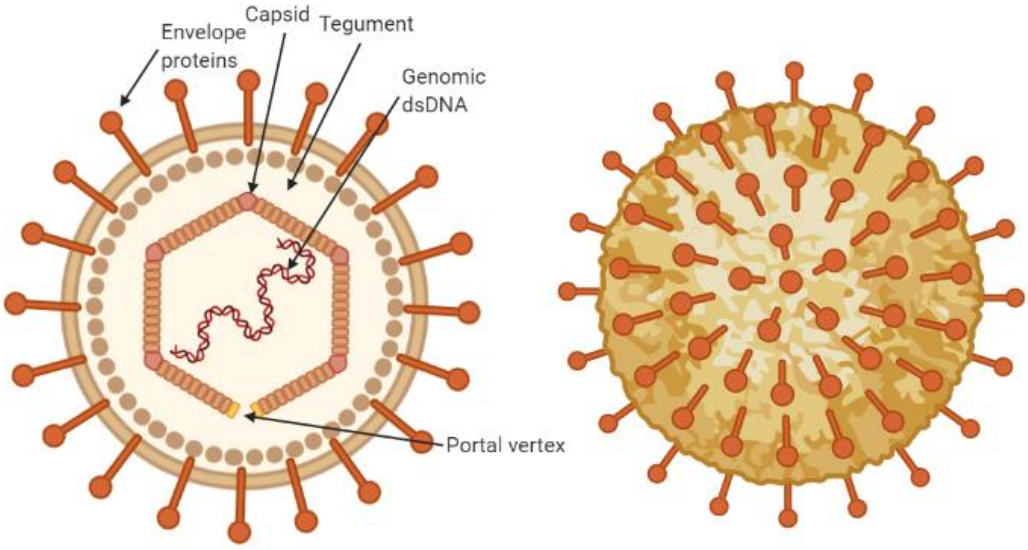

***Figure 1.1: Epstein-Barr virus structure**. Adapted from "Principles of Virology" Flint, J. et al. (70).*

1.5.1 Epstein-Barr virus initial infection and latency stages

Primary Epstein-Barr virus infection often result in a self-limiting disease, known as mononucleosis, due to an abnormal EBV-specific immune response (71). EBV infects and enters B lymphocytes through binding of the viral envelope glycoprotein gp350 to the CD21 receptor on the surface of B cells, in addition to binding of a second glycoprotein, gp42, to the HLA class II molecule as co-receptor (69, 72). After the initial infection, EBV goes into a latent state, most commonly in resting memory B cells and sometimes in epithelial cells, T cells or natural killer (NK) cells (69).

Epstein-Barr virus' entry and effect on epithelial cells is poorly understood, but the role of EBV in the pathogenesis of nasopharyngeal carcinoma and gastric adenocarcinoma is recognized (73). EBV is shown to infect epithelial cells through EBV-positive B cells and the virus must undergo an initial round of replication in primary B cells before it can access its permissive epithelial targets (74). It is also shown that virus captured on the surface of recently exposed primary B cells is highly infectious for the epithelium, as the B cell function as a carrier for EBV to entering epithelial cells (74).

Epstein-Barr virus has three different latency stages, type I, II and III, where it shuts down its protein expression and maintains its viral genome through expression of certain latent genes that is reported to have oncogenic properties (68, 75). EBV genes expressed during the latent infection include six nuclear antigens (EBNA-1, 2, 3A, 3B, 3C and leader protein (LP)), three latent membrane proteins (LMP-1, 2A and 2B), two EBV-encoded small RNAs (EBER-1 and 2), and two major clusters of microRNAs (69, 76). The two clusters of miRNAs consist of the BHRF1 (BamHI fragment H rightward open reading frame 1) cluster and the BART (BamHI fragment A rightward transcript) cluster (45). In total, is 44 miRNAs found to be encoded by EBV, which directly targets host or viral mRNAs (77). The BAMHI A rightward transcripts (BARTs) and the BART-encoded microRNAs (miR-BARTs) are expressed independently of the latency type displayed by the infected tumor cells (78). The BART miRNAs are highly expressed in EBV-associated epithelial malignancies and may induce malignant transformation (26).

1.5.2 Epstein-Barr virus in cancer

Epstein-Barr virus (EBV) was the first oncovirus to be discovered, and was originally identified in Burkitt lymphoma cells (69, 79). EBV infection is not generally related to cancer development, but EBV is well known to be linked to several specific human cancers such as Burkitt's lymphoma, Hodgkin's lymphoma, nasopharyngeal carcinoma, post-transplant lymphoma and some types of gastric cancers (69, 80).

An intricate interplay of host cell factor and viral gene expression is probably involved in the regulation of the growth and transformation properties of EBV-infected epithelial cells (26). In nasopharyngeal cancer (NPC) cells, a lytic activation of EBV promotes genome instability and drives the progression of NPC cells to acquire a more malignant phenotype (26). This suggest that there is an interplay between lytic and latent EBV genes in the pathogenesis of epithelial malignancies (26). There has been detected high levels of BamHI A rightward transcripts (BARTs) expressed in both NPC and EBV-associated gastric cancer (EBVaGC), suggesting their involvement in epithelial malignancies (26). Studies have also revealed a positive association between EBV infection and CRC (44, 46, 81-83).

1.5.3 BamHI A rightward transcripts microRNAs (miR-BARTs)

Epstein-Barr virus encodes for 25 pre-miRNAs producing at least 44 mature miRNAs, where 25 miRNAs have been identified in CRC and most of them were located in the BamHI A rightward transcripts (BARTs) (32, 44). The BART miRNAs (miR-BARTs) are transcribed from a large intron in the BART transcript, where they share a common 3'terminus and are derived from intron processing and a series of alternative splicing (60, 84).

MicroRNA-BARTs may contribute to tumorigenesis by evading growth suppressors and immune destruction, activating invasion and metastasis and resisting cell death (26). BART miRNAs have been found to regulate and inhibit both CD4 and CD8-mediated immune responses to infected cells (27, 28), stimulate tumor cells survival in culture (30) and enhance tumor growth *in vivo* (29). The miR-BARTs are shown to promote epithelial cell survival by targeting multiple pro-apoptotic cellular genes that could contribute to the EBV-mediated epithelial carcinogenesis (45).

BARTs are abundantly expressed at extreme high levels in EBV-infected epithelial cancers and play a crucial role in EBV-associated epithelial malignancies (26). MicroRNAs from EBV are found to be highly upregulated in tumor samples compared to paired normal samples (26, 44-46). In a meta-analysis of CRC samples, Mjelle et al. (44) identified 25 miRNAs from EBV, where most of them were located in the BART cluster. The miRNA EBV-miR-BART10-3p was validated as significantly increased in CRC tumor samples (44).

The EBV originated miRNA, EBV-miR-BART10-3p, is shown to effect both nasopharyngeal carcinoma (NPC) and Epstein-Barr virus (EBV)-associated gastric carcinoma (EBVaGC) (85, 86). It promotes invasion and migration capabilities in NPC cells by directly targeting the *BTRC* gene, which encodes an important component of the β-TrCP (beta-transducin repeat containing E3 ubiquitin protein ligase) (86, 87). In EBVaGC, EBV-miR-BART10-3p is shown to regulate cell proliferation and migration by targeting the tumor suppressor gene *DDK1*, contributing to EBVaGC metastasis (85). The miRNA is also shown to suppress the expression of IL-12B in infected cells and activate the *Wnt* pathway, thereby promoting cell proliferation and epithelial malignancy (28, 76, 88).

1.6 Colon cancer tissue derived spheroids

A cancer tissue- or tumor derived-spheroid is classified as floating spheres that serve as surrogate systems to evaluate tumor-related characteristics *in vitro*, reconstituted in the absence of non-tumor cells (89).

1.6.1 Application of colon cancer derived spheroids

Methods for propagating primary cancer cells in the laboratory range from conventional 2D cell cultures to more advanced 3D culture systems (90). Primary models of CRC such as cancer tissue-originated spheroids (CTOSs) and patient-derived organoids (PDOs) are being established with increasing success rate (90-92). Compared to 2D cell cultures, maintain CTOSs or PDOs the characteristics of cancer cells from the original patients' tissue and mimics the *in vivo* tumor conditions more closely in regards to cell morphology and organization, cell hierarchy and heterogeneity, protein and gene expression patterns, growth

patterns and distribution of profiling and apoptotic cells, cell-cell and cell-matrix interactions and metabolic gradients of for example oxygen and drug penetration (90, 92, 93).

Studies have shown that there is an overall genetic resemblance between the primary tumor and the established model even after long-term culturing (91, 94, 95). Some examples of applications for CTOSs or PDOs can be to test the therapeutic response of cancer cells obtained from the patient's own tumor towards a variety of drugs under controlled experimental conditions, disease modeling or to study the colorectal microbiota (90, 96).

Organoids or CTOSs provide the opportunity to study the impact of different biological systems, for instance bacteria, on the intestinal epithelium in a controlled environment using for example co-culture experiments (97). As the human microbiota has been shown to have an impact on CRC in terms of initiation and progression, the CTOSs model can be used in co-culture with specific microbes, microenvironment or different cell types shown to interact with CRC cells (97-99). For example, has *F. nucleatum* in co-culture with CRC spheroids been shown to proliferate in the tumor spheroids and alter the microenvironment by assembling biofilm-like structures (100). Microinjection can also be used to introduce microbes to CRC spheroid models (101). The microinjection of microbes into the lumen of a spheroid has been shown in a gastrointestinal spheroid model, which can be extended to CRC (101).

1.6.2 Cancer tissue-originated spheroids

Kondo et al. (92) have established a preparation method for cancer tissue-originated spheroids (CTOSs), which is based on the principle that cell-cell contact must be maintained throughout the preparation and culture of cancer cell clusters (92). The CTOSs method gives a high recovery rate and highly purified cancer cells, in addition to a stable CTOSs culture for further experiments (96).

The cancer tissue-originated spheroid (CTOS) method is a distinct technique for preparing and culturing organoids without dispersing the cancer cells into single cells (92). In this method the cell-cell interactions are maintained between cancer cells during the enzymatic digestion of cell-matrix interaction, and the subsequent culturing (96). A CRC tissue sample is digested, and the resultant tissue fragments and cells are passed through several mesh filters (96). The epithelial cancer fragments trapped by the filters are used for further culture and

rapidly form spheroids (CTOSs) with minimal cell death, as the cell-cell anchorage prevents triggering of anoikis (96, 102). The CTOSs method enables easy collection of the population of purified cancer cells, since blood cells, fibroblasts and dead cancer cells pass through the filter, and therefore allows for preparation of CTOSs from the primary tumor with high viability, efficiency, and purity (92, 96). The disadvantages of the CTOSs method is technical difficulties, as it requires craftmanship to prepare CTOSs from individual patients, and limited access to patient samples (96).

2 Aims of the study

The aim of this study was to discover new genes related to *F. nucleatum* and EBV-miR-BART10-3p. Specifically, we aimed to validate the human target genes, *SAP18* and *CCND1*, of EBV-miR-BART10-3p in colorectal cancer cells. Further we aimed to validate changes in gene expression of genes *CSF2* and *CXCL8* in colon cancer cells in co-culture with *F. nucleatum*. We aimed to investigate changes in migration and proliferation of colon cancer cells in co-culture with *F. nucleatum* and determine the localization of *F. nucleatum* in colon cancer cells.

Finally, we wanted to establish a colorectal cancer patient derived spheroid model, which can be used to investigate the interaction and impact of colon microbiota in colorectal cancer and be used as an alternative to cell lines and mouse models in drug screening and general CRC research.

3 Materials and methods

3.1 Materials

Materials, instruments, and reagents used in this study are listed in supplementary table S3.

3.1.1 Cell lines, bacteria, and miRNA

Cell lines

Several human colorectal cancer cell lines were used in the current project. Cell culture work were performed in sterile fume hoods using sterile techniques. Cell lines were grown in T-75 culture flasks with filter caps and incubated at 37 °C with 5 % CO_2. Cell lines were passaged two to three times a week when confluent.

DLD-1 and LS411N were cultured in RPMI-1640 medium (Sigma-Aldrich) and SW480 and SW620 were cultured in Dulbecco's Modified Eagle Medium (DMEM) (Sigma-Aldrich). All culture mediums were supplemented with 10 % fetal bovine serum (FBS) (Sigma-Aldrich) and 5 % Penicillin-Streptomycin (Sigma-Aldrich). RPMI-1640 was also supplemented with 5 % L-Glutamine (Sigma-Aldrich).

Bacteria strains

In-house *Escherichia coli* DH5α cells were cultured in Lysogeny broth (LB) at 37 °C on shaking.

Fusobacterium nucleatum subsp. Nucleatum (25586™ ATCC®) were purchased from ATCC, cultured on Fastidious Anaerobe Agar (F.A.A) with horse blood agar plates (FHB) (Thermo Fischer Scientific) and in Tryptic Soy Broth medium (TSB) (Sigma-Aldrich) under anaerobic conditions at 37 °C. The anaerobic conditions were achieved by the use of an anaerobic jar (Sigma-Aldrich) and anaerobic atmosphere generation bags (Sigma-Aldrich), as shown in figure 3.1. The anaerobic environment was monitored by an anaerobic indicator test (Sigma-Aldrich) that is saturated with resazurin solution, changing color from pink to white indicating anaerobic conditions.

Figure 3.1: Anaerobic jar for cultivation of F. nucleatum. *Anaerobic conditions were achieved by anaerobic atmosphere generation bags (white bag) and the anaerobic conditions were monitored by an anaerobic indicator test (pink patch on wall of anaerobic jar). The anaerobic indicator change color from pink to white indicating anaerobic conditions. Tryptic soy broth medium containing F. nucleatum in tubes with blue cap. F.A.A. agars were incubated in the same manner.*

MicroRNA mimics

EBV-miR-BART10-3p mimic (MC12577, Thermo Fischer Scientific) and non-targeting miRNA mimic (Thermo Fischer Scientific) were obtained from Ambion, shown in table 3.1. The non-targeting miRNA mimic is a random sequence miRNA mimic molecule that has been validated to not produce identifiable effects on known miRNA function (103).

Table 3.1: MicroRNA mimics, miRBase accession number, manufacturers catalog number and mature miRNA sequence.

MicroRNA mimic	**miRBase Accession number / Catalog number**	**Mature miRNA Sequence**
EBV-miR-BART10-3p	MIMAT0003420 / 4464066	UACAUAACCAUGGAGUUGGCUGU
miRNA Mimic Negative Control #1	– /4464058	Not available

3.2 Cell migration assay

The effect *F. nucleatum* has on cell migration was evaluated by the use of culture inserts for self-insertion (Ibidi) in DLD-1 cells. The culture insert creates a 500 µm +/- 100 µm gap in the confluent cell layer, making it possible to get an accurate wound in the cell layer to monitor, as shown in figure 3.2.

DLD-1 cells (~$6.0*10^5$) were cultured in complete medium without antibiotics. MOI (multiplicity of infection) of 300 of *F. nucleatum* were added to the cells separately and incubated for approx. 5 h. Cells were then washed twice with PBS, resuspended in medium with antibiotics, transferred to the culture inserts and incubated until the next day. The next day, the gap was removed, and pictures of the gap were taken at 0 h, 24 h, 48 h and 72 h with microscope EVOS 1 at 10x magnification. Cells without bacteria were treated the same way. Images were processed and area of wound was measured using ImageJ (104). Statistical analyses were performed using GraphPad Prism 8, performing one-tailed paired student t-test for comparing treatment at different time points. Two-way ANOVA with multiple testing was also performed to compare timepoints with different treatment. The result is presented as percentage of wound closure.

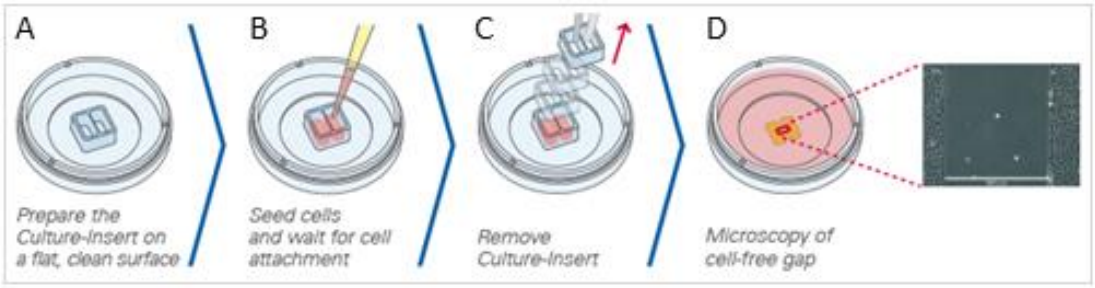

Figure 3.2: Principle of migration assay. *A) Culture insert is placed on a flat, clean surface in a 6-well plate well. B) Cells co-cultured with bacteria are reseeded into the chambers and outside (not showed in figure) of the chamber insert. C) The next day, the cells have attached to the surface and the culture insert is removed. D) Cell gap is monitored by microscopy and pictures of gap were taken at 0 h, 24 h, 48 h and 72 h. Figure adapted from Ibidi (105).*

3.3 Cell proliferation assay

The effect of *F. nucleatum* has on cell proliferation in DLD-1 and LS411N cells, was evaluated by the use of µ-Slide 8 well 500-grid (Ibidi). The µ-Slide 8 Well 500-grid has eight

chambers with gridded bottoms, allowing for cultivation and live cell imaging in same chamber and making it easy to evaluate the cell proliferation, as shown in figure 3.3.

DLD-1 (~$1.0*10^4$) and LS411N (~$5.0*10^5$) cells were cultured in complete medium without antibiotics. A MOI of 500 of *F. nucleatum* and *E. coli* were added to the cells and incubated for 5 h. Cells were washed twice with PBS and resuspended in 2 ml of complete medium with antibiotics. A volume of 300 µl of the cell suspension were transferred to the well of an µ-Slide 8 Well Grid-500. The wells were monitored by use of microscope and picture with EVOS 1, and pictures were taken at 0 h, 24 h, 48 h and 72 h. The pictures were processed using ImageJ.

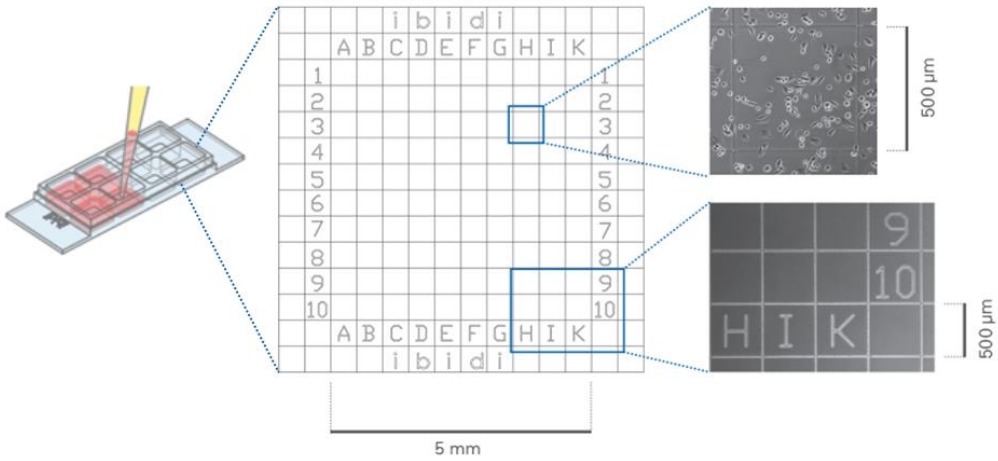

Figure 3.3: Cell proliferation principle and layout of µ-slide 8 well Grid-500. *Allows for cultivation and live cell imaging to be conducted in one single chamber. Figure adapted from Ibidi (106).*

3.4 RNA isolation

Total RNA was isolated from frozen cell pellets using the Total RNA purification Kit (Norgen biotek corp). In brief, Buffer RL (350 µl) were added to the frozen cell pellet and vortexed until lysed. 96% ethanol (300 µl) were added to the lysate and vortexed additionally. Lysate was loaded onto the membrane in spin columns provided in the kit. RNA bound to the column and contaminants were washed away before the column were transferred to a new elution tube and RNA were eluted using nuclease-free water (25 µl). Isolated RNA was stored at -20 °C.

Isolated RNA was measured using NanoDrop™ ND-1000 spectrophotometer (Thermo Scientific) to give an indication on RNA purity and concentration.

3.5 Reverse transcription PCR

Complementary DNA (cDNA) was synthesized by reverse transcriptase (RT) using the High-Capacity RNA-to-cDNA kit (Applied Biosystems). The RT-enzyme produces cDNA from an RNA template under optimized conditions.

The kit consists of a 2x RT Buffer Mix composed of dNTPs, random octamers and oligo (dT-16) and 20x RT Enzyme Mix composed of MuLV (murine leukemia virus) and RNase inhibitor protein. The reverse transcriptase reactions were mixed as shown in table 3.2 and processed in a thermal cycler with conditions shown in table 3.3. cDNA was stored at -20 °C until use.

Table 3.2: Components and volume per reaction for reverse transcriptase reaction

Component	Volume per reaction
2X RT Buffer Mix	10.0 µl
20X RT Enzyme Mix	1.0 µl
RNA Sample	Up to 2 µg
Nuclease-free H_2O	Quantity sufficient to 20 µl
Total per reaction	20.0 µl

Table 3.3: Thermal cycler conditions for reverse transcriptase reaction. Table showing stage, temperature (°C) and time (min) for each step.

Step	Stage	Temperature (°C)	Time (min)
1	cDNA synthesis	37	60
2	Stop reaction	95	5
3	Hold	4	Forever

3.6 RNA-sequencing of colon cancer cells co-culture with bacteria and transfection with EBV-miR-BART10-3p mimics

DLD-1, LS411N, SW480 and SW620 cells were co-cultured with 600 MOI of *F. nucleatum*, *E. coli* and corresponding volume of TSB, in appropriate complete medium without antibiotics for 6 h at standard cell culture conditions (37 °C, 5 % CO_2). Cells were then washed twice with PBS and medium changed to appropriate complete medium with antibiotics and incubated additionally 24 h under same cell culture conditions. Cells were then harvested, and RNA isolation was performed as described above.

DLD-1, LS411N, SW480 and SW620 cells were transfected with EBV-miR-BART10-3p mimic and non-targeting miRNA mimic using the transfection agent Lipofectamine RNAiMAX (Invitrogen) according to manufactures protocol. The transfected cells were incubated for 48 h under standard cell culture conditions, harvested and RNA isolation was performed as described above.

mRNA sequencing was performed using the SENSE mRNA-Seq Library Prep Kit V2 (Lexogen). The cDNA/sequencing libraries were sequenced with 75 base pair (bp) single read by the Genomic Core Facility at NTNU.

TargetScan was used to predict binding sites of EBV-miR-BART10-3p to the human target genes.

3.7 Cell culture experiments

3.7.1 Transfection with EBV-miR-BART10-3p mimic

SW620 cells were transfected with EBV-miR-BART10-3p mimic and non-targeting miRNA mimic to a final concentration of 0.05 nmol using the transfection agent Lipofectamine RNAiMAX (Invitrogen) according to manufacturer's protocol. The transfected cells were incubated for 24 h at standard cell culture condition and harvested. RNA isolation and reverse transcription was performed as described above.

3.7.2 Co-culture with *F. nucleatum* and *E. coli*

DLD-1 and SW620 cells were co-cultured with *F. nucleatum* and *E. coli* in two different experiment layouts, concentration experiment with different multiplicity of infection (MOI) and timeseries experiment with same MOI and different incubation time. In both experiments, were DLD-1 and SW620 cells cultured in complete medium without antibiotics.

For the concentration experiment, *F. nucleatum* and *E. coli* were added to the cells at 0, 0.1, 1, 10 and 100 MOI, followed by incubation for 6 h in standard cell culture conditions. For the timeseries experiment, *F. nucleatum* and *E. coli* at 600 MOI were added to the cells, followed by harvesting at 0 h, 3 h, 6 h, 12 h, and 24 h. RNA isolation and reverse transcription were performed as described above.

3.8 Real-time quantitative PCR

Real-time quantitative PCR (qPCR) was used to determine the relative gene expression (log2) of the target genes, in treated vs untreated samples using the quantitative comparative C_T method ($\Delta\Delta C_T$). The threshold was set above the background and within the exponential phase of the amplification curve.

The change in relative expression of target gene is calculated for all samples in experiment set ups described above. Real-time qPCR data were analyzed using equation [2], where $\Delta\Delta C_T$ is calculated as in equation [1]. X is any time point or concentration and 0 represent the expression of the target gene normalized to the endogenous control ACTB at 0 MOI or 0 h (start point of experiment). The mean C_T values for both the target and endogenous control genes were determined at time or concentration 0 and used in equation [2]. The mean and SD or SEM for each sample is calculated of three technical replicates for co-culture with *F. nucleatum* and *E. coli*, and three biological replicates for transfection with EBV-miR-BART10-3p and non-targeting miRNA mimics. In this analysis the time and concentration at 0 should be 1.

$$\Delta\Delta C_T = \left(\Delta C_{T,\ target} - \Delta C_{T,ACTB}\right)_x - \left(\Delta C_{T,\ target} - \Delta C_{T,ACTB}\right)_0 \quad [1]$$

$$Relative\ expression\ of\ target = 2^{-\Delta\Delta C_T} \quad [2]$$

The real-time qPCR reactions were carried out on a Step One Plus Real-Time PCR system (Applied biosystems) with TaqMan Universal Master Mix II (Applied Biosystems) and TaqMan Gene Expression assays for the specific genes (table 3.6). The TaqMan Universal Master Mix II, no UNG, contains AmpliTaq Gold DNA Polymerase Ultra Pure, dNTPs (with dUTP), ROX Passive reference dye and optimized buffer components. The TaqMan Gene Expression Assays, listed in table 3.6, contains gene specific target primers and a sequence-specific probe labeled with FAM.

The TaqMan qPCR employs target specific primers and a fluorogenic non-extendable probe to detect a specific PCR product as it accumulates during the PCR. The probe is a short, sequence specific oligonucleotide labeled with a fluorescent reporter dye (FAM) at the 5'end and a quencher at the 3'end forming a donor-acceptor FRET (fluorescent resonance energy transfer) pair (107). The probe hybridizes to the target sequence downstream for one of the target specific primers (108). The upstream primer is extended by the Taq DNA polymerase, leading to the disruption of the FRET pair and releasing the quencher from the probe, increasing the reporter dye signal (107). Principle is described in figure 3.4. The increase in fluorescence intensity is proportional to the amount of accumulated PCR product. The higher the starting copy number of the target sequence, the earlier a significant increase in fluorescence is observed.

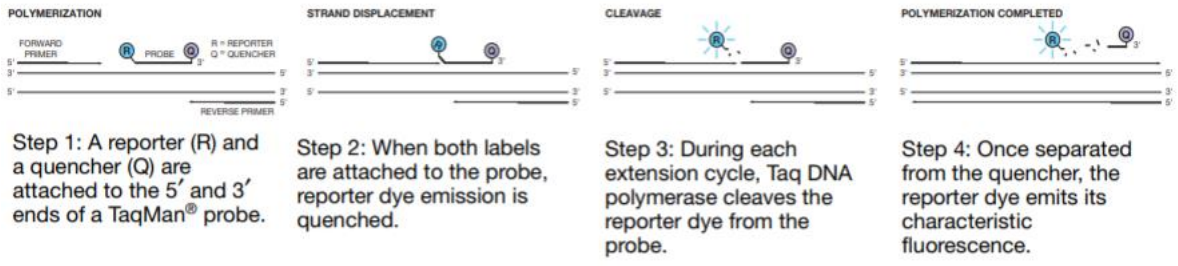

Figure 3.4: Principle of real-time qPCR with use of TaqMan gene expression probes with FAM-reporter (P) and MGB-quencher (Q). *Figure from Applied Biosystems (108).*

A real-time qPCR mastermix was prepared for the respective probes (table 3.6) as shown in table 3.4 and added to the wells of a MicroAmpTM Fast Optical 96-well reaction plate. The reaction plate was mixed gently and centrifuged briefly before it was loaded into Step One Plus RealTime machine with conditions shown in table 3.5.

Table 3.4: Real-time qPCR mastermix components and volume (µl)

Components	Volume (µl)
	1x
TaqMan FAM-probe	1.0
TaqMan Universal Master Mix II, no UNG	10.0
cDNA template (1 to 100 ng)	4.0
Nuclease-free water	5.0
Total	20.0

Table 3.5: Thermal cycle conditions for real-time qPCR reaction showing stage, temperature (°C) and time for each step

Stage		Temperature (°C)	Time (mm:ss)
Hold		50	2:00
Hold		95	10:00
Cycle (40 Cycles)	Denaturation	95	0:15
	Anneal/Extend	60	1:00

Table 3.6: qPCR TaqMan gene expression probes with FAM-MGB. *"Gene symbol" is the official gene symbol; "Gene name" is the gene name; "RefSeq" is the NCBI reference sequence name; "Assay ID" is the name of the assay from the producer; "Assay" indicates in which experiment the gene was studied.*

Gene symbol	Gene name	RefSeq	Assay ID	Assay
ACTB	Actin beta	NM_001101.3	Hs99999903_m1 Hs01060665_g1	EBV / *F. nucleatum*
CXCL8	C-X-C motif chemokine ligand 8	NM_000584.3	Hs00174103_m1	*F. nucleatum*
CSF2	Colony stimulating factor 2	NM_000758.3	Hs00929873_m1	*F. nucleatum*
CCND1	Cyclin D1	NM_053056.2	Hs00765553_m1	EBV
SAP18	Sin3A associated protein 18	NM_005870.4	Hs00705532_s1	EBV

3.9 Luciferase assay and co-transfection with vector and EBV-miR-BART10-3p

We investigated the direct effect of EVB-miR-BART10-3p on the genes of interest, *SAP18* and *CCND1*, by co-transfection of miRNA mimic and non-targeting miRNA mimic together with vectors containing the 3'UTR or target site of genes of interest, followed by luciferase assay measurements.

To validate the targets of EBV-miR-BART10-3p we used luciferase reporters that contain either the whole 3'UTR of the gene or interest, or part of the 3'UTR containing only the target site and a few flanking nucleotides. The principle of luciferase reporters is described in figure 3.5. The luciferase gene is transcribed from the transfected vector into a mature mRNA with a 3'UTR that can be targeted by a co-transfected miRNA mimic. When the miRNA is targeting the 3'UTR of the luciferase transcript by using canonical miRNA targeting (58), the transcripts are degraded and less luminescence from the luciferase genes is produced due to reduced translation of the luciferase mRNA. The effect of the miRNA on the target gene can be measured by comparing the luminescence from cells that are co-transfected with the vector and the miRNA with the luminescence from the cells co-transfected with the vector and a negative control miRNA. Less luminescence should be observed in cells containing both the miRNA and the vector. In this project we use the whole 3'UTR of the gene *SAP18* and *CCND1* in 3'UTR LightSwitch vectors in addition to a psiCHECK™-2 vector containing a 46 bp long region of the 3'UTR of *CCND1* with a predicted 8-mer target site.

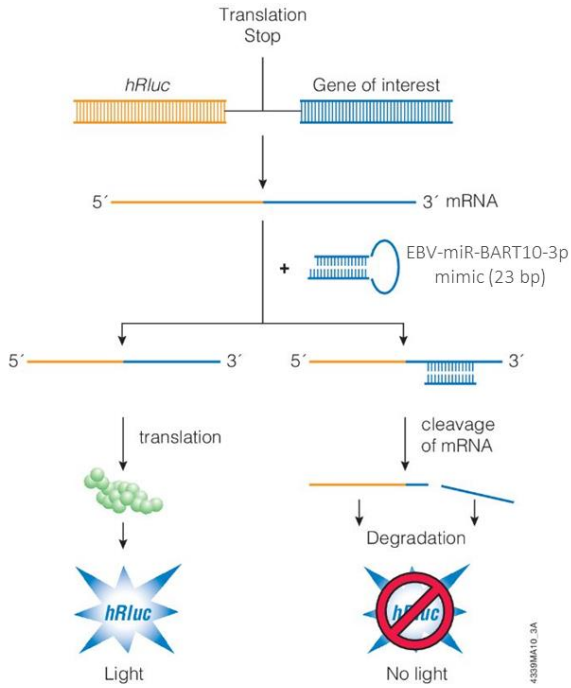

Figure 3.5: Mechanism of action of 3'UTR luciferase vectors, in co-transfection with EBV-miR-BART10-3p. *The gene of interest is cloned into the vector, at the 3'end of the Renilla luciferase gene and its stop translational codon. In the mammalian cell line, the fusion of the Renilla luciferase gene and the gene of interest is transcribed. In co-transfection with EBV-miR-BART10-3p, the EBV miRNA will bind to the target mRNA, and the mRNA will be cleaved, and subsequently degrade and decrease the Renilla luciferase signal. Adapted from Promega (109)*

3.9.1 Vectors and insert

3.9.1.1 psiCHECK™-2 vector

The psiCHECK™-2 vector (Promgea), figure 3.6A, includes two luciferase reporter genes, *Renilla (hRluc)* and firefly (*hluc*+), in addition to a coding region for the β-lactamase resistant gene (Amp^r). The differences in the luciferases makes it possible to selectively discriminate between their respective bioluminescence. The *Renilla* gene is the primary reporter gene, and the gene of interest, for instance its 3'UTR sequence, is ligated downstream from this between the restriction sites for NotI and XhoI. The luminescence measured from the *Renilla* luciferase protein is proportional to the amount of protein produced and can thereby indicate the effect of the miRNA on the protein output. For instance, a vector containing a functional miRNA site within the 3'UTR of the *Renilla* luciferase gene should produce less luminescence compared to a vector without a functional target site, or if the miRNA is not present in the cell. The firefly luciferase functions as an internal luminescence control that is

not affected by the co-transfected miRNA. The *Renilla* luciferase signal is normalized to the firefly luciferase signal (109).

Firefly luciferase is a 61 kDa monomeric protein and photon emission (light) is achieved through oxidation of beetle luciferin in a reaction that requires ATP, Mg^{2+} and O_2 (figure 3.6B). Reagent for quantifying firefly luciferase activity incorporates coenzyme A to provide enhanced reaction kinetic by promoting rapid enzymatic turnover, resulting in an extended "glow" luminescent. *Renilla* luciferase is a 36 kDa protein, composed of 3 % carbohydrate when purified from its natural source, *Renilla reniformis*. The luminescent reaction catalyzed by *Renilla* luciferase utilizes O_2 and coelenterate luciferin (coelentrazine). The kinetics of the *Renilla* luciferase reaction provides a glow-type luminescent signal that decays slowly over the course of measurement (110).

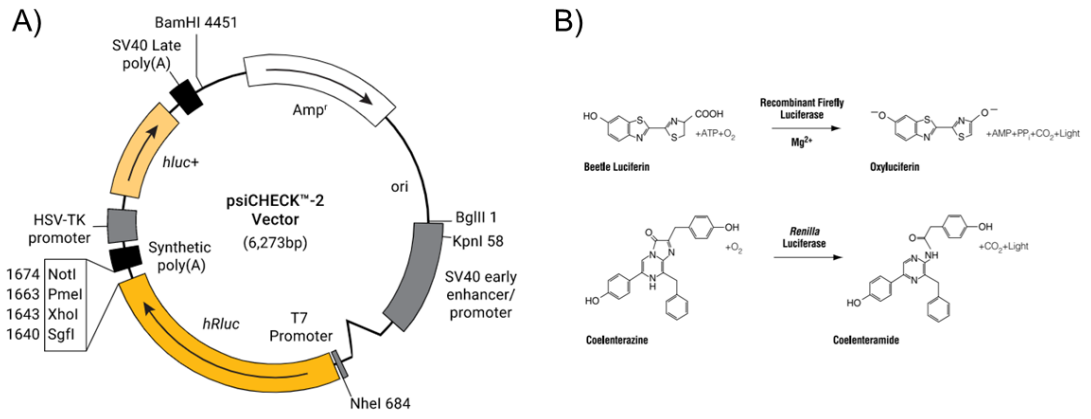

Figure 3.6: Schematic figure of psiCHECK™-2 vector and principle of luciferase reactions. *A) Schematic figure of psiCHECK™-2 vector, showing Renilla (hRluc) and firefly (hluc+) luciferase genes, cutting sites, β-lactamase resistant gene (Amp^r), promotors and poly(A) tails. Figure from Promega (109). B) Bioluminescent reactions catalyzed by the firefly and Renilla luciferases. Figure from Promega (110).*

The insert of the gene *CCND1* consists of a 46 bp sequence that contain an 8-mer EBV-miR-BART10-3p target site from the 3'UTR of *CCND1*. The *CCND1* 3'UTR target site for EBV-miR-BART10-3p is shown in supplementary figure S2. The sense and antisense sequence of the *CCND1* 8-mer target site (table 3.7) were acquired from Integrated DNA technologies (224365708). The sense and antisense sequences were annealed together by mixing the two oligos in equal molar amounts, incubated at 94 °C for 2 min and gradually cooled.

Table 3.7: CCND1 3'UTR 8-mer EBV-miR-BART10-3p target site sense and antisense sequences

Sequence direction	Nucleotide sequence
Sense	5'-/5Phos/TCG AGG TTT TGG GTA TGT TTA ATC TGT TAT GTA CTA GTG TTC TGG C-3'
Antisense	5'-/5Phos/GGC CGC CAG AAC ACT AGT ACA TAA CAG ATT AAA CAT ACC CAA AAC C-3'

3.9.1.2 3'UTR GoClone vector

The pre-cloned 3'UTR GoClone vector (Switchgear Genomics) includes one optimized luciferase gene, *Renilla* (RenSP), and a coding region for the β-lactamase resistant gene (Amp^r), shown in figure 3.7A. The insert of the entire 3'UTR of *CCND1* and *SAP18* consists of 3400 bp and 1589 bp respectively and is ligated downstream of the luciferase gene. A random control – R04_3UTR (S890004) was also included.

The *Renilla* luciferase protein catalyzes oxidation of its coelenterazine substrate producing light to be measured, figure 3.7B. By the optimized RenSP luminescent reporter gene, in addition to holding a protein domain that increases the half-life of the RenSP protein, the overall enzymatic activity (light output) is increased, which allows for a stabilized production of light (111).

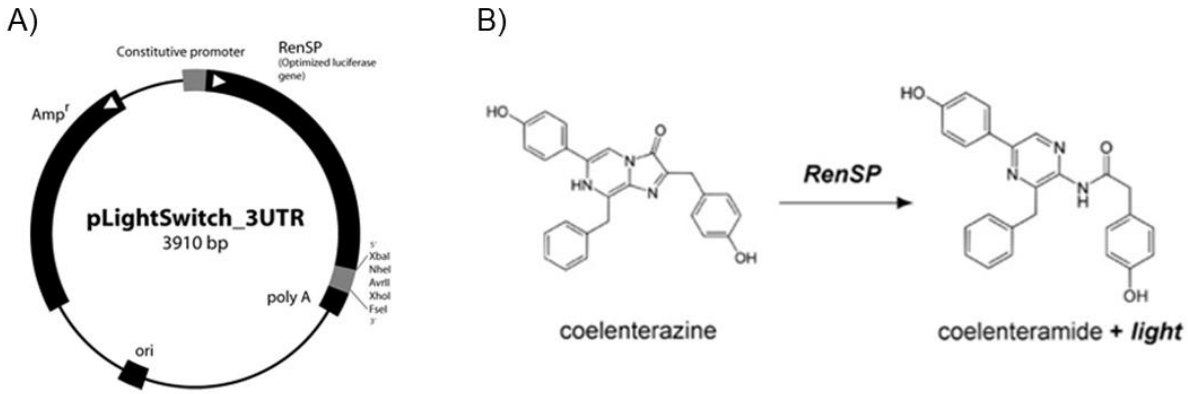

Figure 3.7: Schematic figure of 3'UTR LightSwitch vector and principle of luciferase reaction. *A) Schematic figure of 3'UTR LightSwitch vector showing the optimized luciferase gene (RenSP), β-lactamase resistant gene (Amp^r), promotor, poly(A) tail, and site of 3'UTR insert is indicated. B) Bioluminescent reaction catalyzed by RenSP luciferase. Figures from Switchgear Genomics (111).*

3.9.2 Construction of psiCHECK™-2 vector with *CCND1* 8-mer 3'UTR target site insert

Construction of the psiCHECK™-2 vector with insert of the *CCND1* 8-mer 3'UTR target site is performed using the following steps: restriction cutting of psiCHECK™-2 vector, PCR cleanup or gel extraction of restriction cut psiCHECK™-2 vector, ligation of psiCHECK™-2 vector and *CCND1* target site insert, transformation by heat shock and verification of insert by gel electrophoresis and Sanger sequencing.

3.9.2.1 Restriction cutting of psiCHECK™-2 vector

Restriction enzyme cutting was performed by the use of the restriction enzymes XhoI (New England Biolabs) and NotI-HF® (New England Biolabs), and CutSmart Buffer (New England Biolabs). The components were mixed as shown in table 3.8 and incubated overnight at 37 °C. The restriction cut psiCHECK™-2 vector was verified by a 1 % gel electrophoresis and should produce a band at approximately 7000 bps.

Table 3.8: Components and volume for restriction cut reaction of psiCHECK™-2 vector

Component	Volume
psiCHECK™-2 vector	1 µg
10X CutSmart Buffer	5 µl
XhoI	1.0 µl
NotI-HF	1.0 µl
Nuclease-free Water	Up to 50 µl
Total	50 µl

3.9.2.2 Purification of restriction cut psiCHECK™-2 vector

The QIAquick PCR purification Kit (QIAGEN) was used to purify the restriction cut psiCHECK™-2 vector from impurities like nucleotides, enzymes, salts, etc. In brief, the binding buffer is added to the restriction cut psiCHECK™-2 vector product and applied to the

QIAquick spin column. Single nucleotide left-overs from the restriction cutting and very short nucleic acids are washed away, and the pure DNA is eluted with nuclease-free water.

Monarch® DNA Gel Extraction kit (New England BioLabs) was used to excise and purify the restriction cut psiCHECK™-2 vector products. The DNA fragment was excised from the agarose gel using a scalpel and transferred to a microcentrifuge tube. Four volumes of Monarch Gel Dissolving buffer were added to the microcentrifuge tube, and incubated at 50 °C on a heating block with periodically vortexing for approximately 10 min. The dissolved gel solution was added to a column in a collection tube and spun for 1 min at max speed in a tabletop microcentrifuge. The column was washed twice with washing buffer, then transferred to a clean microcentrifuge tube and DNA was eluted with nuclease-free water.

Gel extraction gave low output when measuring DNA concentration using NanoDrop™ ND-1000 spectrophotometer, therefore PCR purification kit was used for purifying cut psiCHECK™-2 vector, instead of the abovementioned gel extraction method.

3.9.2.3 Ligation of psiCHECK™-2 vector and insert

Purified and restriction cut psiCHECK™-2 vector and the annealed oligo insert of *CCND1* were cloned together by a ligation reaction using 2x Ligase buffer (New England Biolabs) and Quick Ligase (New England Biolabs). Components were mixed together as shown in table 3.9 and incubated in a 25 °C water bath for 5 min.

Table 3.9: Components and volume for ligation dependent cloning reaction of psiCHECK™-2 vector and insert

Component	Volume
psiCHECK™-2 vector	1 µl
Annealed oligo CCND1	Approx. 10 µl
2X Ligase Buffer	10 µl
Quick Ligase	1 µl
Nuclease-free water	Up to 25 µl
Total	25 µl

3.9.2.3 Transformation by heat shock

Transformation by heat shock is the process where foreign DNA is introduced to competent DH5α *E. coli* cells, for identification and amplification of vectors that contain the desired insert.

In short, the ligation product is mixed with competent DH5α *E. coli* cells and incubated on ice for 15-20 min. The reaction is transferred to a 42 °C water bath for 50 sec, and the increase in temperature creates pores in the plasma membrane of the bacteria, allowing the vector DNA to enter the bacteria cell. The reaction is then placed on ice for minimum 2 min, which closes the pores of the plasma membrane. Nutrient rich SOC medium is added and the reaction is incubated in a shaking incubator at 37 °C for 60 – 90 minutes at 300 rpm. The cells are then spun and plated onto prewarmed Amp-LB dishes, allowing only the bacteria with vector to grow, due to the Ampicillin-resistant gene in the plasmid. The dishes are incubated at 37 °C overnight. The next day, separate colonies are picked from the plate and transferred to Amp-LB medium and incubated in a shaking incubator at 37 °C at 300 rpm overnight. The third day, the vectors are purified from the bacterial cultures by using Wizard® *Plus* Miniprep DNA Purification system (Promega). The vectors insert is verified by gel electrophoresis and sanger sequencing. Detailed protocol for heat shock transformation is found in supplementary protocol S1.

3.9.2.4 Purification of ligated and heat shocked psiCHECK™-2 vector

The Wizard® *Plus* Minipreps DNA Purification Systems (Promega) is used to purify the vectors from the bacterial cultures. In brief, bacterial cells were pelleted for 2 min at 10 000xg in a microcentrifuge. The pellet was resuspended in Cell Resuspension solution (250 µl), Cell Lysis Solution (250 µl) was added and the tube was mixed by inverting the tube four times. Alkaline Protease Solution (10 µl) was added and mixed by inverting four times, to inactivate endonucleases and other proteins released during the lysis of bacterial cells. Neutralization solution (350 µl) was added and mixed by inverting four times, and the lysate was centrifuged at max speed for 10 min. The cleared lysate supernatant was transferred to a Spin Column and DNA bound to the column by centrifugation at max speed for 1 min. The column was washed first with Column Wash (750 µl) Solution and then Column Wash Solution (250 µl). The

column is then transferred to a microcentrifuge tube and eluted in nuclease-free water (50 µl). The purified vectors were stored at -20 °C.

3.9.2.5 Verification of *CCND1*-insert

The insert of *CCND1* 8-mer 3'UTR in the psiCHECK™-2 vector was verified by performing Sanger sequencing of the region of the vector containing the insert.

The heat shocked bacteria stocks were lysed by boiling to release the vector DNA for PCR and gel electrophoresis. Bacteria stock (500 µl) was transferred to a microcentrifuge tube and spun at 6000 rpm for 5 min. The supernatant was removed, cell pellet was resuspended in sterile water and boiled at 95 °C on shaking for 10 minutes. The lysed cells were spun at max speed of 2 min and the supernatant (200 µl) was transferred to a new microcentrifuge tube for PCR reaction with primers specific for the psiCHECK™-2 vector and *CCND1* insert, shown in table 3.10.

Primers were designed to amply a region of the plasmid containing the insert. The *CCND1* forward primer was designed to overlap the *CCND1* insert, meaning that the primer would only bind if the insert was present in the vector, thereby indicating a successful cloning procedure. Using this technique, we could easily screen multiple colonies from the cloning by running the PCR products on an agarose gel and identify the expected PCR product.

Table 3.10: Base pair sequence and melting temperature (Tm) of the psiCHECK™-2 reverse primer and CCND1 forward primer

Primer	**Base pair sequence**	**Tm (°C)**
psiCHECK™-2 reverse	5'- ACC CTA ACC ACC GCT TAA GC-3'	57,4
CCND1 forward	5'- GGT ATG TTT AAT CTG TTA TGT ACT A-3'	48,3

Q5® High-Fidelity PCR Kit (New England Biolabs) and the above-mentioned primers were used to perform PCR reaction of the vectors from lysate. The components were mixed together as shown in table 3.11 and placed in a thermal cycler with conditions shown in table 3.12.

PCR products were mixed with loading dye and loaded onto a 1% agarose gel. Bands present at 194 bp, indicates that the insert was successfully cloned into the vector.

Table 3.11: Components and volumes for Q5 High fidelity PCR reaction

Component	Volume per reaction (µl)
5x Q5 Reaction Buffer	5.0
10 mM dNTPs	0.5
10 µM CCND1 forward primer	1.25
10 µM psiCHECK™-2 reverse primer	1.25
Template DNA (lysate)	2.0
Q5 Hot Start High Fidelity DNA Polymerase	0.25
5X Q5 CG Enhancer	5.0
Nuclease-Free Water	9.75
Total	20.0

Table 3.12: Thermal cycle conditions for PCR reaction with CCND1 forward primer and psiCHECK™-2 reverse primer

Step	Cycles	Temperature (°C)	Time
Initial denaturation	1	98	30 sec
Denaturation Annealing Extension	35	98	30 sec
		40	30 sec
		72	2 min
Final extension	1	72	2 min
Hold	1	4	Forever

The vectors presenting a band at 194 bp after gel electrophoresis, were sequenced by Sanger sequencing. The sequencing was performed by GATC. For sequencing, vector with insert was mixed with the reverse primer (table 3.10) and nuclease-free water according to table 3.13.

Table 3.13: Components and volume for sanger sequencing of psiCHECK™-2 vector with CCND1 insert

Component	**Amount**
psiCHECK™-2_CCND1 vector	500 ng
psiCHECK™-2 reverse primer	2.5 µl
Nuclease-free water	Up to 10 µl
Total	10 µl

3.9.3 Luciferase assay

3.9.3.1 Transfection of miRNA mimics and vectors

SW620 cells were seeded with a density of 25 000 cells per well in a 96-well tray and incubated for approx. 24 h. Vectors (100 µg) and EBV-miR-BART10-3p miRNA or non-targeting miRNA mimic (10 µM) were co-transfected to cells using DharmaFECT DUO Transfection Reagent (0.5 µl) (Thermo Scientific), according to manufacturer's protocol, and incubated for 24 h before lysis and detection. Dual-Luciferase® Reporter Assay System (Promega) was used for detection of the psiCHECK™-2 vectors and LightSwitch Luciferase Assay System (SwitchGear Genomics) was used for detection of 3' UTR GoClone vectors. Luminescence was measured using FLUOstar Omega plate reader (BMG Labtech). Each assay was performed with at least two biological replicates, with four technical replicates each.

3.9.3.2 Dual-Luciferase® Reporter Assay System

The transfected cells were lysed by adding 1x Passive Lysis Buffer to the wells of the 96-well plate and were incubated at room temperature on a rocking platform for 15 minutes. The Luciferase Assay Reagent II (LAR II) were added to the lysed cells, and firefly luciferase signal was measured. The Stop & Glo® Reagent was prepared right before use, added to the

wells and *Renilla* luciferase signal was measured. Luminescence measurement time was set to 2 seconds.

The luminescence signal was normalized by dividing the firefly luminescence on the *Renilla* luminescence. The specific activity of EBV-miR-BART10-3p miRNA mimic on the target gene were calculated by dividing the EBV-miR-BART10-3p miRNA mimic results on the non-targeting miRNA mimic results, giving the ratio for downregulation. Non-transfected cells were used as control for the background signal. Empty psiCHECK™-2 vector was used as control.

3.9.3.3 LightSwitch Luciferase Assay System

Assay Solution consisting of Assay Buffer and 100x Assay Substrate is added to the transfected cells and incubated for 30 minutes protected from light before luciferase signal were measured. The Assay Solution serves as both lysis buffer and luminescence creator.

The luminescence signal was normalized by dividing the signal from the EBV-miR-BART10-3p mimic transfected cells to the signal from the non-targeting miRNA mimic transfected cells. The results were then normalized to the control (R04_3UTR) and outliers were removed before calculating the average across technical replicates.

3.10 Sandwich Enzyme-linked Immunosorbent assay (ELISA)

Sandwich Enzyme-linked Immunosorbent assay (ELISA) (R&D Systems) was performed to determine the concentration of CXCL8 in DLD-1 cell culture supernatants from timeline and concentration experiment with *F. nucleatum* and *E. coli.* Cell culture experiment layout is described above. Cell culture supernatants were generated by harvesting medium from co-culture assays, centrifuged at 500xg for 5 min, and collection of supernatants. The cell culture supernatants were stored at -20 °C until ELISA was performed.

Figure 3.8 describes the principle for direct sandwich ELISA. Monoclonal antibody specific for CXCL8 is precoated onto a microplate. CXCL8 standards ranging from 0 pg/ml to 2000 pg/mL and cell culture supernatants were added to the wells and any CXCL8 present would bind to the immobilized antibody. Washing steps were performed to wash away any unbound substances. An enzyme-linked polyclonal antibody specific for CXCL8 were added, followed

by additional washing steps. Substrate solution were added, and the active substances hydrogen peroxide and tetramethylbenzidine changed the wells color to blue. The reaction was stopped by adding stop solution containing 2N sulfuric acid, changing the color to yellow (112). Absorbance was measured at 450 nm and 540 nm with the FLUOstar Omega plate reader (BMG Labtech). Wavelength correction was done by subtracting absorbance at 540 nm from absorbance at 450 nm. Standard curves (supplementary figure S5) were made from IL-8 standard results, and concentrations for samples were calculated.

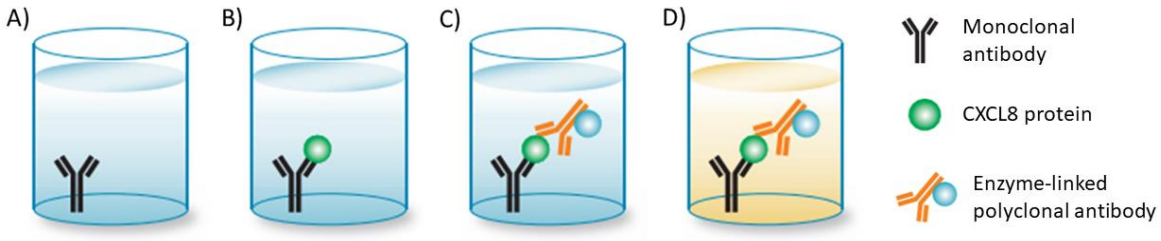

Figure 3.8: Overview of sandwich ELISA principle. *A) Monoclonal antibody is coated on microplate. B) The monoclonal antibody binds and immobilizes CXCL8 present in sample. C) Enzyme-linked polyclonal antibody specific for CXCL8 is added to the well. Substrate solution is added, and the active substances hydrogen peroxide and tetramethylbenzidine changes the color of the well to blue. D) Stop solution is added, containing 2N sulfuric acid, changing color to yellow and absorbance is measured. Figure adapted from Bio-Rad Laboratories, Inc (113).*

3.11 Confocal Laser Scanning microscopy and fluorescent staining

Fluorescent staining and confocal laser scanning microscopy were used to visualize the intra- and extracellular localization of *F. nucleatum* in DLD-1 cells.

Confocal laser scanning microscopy allows for imaging in the same focal plane, that is, where the focus of the lens hits the sample. The principle of laser scanning microscopy, figure 3.9, is based on that the laser scanning microscope (LSM) technique project the light of a laser through a high-NA objective onto a certain plane of interest as a nearly diffraction-limited focus. The excitation light is projected onto the sample by a beam splitter and through the objective, allowing for precise focus and correct wavelength of light to hit the sample. The light emitted from the fluorophore in the sample, is projected onto a variable pinhole diaphragm by the same objective and a tube lens. The focus inside the specimen and the pinhole are situated at optically conjugated points (confocal imaging), passing only the light emitted from the object plane of interest through the pinhole and unwanted light is focused

outside the pinhole. The tube lens gathers the emitted light from the objective plane of interest and directs it through the pinhole, allowing for its detection by a detector. The detector converts the optical information into electric signals, allowing for the image of any object plane to be generated and stored within seconds (114).

The Zeiss LSM 510 META confocal microscope allows for multichannel imaging, making it possible to visualize several components in the sample at same focus simultaneously.

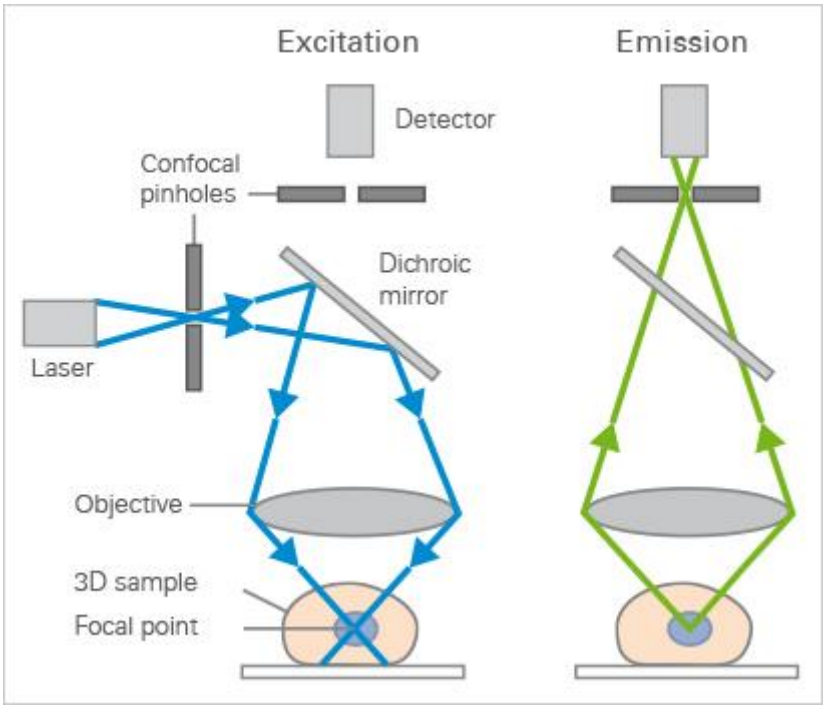

Figure 3.9: Principle of confocal microscopy. *Excitation and emission light pathways in a basic confocal microscope configuration. Figure from Ibidi (115)*

DLD-1 cells were seeded into confocal microscope dishes (VWR) and incubated until the next day. The confocal dishes have a glass bottom making them optimal for confocal microscopy. CFSE stained and unstained *F. nucleatum* were added to separate confocal dishes containing DLD-1 cells and were incubated for 2 h. The cells were then fixated, and F-actin was stained with Rhodamine Phalloidin. To visualize the cell nucleus, it was stained with DAPI. Confocal microscopy was performed by using the Zeiss LSM 510 META confocal microscope with the lasers Argon 488 nm, diode 561 nm and diode 405 nm, for CFSE, Rhodamine Phalloidin and DAPI, respectively.

F. nucleatum was stained with the fluorescent stain CFSE [5-(and-6) carboxylfluorescein diacetate succinimidyl ester] (Invitrogen). CFSE crosses the membrane of the bacteria, and intracellular esterases cleave the acetate groups and generate the fluorescent carboxylfluorescein molecule. The succinmidyl ester group reacts with primary amines in the bacteria, crosslinking the dye to intracellular proteins (116). For staining, 500 MOI of *F. nucleatum* was centrifuged at 4000xg for 5 min. The cell pellet was resuspended in 2 ml of 10 µM CFSE and incubated at 37 °C for 30 min and the fluorescent labeling was terminated by pelleting of bacteria and washing with PBS to remove excess CFSE-stain. Bacteria were then resuspended in PBS and a 23-gauge needle was used to create a single bacterial suspension. Stained *F. nucleatum* (45 µl) and unstained *F. nucleatum* (45 µl) was added to 100 000 cells DLD-1 cells in confocal dishes and incubated for 2 h before the cells were fixated and stained with Rhodamine Phalloidin. CFSE has a peak excitation/emission of 494/521 nm and Argon laser 488 nm was used (117).

DLD-1 cells were stained with a high-affinity F-actin probe conjugated to the red-orange fluorescent dye tetramethylrhodamine (TRITC). The phallotoxin is isolated from the deadly *Amanita phalloides* mushroom and consist of a bicyclic peptide that bind to F-actin (118). For fixation and Rhodamine Phalloidin staining, cells were washed twice with pre-warmed PBS and fixed with 4 % formaldehyde solution in PBS for ten minutes in room temperature and washed away twice with PBS. The methanolic stock solution of Rhodamine Phalloidin was diluted 1:40, and 200 µl was added to the cells and incubated for 20 minutes in room temperature, before additional washing to remove excess staining solution. The dye Rhodamine Phalloidin has a peak excitation/emission at 540/565 nm and diode laser 561 nm was used for confocal microscopy.

The cell nucleus was stained with DAPI (4’,6-diamidino-2-pheynylidole), a blue-fluorescent DNA stain that gives a 20-fold enhancement of fluorescence upon binding to AT regions of dsDNA (119). Diluted DAPI staining solution (0.1 µg/ml) was added to the fixed cells and incubated for 15 minutes at room temperature. Excess staining solution was washed away and 200 µl of PBS was added to avoid drying of the cells. DAPI has excitation/emission at 358/461 nm and diode laser 405 nm was used.

3.12 Data and statistical analysis

Image processing and area measuring were done by ImageJ (104). Statistical analysis and graphical display were done by GraphPad Prism software version 8 (Software MacKiev, GraphPad, San Diego, CA).

Student's t-test was performed to evaluate the differences between start point of analysis and increase in concentration or time. P-values ≤ 0.05 were considered significant. Two-way ANOVA was performed to evaluate the significance of treatment (co-culture with bacteria) and time or concentration. P-values are classified after level of significance: ns p-value > 0.05, *p-value ≤ 0.05, **p-value ≤ 0.01, ***p-value ≤ 0.001, ****p-value ≤ 0.0001.

3.13 Cancer tissue-originated spheroids

3.13.1 Initial phase of methods development

The establishment of patient tissue-originated spheroids was performed in collaboration with the research group 'Systems Biology for Oncology' at St. Olavs Hospital and NTNU, for the project "Personalized drug screens: Patient derived spheroids for colon cancer therapy", with project leader Åsmund Flobak. The cancer tissue-originated spheroids were prepared using a modified version of the protocol published by Kondo et al. (92).

Primary tumor tissue was collected from 17 Patients with colorectal cancer adenocarcinoma stage I – IV undergoing surgical resection of their primary tumor at St. Olavs Hospital, Trondheim, Norway. The patients had not received chemo-radiotherapy prior to tumor resection and tissue samples were confirmed as tumor or normal tissue by the gastrointestinal surgeon. Written consent was acquired from each patient. The study was approved by the Regional Committees for medical and health research ethics (REK 2019/246).

The cancer tissue-derived spheroids were prepared and cultured according to the following procedure in the initial phase of methods development, with crucial steps showed in figure 3.10. Tumor tissues were washed in HBSS, visible fatty and necrotic areas were removed with a scalpel and the tissue was minced into 1-2 mm pieces. Tissue was digested in supplemented DMEM with Liberase DH in a 37 °C water bath with shaking for 2 h. The tissue suspension

was filtered sequentially through a 500 µm mesh filter and 40 µm cell strainer. Tissue retained by the 40 µm filter were collected, supplemented serum-free stem cell medium was added, and the tissue suspension was incubated for 24 h. CTOSs were then seeded in collagen solution consisting of Cellmatrix type I-A, DMEM and reconstitution buffer in a 3.5 cm non-treated dish and supplemented serum-free stem cell medium was added. The dish was then incubated at 37 °C in a 5% CO_2 humidified incubator. List of materials and detailed protocols are found in supplementary table S10 and supplementary protocol S2 and S3.

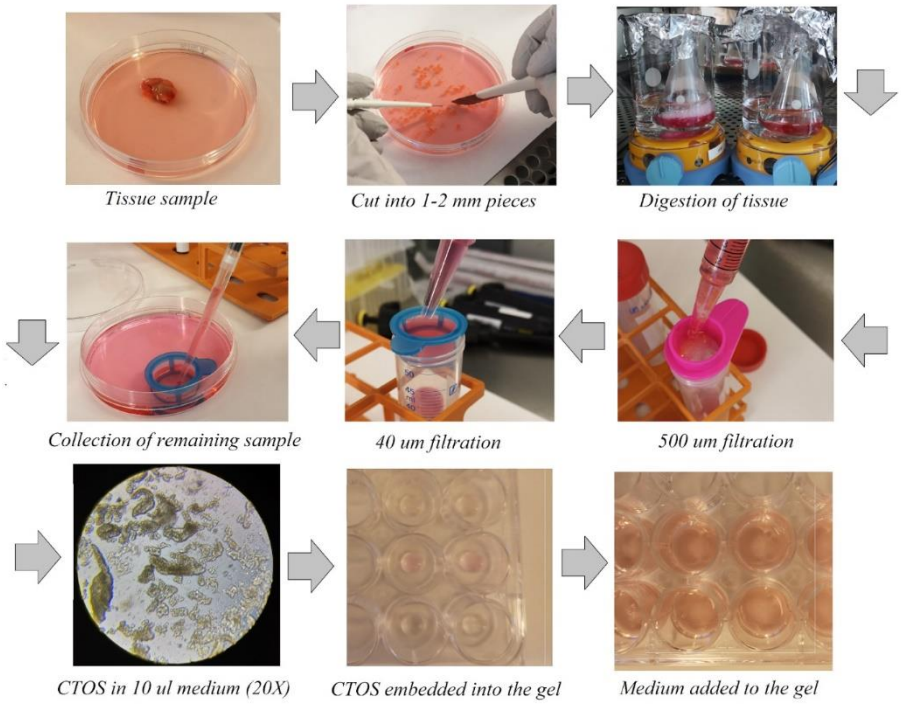

Figure 3.10: CTOSs preparation protocol from the initial phase. *Colorectal tumor tissue from patient was visually assessed, and visible fatty and necrotic areas were removed before the tumor tissue was cut into 1-2 mm large pieces. Minced tumor tissue was further digested with enzyme Liberase DH at 37 °C for 2 h. The digested tumor tissue was filtrated through a 500 µm filter and captured by a 40 µm filter. Tissue between 40 – 500 µm in size were then collected, and the number of CTOSs collected were counted manually in a light microscope. The CTOSs were then embedded into gel for further growth, and serum-free stem cell medium was added to the gels.*

After approximately two weeks of culture, the CTOSs were split and re-seeded for expansion. During splitting, the gels were digested in DMEM with collagenase type IV at 37 °C for 1 h, and the CTOSs were released from the digested gel by pipetting. CTOSs were resuspended in HBSS containing 1% BSA and mechanically teared apart by the use of 23 g needles. Fragmented CTOSs were transferred to serum-free stem cell medium and incubated in a 5 %

CO_2-humidified incubator at 37 °C overnight. CTOSs were seeded according to the protocol in supplementary S3. Detailed protocol for splitting is found in supplementary protocol S4. A CTOSs "line" is classified as established when the CTOSs are capable to be split, frozen and thawed.

3.13.2 Optimization phase with methods improvements

Following initial use of the protocol described above, an optimized protocol based on the protocols from Kondo et al. (92) and Jeppesen et al. (90), was developed. The protocol is optimized with regards to comparing digestive enzymes and seeding gels, giving a greater spheroid outcome in terms of viability and number of spheroids. Figure 3.11 describes the protocol in regards of optimization steps, and a detailed protocol is found in supplementary protocol S5 for preparing and culturing.

Tissue sampling and classification were performed as described in the initial phase of methods development. Tumor tissue was washed in HBSS, visible fatty and necrotic areas were removed with a scalpel and sample was cut in half. The two half tissue samples were minced into 1 – 2 mm pieces and digested in supplemented DMEM with Liberase DH for 2 h or collagenase II for 20 min, respectively, in a 37 °C water bath with stirring by a magnet bar. The tissue suspensions were filtered sequentially through a 500 µm pluriStrainer and 40 µm cell strainer. Tissue retained by the 40 µm filter was collected. CTOSs were counted and seeded into four different gels – Cellmatrix Type I-A, Matrigel, Cultrex and Geltrex (specifics are listed in supplementary table S10). Supplemented serum-free stem cell medium was added, following incubation at 37 °C in a 5 % CO_2-humidified incubator.

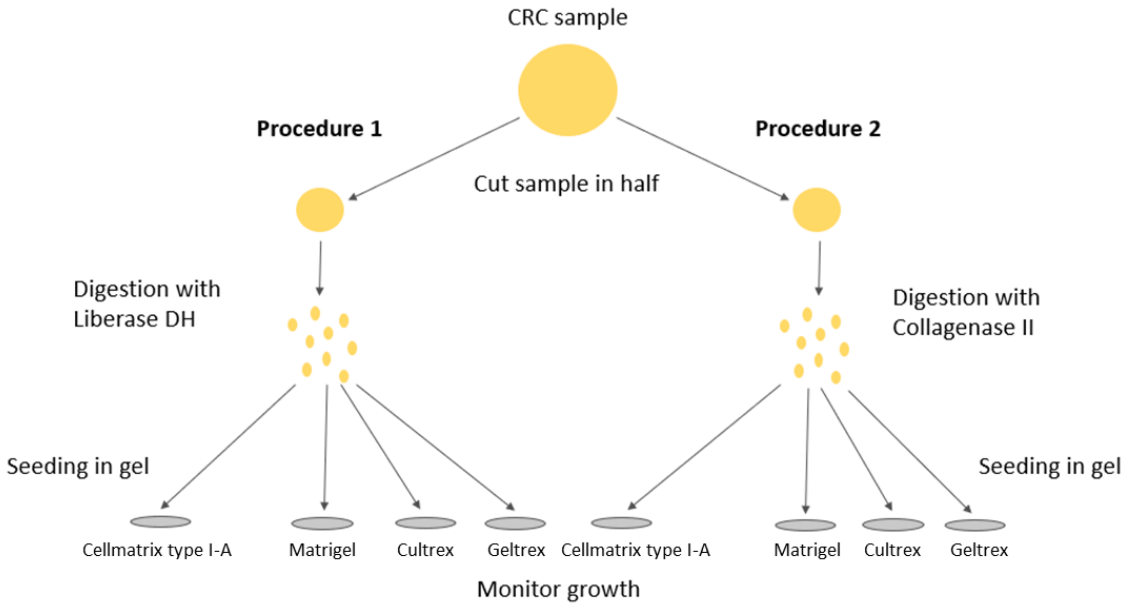

Figure 3.11: Procedure for optimization phase of methods development, considering digestive enzyme and seeding in gel. *The two procedures utilize different digestive enzymes and four different gels for seeding. Procedure 1 uses the original digestive enzyme, Liberase DH, and procedure 2 uses Collagenase II for digestion. Figure by Folkesson, E. (unpublished work).*

For splitting of the CTOSs, the gels were digested with DMEM and collagenase type IV at 37 °C for 1 h and CTOSs were released from the gels by pipetting. CTOSs were washed in PBS, resuspended in DMEM and collagenase type II and incubated for 20 min at 37 °C in a water bath, to split the CTOSs. After incubation, were the CTOSs washed in HBSS and filtered through the 500 µm pluriStrainer filter and subsequently the 40 µm cell filter. CTOSs restrained from the 40 µm filter were collected, resuspended in 0.4 ml HBSS, and counted by the use of a glass slide and light microscope.

Following splitting, the CTOSs were resuspended in a 7:2:1 volume of Cellmatrix type I-A, DMEM and reconstitution buffer. The reconstituted gel-solution (50 µl) was added to a prewarmed 24-well plate, and incubated at 37 °C for 30 min, for the gel to set. Serum-free stem cell medium was added to the wells and incubated overnight at 37 °C before medium was changed again. Medium was changed every third day, thereafter.

For freezing, the CTOSs were resuspended in fetal calf serum (FCS) achieving a spheroid density of 210 spheroid per ml, based on the count done following digestion with collagenase

type II. DMSO was then added to a concentration of 5 % of final volume. Cryovials were put in an isopropanol box and stored at -80 °C until further use.

For thawing of the CTOSs, the cryovial containing CTOSs from LN_2 storage was immediately placed in 37 °C water bath, allowing rapid thawing. The contents of the cryovial were transferred dropwise to serum-free stem cell medium and the cryovial were washed three times to retain all spheroids. The CTOSs were centrifuged and resuspended in 7:2:1 volume of Cellmatrix I-A, serum-free stem cell medium and reconstitution buffer, and plated out in 50 µl gel drops on a prewarmed 24-well plate. The plate was incubated for 30 min at 37 °C, followed by addition of 0.5 ml of serum-free stem cell medium and incubate overnight at 37 °C. Medium was changed the following day, and the spheroids were monitored daily following thawing. Medium was then changed every third day.

Detailed protocols for splitting, freezing, and thawing of CTOSs are found in supplementary protocol S6 and S7.

4 Results

4.1 Screening for candidate genes using RNA-sequencing

RNA-sequencing was performed to discover and identify genes regulated in CRC cell lines in co-culture with *F. nucleatum* or *E. coli*, and transfection with EBV-miR-BART10-3p mimic. For the bacteria co-culture experiments, we observed large differences in gene expression between different cell lines, irrespectively of the co-culture, indicating that the cell lines have different transcriptional programs (supplementary figure S6 and S7). We also observed large differences between the treatments, however, differences varied between the different cell lines (supplementary figure S6 and S7). For the cell line DLD-1 we detected 3 significant genes comparing *F. nucleatum* co-cultured cells to non-treated (TSB) cells. However, 567 genes had an absolute log2 fold change above 1, indicating that many genes were affected by the treatment. For DLD-1 we detected 1 significant gene comparing *E. coli* co-cultured cells and non-treated (TSB) cells, and 550 genes with an absolute log2 fold change above 1. For the cell line SW620, we detected 2308 significant genes comparing *F. nucleatum* co-cultured cells to non-treated (TSB) cells, and 702 genes with an absolute log2 fold change above 1. Comparing *E. coli* and non-treated (TSB) cells in SW620, we detected 81 significant genes, and 472 genes with an absolute log2 fold change above 1.

The genes *CXCL8* and *CSF2* were selected for further studies with *F. nucleatum* and the genes *CCND1* and *SAP18* were chosen as potential targets of EBV-miR-BART10-3p. Top hundred differentially expressed genes for co-culture with *F. nucleatum* and *E. coli* is shown in supplementary table S4 – S7, and top differentially expressed genes for transfection with EBV-miR-BART10-3p mimic is shown in supplementary table S8 and S9 for cell lines SW620 and LS411N.

Differentially expressed genes in *F. nucleatum* and *E. coli* co-cultured cells

Two target genes, *CXCL8* and *CSF2*, were chosen for further analysis (figure 4.2). These genes were chosen based on the expression level, significance, and relevance for CRC.

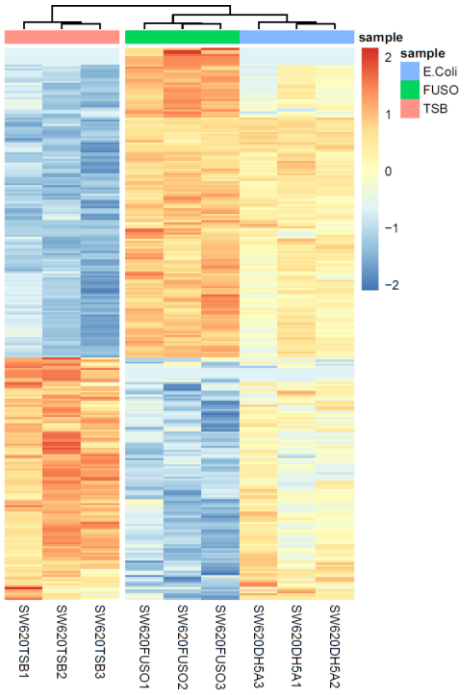

Figure 4.1: Heatmap showing differentially expressed mRNAs after F. nucleatum and E. coli co-culture with SW620 cells. *Red indicating upregulated mRNAs and blue indicating downregulated mRNAs. E. coli = E. coli DH5α, FUSO = F. nucleatum, TSB = non-treated cells.*

Figure 4.1 show a heatmap presenting the differentially expressed mRNAs after *F. nucleatum* and *E. coli* co-culture with SW620 cells. Upregulated mRNAs are presented in red, indicating that there is a difference between mRNA expression in cells treated with *F. nucleatum* and non-treated (TSB) cells. The selected genes, *CXCL8* and *CSF2* both showed increased expression in most of the *F. nucleatum* and *E. coli* co-cultured cells, indicating that they respond to bacterial infection (figure 4.2). Interestingly, *CXCL8* showed higher upregulation in *F. nucleatum* infected cells compared to *E. coli* infected cells for the two cell lines DLD-1 and LS411N, indicating that *F. nucleatum* has a stronger impact on *CXCL8* gene expression in these cell lines. The same is true for the gene *CSF2* in the DLD-1 cell line, however, the general expression level is low in this cell line. In the two SW-cell lines, *E. coli* and *F. nucleatum* have similar effect on the expression of both *CXCL8* and *CSF2*, indicating that they respond to a general infection.

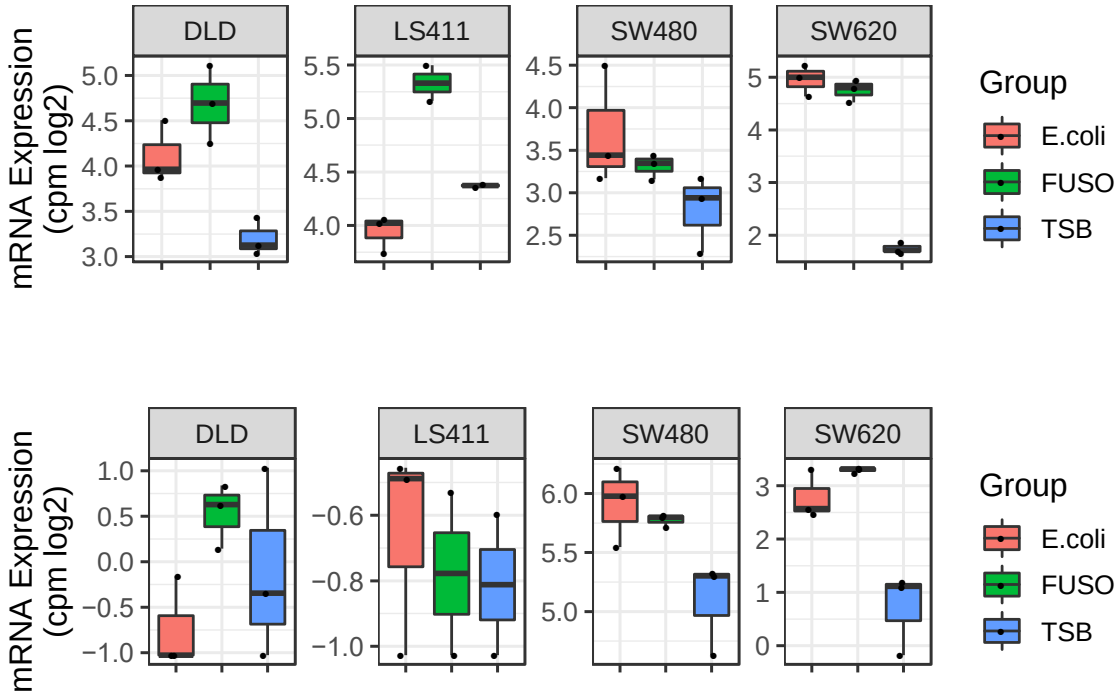

Figure 4.2: mRNA expression of genes CXCL8 and CSF2 after co-culture with E. coli, F. nucleatum and TSB in four different CRC cell lines. *Top: mRNA expression of CXCL8 after co-culture with E. coli, F. nucleatum and TSB in cell lines DLD-1, LS411N, SW480 and SW620. Bottom: Similar as the top plot for gene CSF2. E. coli = E. coli DH5α, FUSO = F. nucleatum, TSB = non-treated cells, cpm = counts per million reads.*

Next, we wanted to investigate in which human tissues these two genes are expressed. We used the Human Protein Atlas resource (120) to investigate the RNA levels across multiple tissues and found that the expression of *CSF2*, figure 4.3, was high in NK-cells, lung and pancreas, and some expression in the colorectal tissues. *CXCL8*, figure 4.4, showed high RNA expression in bone marrow, granulocytes, and lung, in addition to some expression in the colorectal tissues.

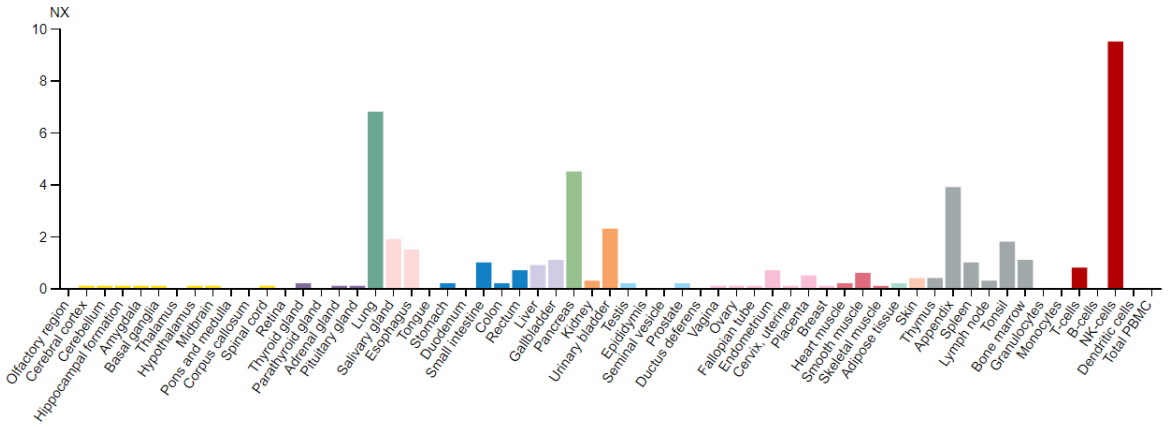

Figure 4.3: RNA CSF2 expression in human tissues. *Showing high expression in NK-cells, lung, and pancreas. Color-coding is based on tissue groups, each consisting of tissues with functional features in common. From The Human Protein Atlas (121).*

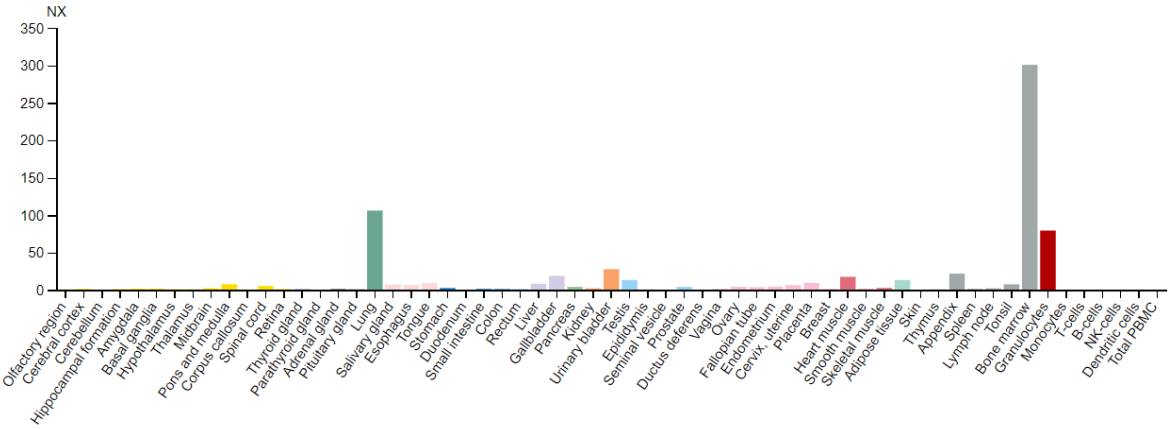

Figure 4.4: RNA CXCL8 expression in human tissues. *Showing high expression in bone marrow, granulocytes, and lung. Color-coding is based on tissue groups, each consisting of tissues with functional features in common. From The Human Protein Atlas (122).*

Differentially expressed genes in EBV-miR-BART10-3p transfected cells

We observed distinct clustering of the samples after transfection of EBV-miR-BART10-3p mimic and non-targeting miRNA mimic (supplementary figure S8), indicating that several genes were affected by the transfection. The RNA-seq showed 16 downregulated genes in both cell lines SW620 and LS411N, comparing EBV-miR-BART10-3p mimic and non-targeting miRNA mimic, presented in figure 4.5, supplementary figure S8 and supplementary table S8 and S9. After overlapping the significantly down-regulated genes with the TargetScan algorithm (123) for miRNA targets, we chose to further validate EBV-miR-BART10-3p targeting the genes *SAP18* and *CCND1*.

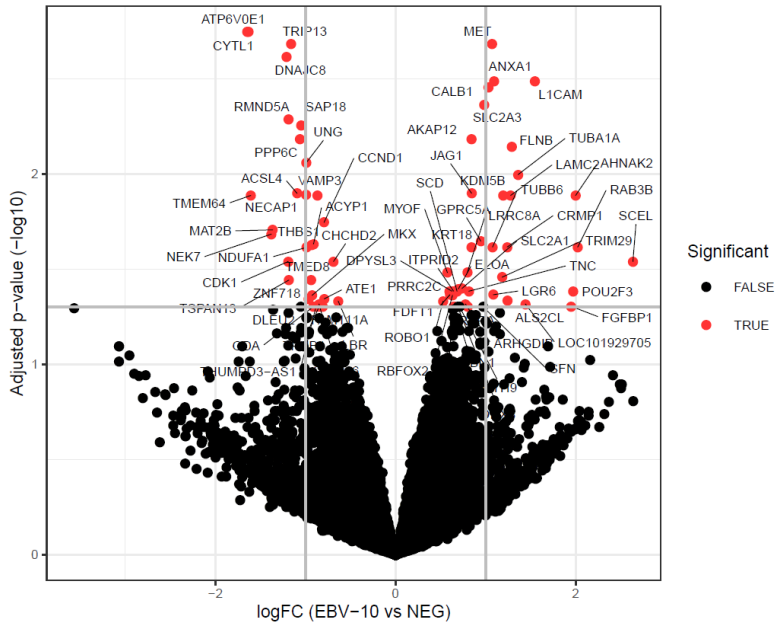

Figure 4.5: Volcano plot visualizing differentially expressed mRNAs after EBV-miR-BART10-3p and non-targeting miRNA transfection in cell line SW620. *Red dots indicate genes significantly upregulated and downregulated from EBV-miR-BART10-3p vs non-targeting miRNA. Selected target genes CCND1 and SAP18 is here shown to be downregulated. EBV-10 = EBV-miR-BART10-3p mimic, NEG = non-targeting miRNA mimic.*

The target genes, *CCND1* and *SAP18*, were both significantly downregulated in EBV-miR-BART10-3p transfected cells compared to the non-targeting control miRNA transfected cells, indicating that EBV-miR-BART10-3p has a negative effect on the expression of these two genes, shown in figure 4.6.

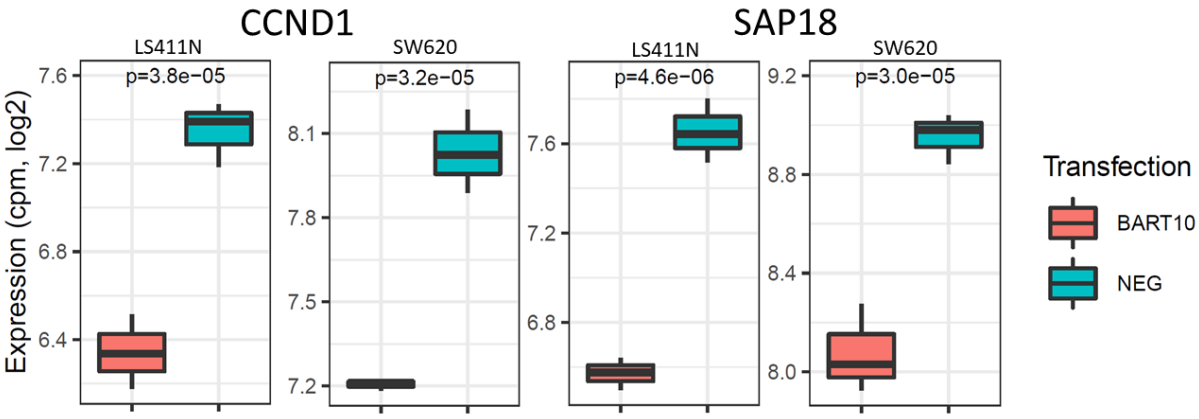

Figure 4.6: Decreased expression of target genes CCND1 and SAP18 in cell lines LS411N and SW620*. P-values ≤ 0.05 indicates significance. The p-values are calculated from a one-sided Wilcoxon rank sum test.*

Target sites for EBV-miR-BART10-3p in the genes of interest, *CCND1* and *SAP18*, were predicted using TargetScan (123). Results are shown in table 4.1 and in supplementary figure S1 and S2, showing binding of the EBV-miRNA-BART10-3p on 3'UTR of target genes.

Table 4.1: Predicted target sites for EBV-miR-BART10-3p in the genes CCND1 and SAP18, from TargetScan. *'Ensembl' and 'Gene symbol' identifies gene, 'miRNA family ID' describes miRNA, 'MSA start' and 'MSA end' describes the start and end position of binding site in the aligned UTR (counting gaps), 'UTR start' and 'UTR end' describes the start and end position of binding site in UTR (not counting gaps) and 'site type' describes binding of miRNA to the 3'UTRs of target genes.*

ENSEMBL	Gene Symbol	miRNA family ID	MSA start	MSA end	UTR start	UTR end	Site type
ENST00000227507	CCND1	EBV-miR-BART10-3p	5222	5249	2150	2155	6-mer
ENST00000227507	CCND1	EBV-miR-BART10-3p	6283	6303	2614	2621	8-mer-1a
ENST00000382533	SAP18	EBV-miR-BART10-3p	59	98	38	45	8-mer-1a

Next, we used Human Protein Atlas resource (120) to investigate the RNA expression of target genes, *SAP18* and *CCND1*, across human tissue. *SAP18*, figure 4.7, showed a moderate expression in all human tissues, with a higher expression in immune cells. *CCND1*, figure 4.8, showed a high expression in the parathyroid gland and liver, with moderate to low expression in the other tissues.

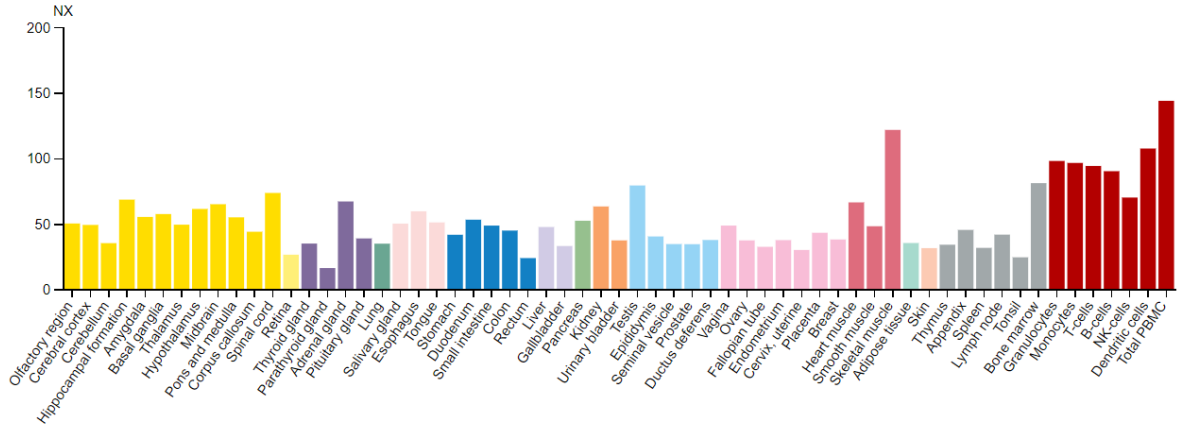

Figure 4.7: RNA SAP18 expression in human tissues. *Showing moderate expression in overall tissue, with higher expression in immune cells. Color-coding is based on tissue groups, each consisting of tissues with functional features in common. From Human Protein Atlas (124).*

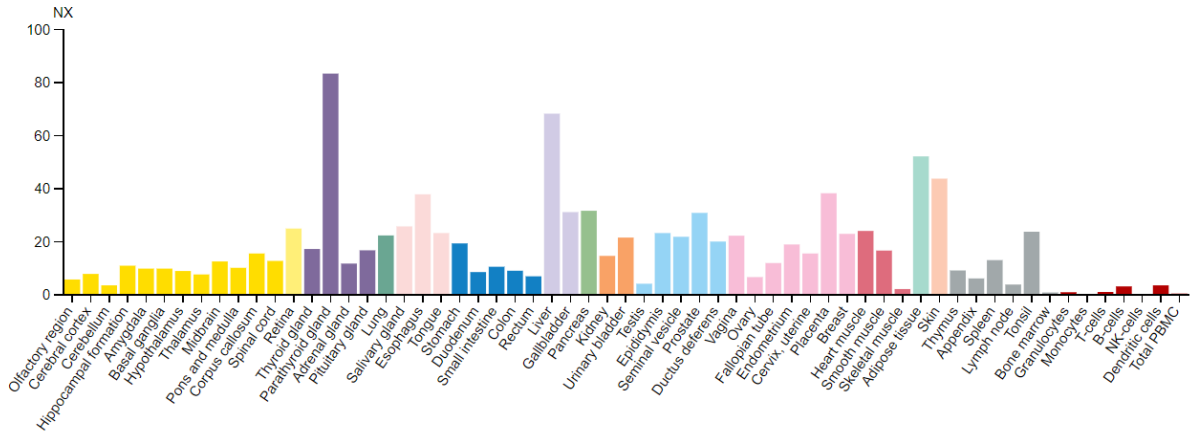

Figure 4.8: RNA CCND1 expression in human tissues. *Showing high expression in the parathyroid gland and liver, with moderate to low expression in the other tissues. Color-coding is based on tissue groups, each consisting of tissues with functional features in common. From Human Protein Atlas (125).*

4.2 *Fusobacterium nucleatum* experiments

4.2.1 Cell migration assay

The direct effect of *F. nucleatum* on CRC cells DLD-1 migration or wound healing properties were examined in an *in vitro* wound healing assay. The non-treated cells and *F. nucleatum* treated cells showed similar wound closure properties (figure 4.9 and 4.10), and there was no significant difference between the two treatments using student t-test between treatments at same timepoint ($p > 0.05$). However, we observed a trend towards more closure in the *F. nucleatum* infected cells for all timepoints. Statistical test (two-way ANOVA) showed significant difference between timepoints ($p=0.008$), but this is expected because of the cells natural wound closure properties.

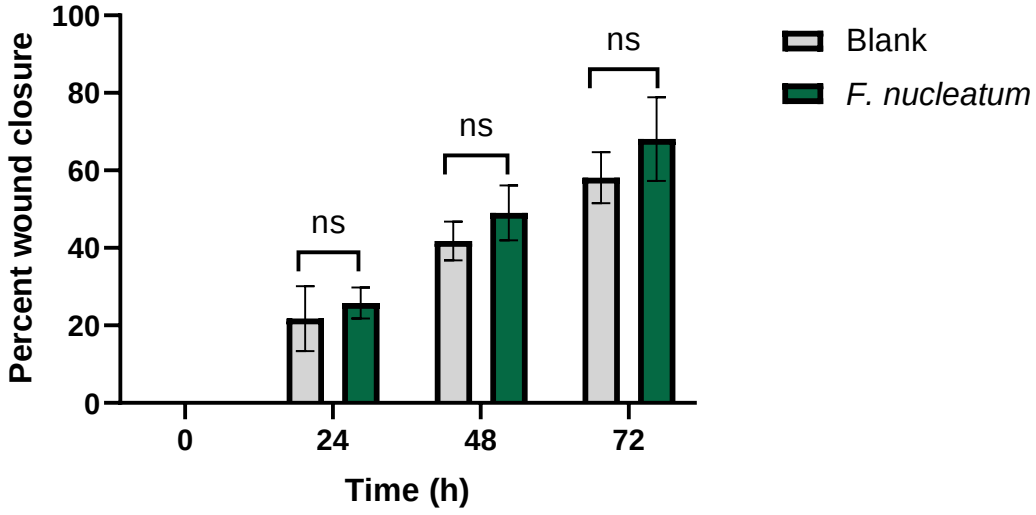

Figure 4.9: Effect of F. nucleatum on migration behavior of DLD-1 cells. *Graph show percent wound closure in DLD-1 cells where cell migration was measured based on the leading edges of the wound. Results show average of three independent biological experiments, with error bars showing SD. One-tailed student-t test gave no significant difference between control (blank) and F. nucleatum co-culture. Two-way ANOVA showed no significant difference between non-treated cells (blank) and co-culture with F. nucleatum (p-value= 0.0897) but did show significant differences between timepoints (p=0.008).*

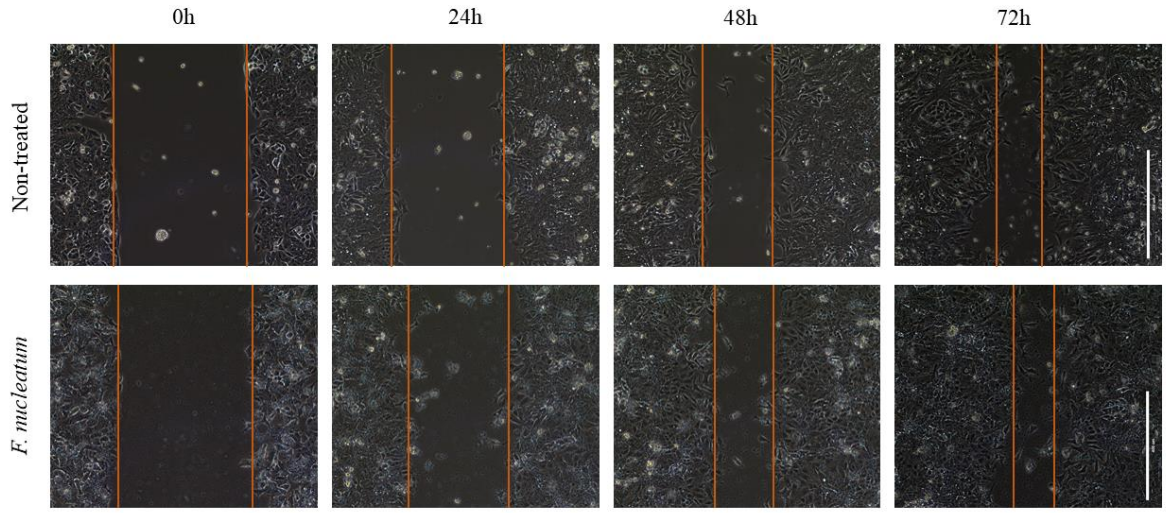

Figure 4.10: Wound closure monitored over time in non-treated DLD-1 cells and DLD-1 cells treated with F. nucleatum. *Top: Wound closure over time in non-treated DLD-1 cells. Bottom: Wound closure over time in DLD-cells co-cultured with F. nucleatum. Straight lines represent the average leading edges of the healing wound. Bar is 400 µl.*

4.2.2 Cell proliferation assay

The effect of *F. nucleatum* and *E. coli* on the proliferative behavior of CRC DLD-1 cells were examined in an *in vitro* cell proliferation assay. *F. nucleatum* treated cells showed a higher number of cells after 72 h compared to non-treated and *E. coli* treated cells, shown in figure 4.11. However, the results cannot be verified because this has only been estimated visually and been performed in one biological replicate.

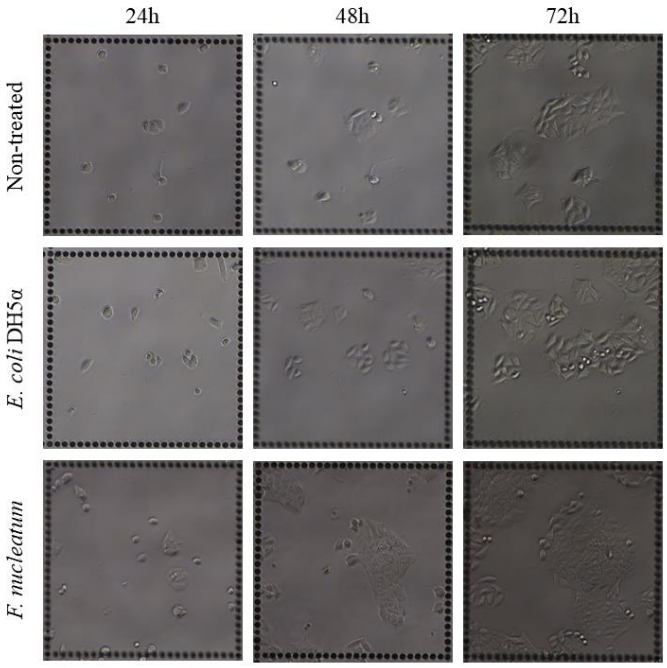

Figure 4.11: The effect of F. nucleatum and E. coli on the proliferative behavior on DLD-1 cells. *F. nucleatum treated DLD-1 cells showed a higher number of cells after 72 h than non-treated and E. coli treated cells. Proliferation result were rated visually of one biological replicate.*

4.2.3 Time series experiment

Next, we applied real-time qPCR and ELISA to investigate the gene expression and secreted protein levels of the cytokine *CXCL8* in DLD-1 cell in co-culture with *F. nucleatum* and *E. coli,* presented in figure 4.12. In co-culture with *F. nucleatum,* the gene expression level peaked at 6 h and 24 h, while the secreted protein level showed a gradually increase with time. In *E. coli* treated cells, both gene expression and secreted protein levels show a stable expression of *CXCL8* with time. Both *F. nucleatum* and *E. coli* stimulated *CXCL8* gene expression and protein secretion were significant elevated across the time course with p-value ≤ 0.05, using unpaired student t-test comparing timepoint 0 h and other timepoints. Two-way ANOVA indicates that both time and treatment is significantly increased by $p \leq 0.05$.

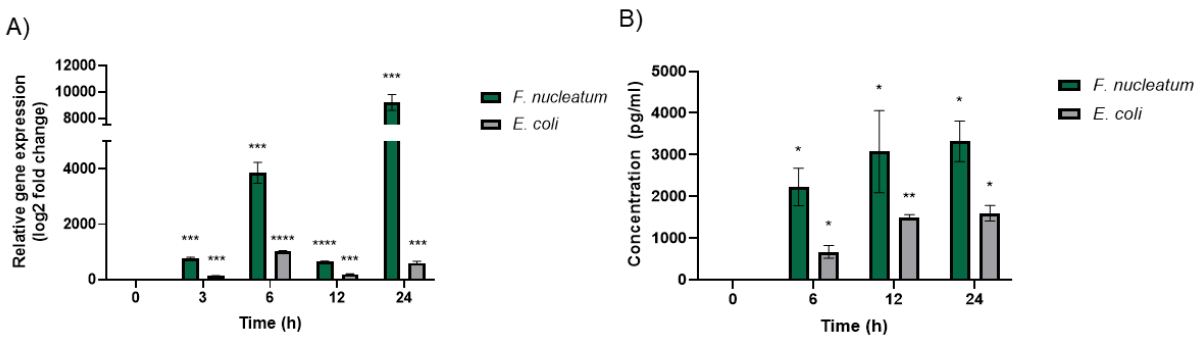

Figure 4.12: Increased gene expression and secreted protein levels of CXCL8 in DLD-1 cells in time series experiment with F. nucleatum and E. coli. *A) Gene expression of CXCL8 in DLD-1 cells showed a gradually increased expression over time for F. nucleatum, while E. coli present a stable expression over time. B) Protein secretion of CXCL8 showed a gradually increasing level over time for F. nucleatum and a stable level for E. coli. Both gene expression and Two-way ANOVA indicates that gene expression and protein secretion is significantly increased in both time and treatment ($p \leq 0.05$). Gene expression were measured by real-time qPCR and are mean of three technical replicates with error bars showing SEM. Protein secretion were measured by ELISA in duplicate with two biological replicates with error bars showing SEM. protein secretion levels of CXCL8 were significantly increased for all time points, ($p \leq 0.05$, two-tailed independent student t-test). * indicates level of significance between 0 h and respective time points: *p-value ≤ 0.05, **p-value ≤ 0.01, ***p-value ≤ 0.001, ****p-value ≤ 0.0001.*

Gene expression levels of cytokine *CSF2* showed upregulation in DLD-1 cells in co-culture with *F. nucleatum* and *E. coli*, measured by real-time qPCR, presented in figure 4.13. Co-culture with *F. nucleatum* showed a gradually significant increased level of *CSF2* with peak gene expression at 24 h ($p \leq 0.05$, two-tailed independent student t-test). *E. coli* treated cells showed a stable expression of *CSF2* with time. Two-way ANOVA indicates that gene expression is significantly increased for both time and treatment ($p \leq 0.05$).

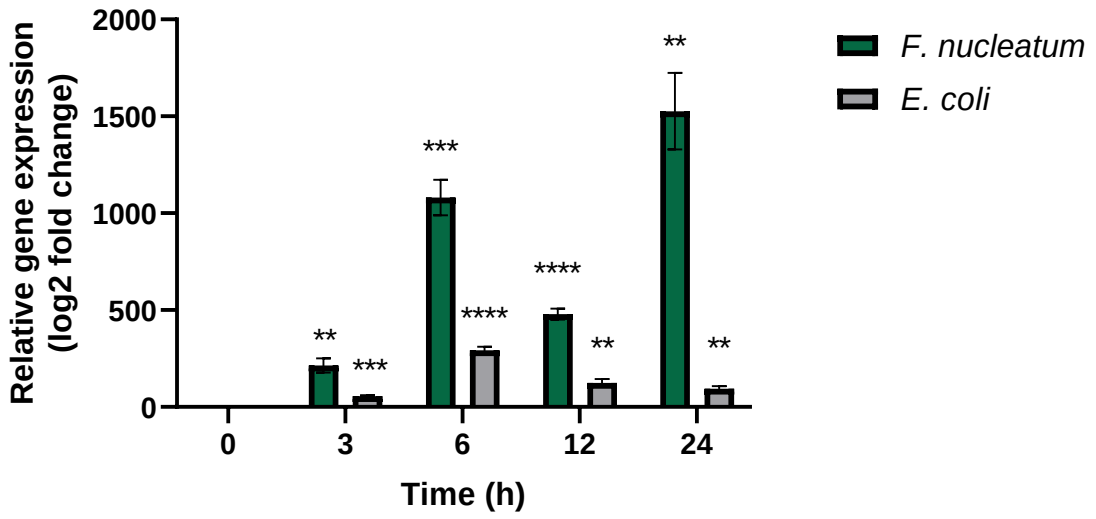

Figure 4.13: Increased gene expression of CSF2 in DLD-1 cells in co-culture with F. nucleatum and E. coli in time series experiment. *CSF2 is significant increased ($p \leq 0.05$, two-tailed independent student t-test) in all time points for both F. nucleatum and E. coli. F. nucleatum treated cells show stable expression of CSF2, while E. coli treated cells show a gradually increasing expression over time. Two-way ANOVA indicates that gene expression is significantly increased for both time and treatment ($p \leq 0.05$). Mean results are from three technical replicates and error bars are SEM. * indicates level of significance between 0 h and respective timepoints: *p-value ≤ 0.05, **p-value ≤ 0.01, ***p-value ≤ 0.001, ****p-value ≤ 0.0001.*

4.2.4 Concentration experiment

Gene expression and protein secretion of cytokine *CXCL8* in co-culture with increasing MOI of *F. nucleatum* and *E. coli* is presented in figure 4.14. The *CXCL8* gene expression showed significant, gradually elevated levels for both *F. nucleatum* and *E. coli* treated cells with increasing MOI. Two-tailed independent student t-test showed significant differences (p-values ≤ 0.05) in gene expression for all concentrations of both *F. nucleatum* and *E. coli*. CXCL8 protein secretion showed a gradually increasing concentration for both *F. nucleatum* and *E. coli* treated cells, but the elevated concentration was only significant for a MOI of 10 of *E. coli* by independent student t-test ($p \leq 0.05$). This can come from large differences between biological replicates.

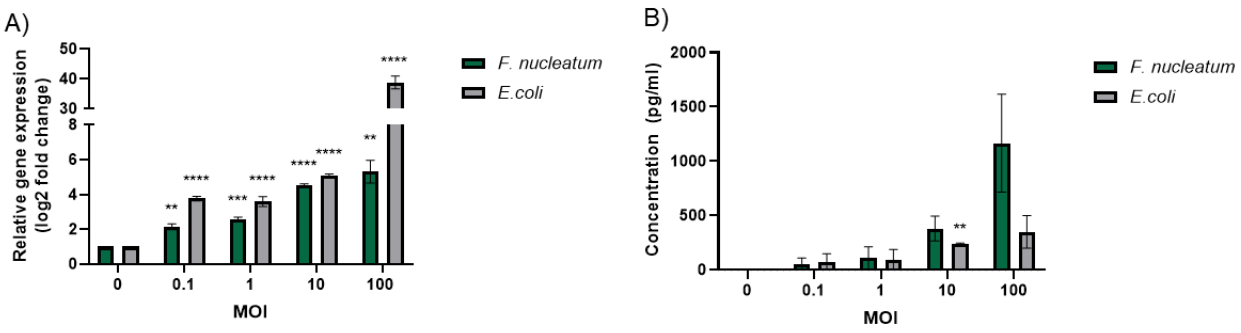

Figure 4.14: Increased gene expression and secreted protein levels of CXCL8 in DLD-1 cells in concentration experiment of co-culture with F. nucleatum and E. coli. *A) Increased gene expression of CXCL8 by co-culture with F. nucleatum and E. coli by increasing MOI, show a significant steady increased gene expression for F. nucleatum and significant gradually increased gene expression for E. coli, across increasing concentration of bacteria ($p \leq 0.05$, two-tailed independent student t-test). Two-way ANOVA for gene expression indicates that both treatment and MOI is significant ($p \leq 0.05$).*
*B) Increased protein secretion levels of CXCL8 in cell supernatants from co-culture with F. nucleatum and E. coli show a gradually increasing protein secretion for F. nucleatum and a steady increasing protein secretion for E. coli, with significant increased protein secretion for 10 MOI co-culture with E. coli ($p \leq 0.05$, two-tailed student t-test). The lack in significance for other concentrations of bacteria can come from large variations between biological replicates. Two-way ANOVA for protein secretion indicates that concentration is significant ($p \leq 0.05$), while treatment is not significant ($p > 0.05$). Mean results are for gene expression from three technical replicates, and for protein secretion two biological replicates and error bars is SEM. *p-value ≤ 0.05, **p-value ≤ 0.01, ***p-value ≤ 0.001, ****p-value ≤ 0.0001.*

Gene expression of cytokine *CSF2* in co-culture with increasing MOI of *F. nucleatum* and *E. coli*, is presented in figure 4.15. The gene expression of *CSF2* gradually increases in *E. coli* treated cells, while *F. nucleatum* treaded cells showed a more stable gene expression. The elevated gene expression is over all significant ($p \leq 0.05$, two-tailed independent student t-test), and two-way ANOVA indicates that both treatment and concentration is significant ($p \leq 0.05$).

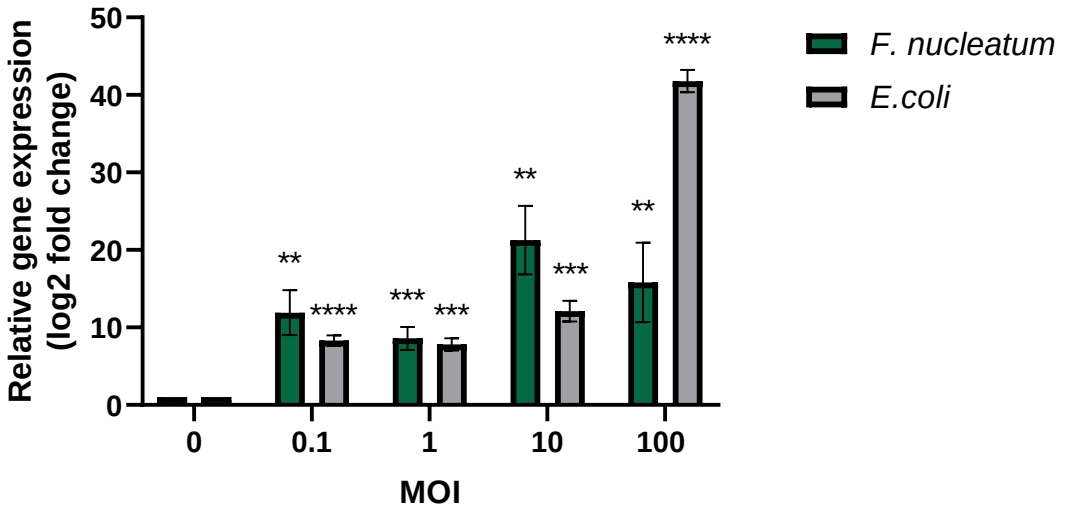

Figure 4.15: Increased gene expression of CSF2 in SW620 cells in concentration experiment of co-culture with F. nucleatum and E. coli*. CSF2 gene expression is significantly gradually increased in E. coli treated cells, and in F. nucleatum treaded cells the gene expression presents a more stable significant increased levels ($p \leq 0.05$, two-tailed independent student t-test). Two-way ANOVA indicates that both treatment and concentration is significant ($p \leq 0.05$). Mean gene expression is from three technical replicates and error bars is SD. *p-value ≤ 0.05, **p-value ≤ 0.01, ***p-value ≤ 0.001, ****p-value ≤ 0.0001.*

4.2.5 Internalization of *F. nucleatum* in DLD-1 cells

Co-culture of DLD-1 cells and *F. nucleatum* was showed by confocal microscopy to visualize and confirm the internalization of *F. nucleatum* in CRC cells. To determine the localization of *F. nucleatum*, was the F-actin in DLD-cells stained with Rhodamine Phalloidin, *F. nucleatum* stained with CFSE and the nucleus was stained with DAPI. CFSE-labeled *F. nucleatum* were co-cultured with DLD-1 cells for 2 h, before fixation and Rhodamine Phalloidin- and DAPI-staining. Upon co-culture of DLD-1 cells and *F. nucleatum*, translocated *F. nucleatum* to the inside of the DLD-1 cells. *F. nucleatum* was found to locate mainly in the cytosol. The internalization of *F. nucleatum* in DLD-1 cells is presented in figure 4.16, 4.17 and 4.18.

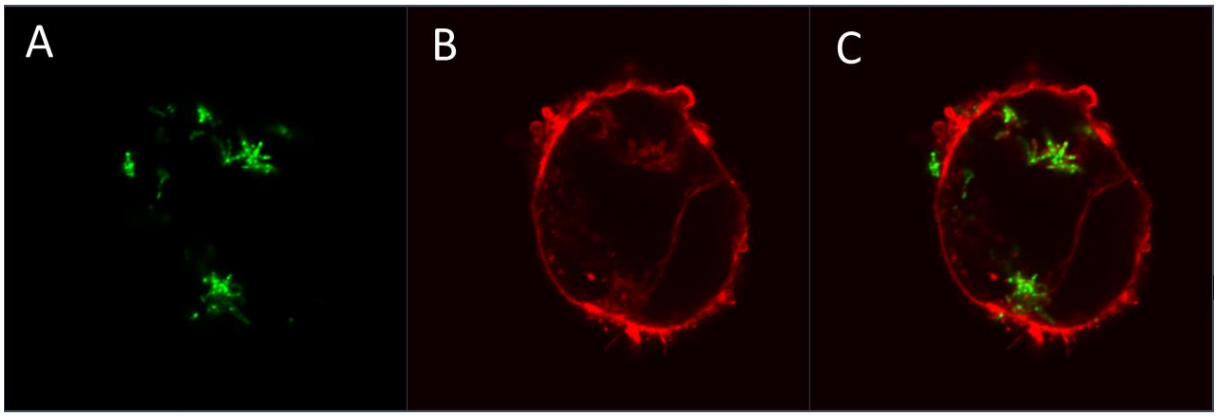

Figure 4.16: Immunofluorescence confocal micrographs of DLD-1 co-cultured with F. nucleatum (MOI of 500) for 2 h (100x). *A) F. nucleatum stained with CFSE (Argon laser 488 nm). B) DLD-1 cell stained with Rhodamine Phalloidin revealing F-actin (Diode laser 561 nm) C) Figure A and B merged to present intracellular localization of F. nucleatum in DLD-1 cell.*

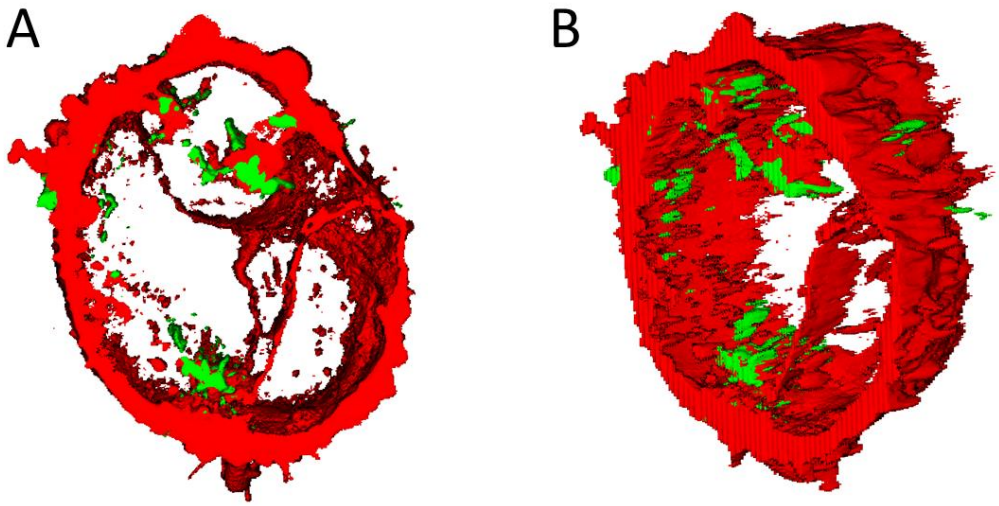

Figure 4.17: 3D-figure of DLD-1 cell infected with F. nucleatum, presenting intracellular localization of F. nucleatum*. 3D-figure made from Z-stack with 81 slices. A) 3D-figure presented from the front and B) 3D-figure presented from the side, showing CFSE-stained F. nucleatum (green) inside of Rhodamine Phalloidin F-actin stained DLD-1 cell.*

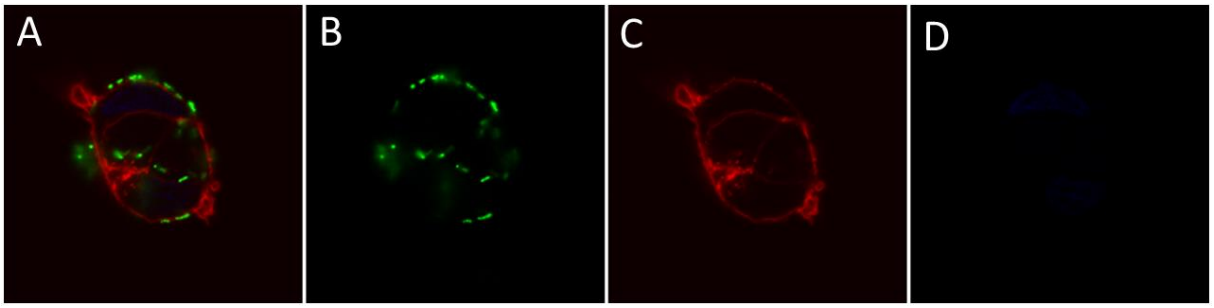

Figure 4.18: Immunofluorescence confocal micrographs of DLD-1 co-cultured with F. nucleatum (MOI of 500) for 2 h (100x), presenting intracellular localization of F. nucleatum*. A) Figure B, C and D merged to present intracellular localization of F. nucleatum in DLD-1 cell. B) F. nucleatum stained with CFSE (Argon laser 488 nm). C) DLD-1 cell stained with Rhodamine Phalloidin revealing F-actin (Diode laser 561 nm). D) Nucleus of DLD-1 cell stained with DAPI (blue) (Diode laser 405 nm)*

4.3 EBV-miR-BART10-3p downregulates genes *CCND1* and *SAP18* when transfected in SW620 cells

4.3.1 Downregulation of *CCND1* and *SAP18* by real-time qPCR

The relative gene expression of target genes *SAP18* and *CCND1* were significantly downregulated after transfection with EBV-miR-BART10-3p mimic, compared to control gene *ACTB* (p-value ≤ 0.05), as shown in figure 4.19.

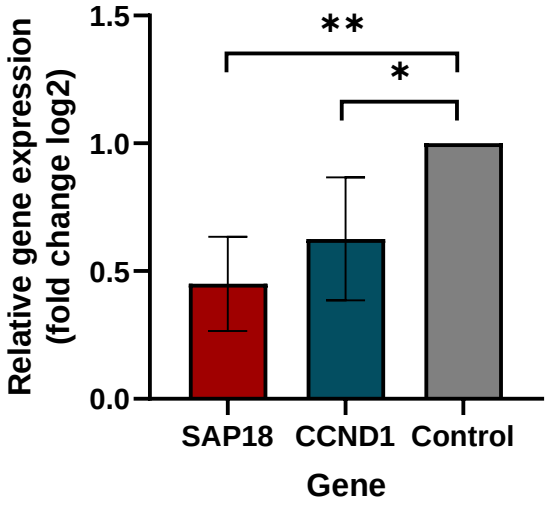

Figure 4.19: Downregulated gene expression of target genes SAP18 and CCND1 genes in SW620 cells when transfected with EBV-miR-BART10-3p mimic*. One-tailed independent student t-test indicates significant downregulation of both SAP18 and CCND1. Mean gene expression is from three biological replicates with six technical replicates each and error bars are SD. *p-value ≤ 0.05, **p-value ≤ 0.01, ***p-value ≤ 0.001, ****p-value ≤ 0.0001.*

4.3.2 Direct downregulation of *SAP18* and *CCND1* when co-transfected with 3'UTR vectors and EBV-miR-BART10-3p mimic

To investigate whether *SAP18* and *CCND1* is directly targeted by EBV-miR-BART10-3p mimic, we used LightSwitch luciferase vectors cloned with the 3'UTRs of *SAP18* and *CCND1*, as well as a psiCHECK™-2 vector with the 8-mer 3'UTR sequence of *CCND1*. Successful insert of 8-mer 3'UTR of *CCND1* in psiCHECK™-2 vector was confirmed by PCR reaction, gel electrophoresis with a band present at 197 bp, and Sanger sequencing, presented in figure 4.20. Entire Sanger sequence of psiCHECK™-2 vector with 8-mer 3'UTR *CCND1* insert is found in supplementary figure S3 and S4.

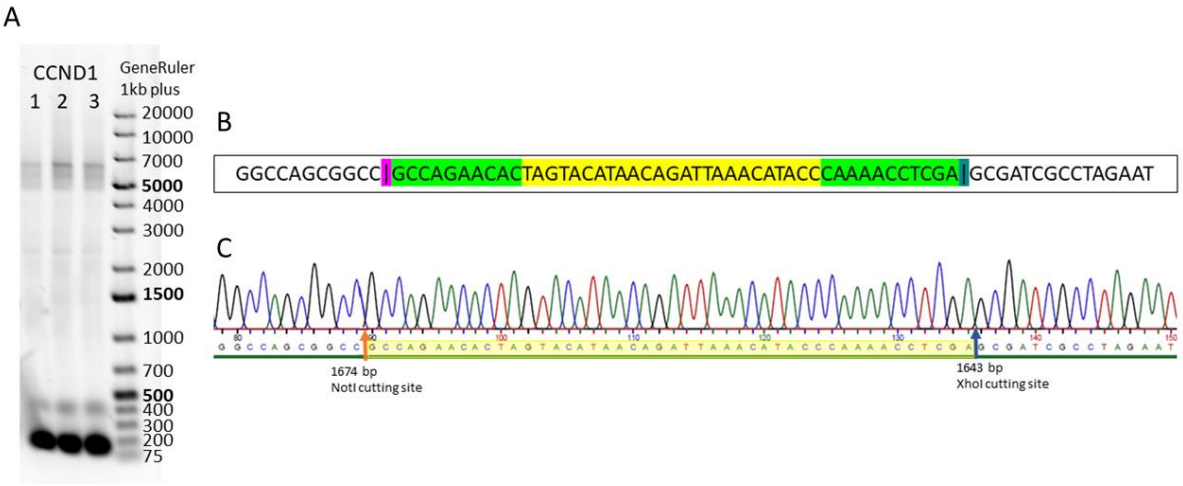

Figure 4.20: Gel electrophoresis and Sanger sequencing of psiCHECK™-2 vector with insert of 8-mer 3'UTR of CCND1. *A) Gel electrophoresis of PCR products of psiCHECK™-2 vector with insert of 8-mer 3'UTR of CCND1. Bands present at 194 bp indicates successful ligation of insert into vector. B) Nucleotide sequence from Sanger sequencing of psiCHECK™-2 vector with insert of CCND1. Yellow indicate CCND1 forward primer used for PCR reaction, green+yellow indicate 8-mer 3'UTR CCND1 insert, pink indicate NotI cutting site and blue indicate XhoI cutting site (straight line not in sequence). C) Sanger sequencing of psiCHECK™-2 with insert of 8-mer 3'UTR to CCND1. Yellow outline indicates insert of CCND1, orange and blue arrows indicate XhoI and NotI cutting site, with nucleotide-number of cutting site in psiCHECK™-2 vector.*

Co-transfection with EBV-miR-BART10-3p mimic and 3'UTR vectors of *CCND1* and *SAP18*, showed significantly downregulation of *SAP18* and *CCND1* using both the psiCHECK2-CCND1 vector with the 8-mer target site and the complete 3'UTR LightSwitch vectors for *SAP18* and *CCND1* (figure 4.21). The luciferase activity for non-targeting miRNA mimic was unchanged, indicating that EBV-miR-BART10-3p recognizes and targets the

SAP18 and *CCND1* 3'UTR directly. These results indicated that EBV-miR-BART10-3p could inhibit the expression of *SAP18* and *CCND1* by directly binding to the predicted EBV-miR-BART10-3p binding site on the 3'UTR sequence of *SAP18* and *CCND1* in CRC SW620 cells.

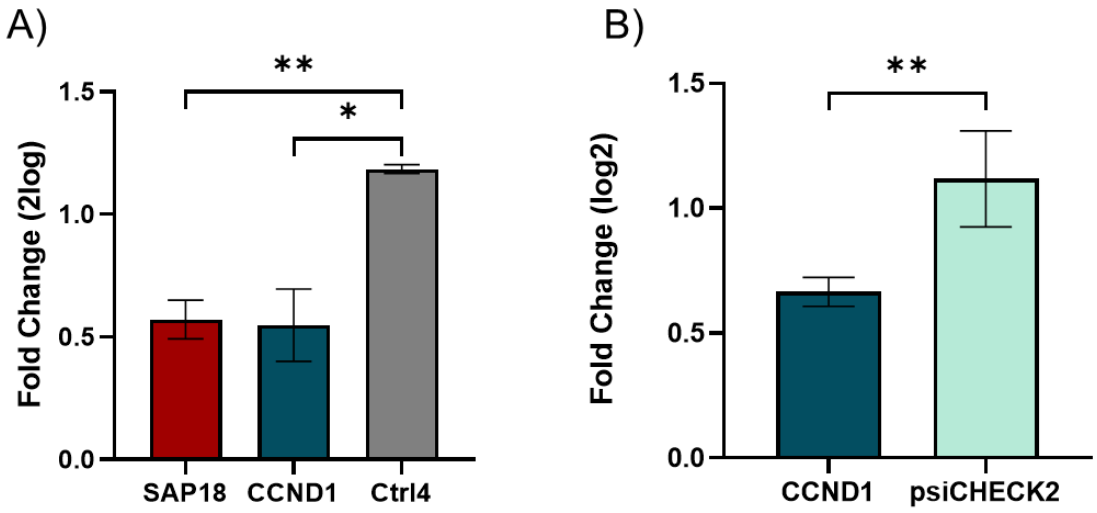

Figure 4.21: Downregulation of SAP18 and CCND1 by co-transfection of EBV-miR-BART10-3p mimic and luciferase vectors containing 3'UTR of genes SAP18 and CCND1. *A) Downregulation of genes SAP18 and CCND1 by co-transfection of EBV-miR-BART10-3p and 3'UTR LightSwitch SAP18 and CCND1 vectors. Both SAP18 and CCND1 showed significant downregulation after co-transfection (independent one-tailed student t-test, $p \leq 0.05$). B) Downregulation of CCND1 by co-transfection of EBV-miR-BART10-3p and 8-mer 3'UTR CCND1-psiCHECK™-2 vector. CCND1 showed significant downregulation when comparing to control psiCHECK™-2 vector (independent one-tailed student t-test, $p \leq 0.05$) *p-value ≤ 0.05, **p-value ≤ 0.01, ***p-value ≤ 0.001, ****p-value ≤ 0.0001.*

4.4 Cancer tissue-originated spheroids

4.4.1 Initial phase of methods development

The cancer tissue-originated spheroids (CTOSs) were prepared using a modified version of the protocol published by Kondo et al. (92). The initial phase protocol for cancer tissue derived spheroids (CTOSs) gave an overall low success rate, as only two of ten tissue samples produced spheroids and the remainder were discarded, presented in table 4.2. Examples of spheroids from CRC-01 is showed in figure 4.22.

Table 4.2: Results from initial phase of method development of colorectal cancer originated spheroids (CTOSs). *Sample ID indicates tumor tissue sample, weigh and/or size is indicated for each sample and result after CTOSs preparation and cultivation.*

Sample ID	Weight (g) / Size	Split/frozen/ discarded
CRC-01	2 pieces, each 1-2 cm	Split + frozen
CRC-02	2 pieces, each 0.5-1 cm	Discarded
CRC-03	0.667 g, 2 pieces	Split + frozen
CRC-04	1.365 g	Discarded
CRC-05	0.852 g	Discarded
CRC-06	0.959 g	Discarded
CRC-07	0.939 g	Discarded
CRC-08	0.227 g	Discarded
CRC-09	0.497 g	Discarded
CRC-10	0.701 g	Discarded

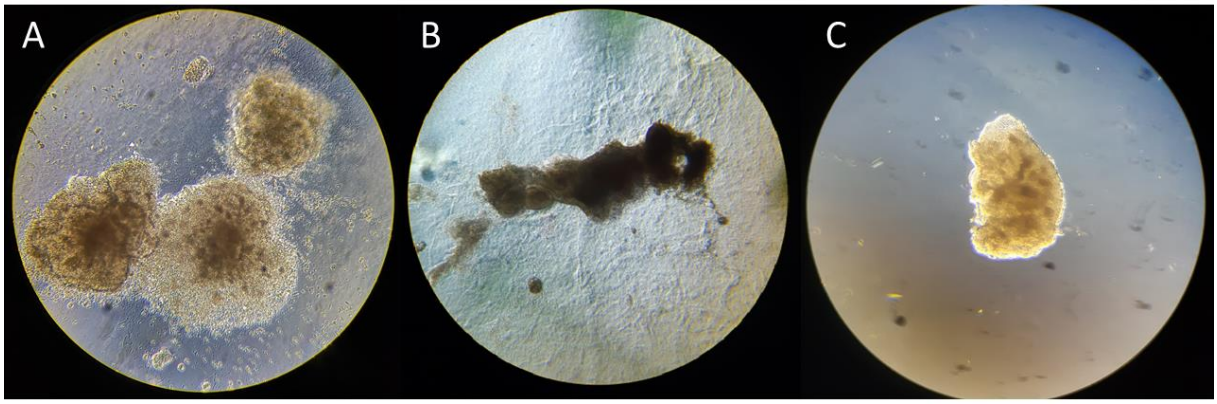

Figure 4.22: Colon cancer tissue-originated spheroids (CTOSs) from CRC-1 in Cellmatrix type I-A. *A) CRC-1 CTOSs after three weeks of incubation. B) CRC-1 CTOS after three weeks of incubation, before splitting. C) CRC-1 CTOS after splitting, freezing, and thawing.*

Experiences and improvements for initial phase of methods development

The digestion step with the enzyme Liberase DH gave a lower output than desired. During the initial phase we found that this can be improved by the use of a water bath and a magnetic stirrer instead of a shaking water bath, giving more manual disturbing of tumor tissue in addition to enzymatic digestion.

The low yield of spheroids can also come from how the spheroids were picked up when adding them into the gel. By centrifuging and removing excess medium, the spheroids get more concentrated and it will be easier to get a higher number of spheroids into the gel.

The Cellmatrix I-A gel was difficult to work with, as it solidified rapidly, caused bubbles, and gave rise to fragile gel drops larger than 80 µl in total volume. This was solved by keeping the components of the gel cold until seeding, working rapidly when seeding gel into wells and reducing the gel drops to 50 µl in total volume. Gel drops also become fragile when adding medium with spheroids to the gel, this was solved by incorporating the spheroids in the originally medium added to the reconstituted gel before plating and incubation.

The splitting procedure was experienced as very manual, as one would physically split each spheroid with needles. It is considered to use an enzyme for the splitting process.

4.4.2 Optimization phase of methods development

Table 4.3 shows tumor samples, weight, number of spheroids derived from digestive enzyme incubation, number of passages before freezing, and success rate. The overall success rate with improvements in the preparation and culturing method was higher than in the initial phase of methods development, with only two out of seven samples being discarded. The two discarded samples were small to begin with, giving few spheroids at start point. An example of a spheroid's growth from day 1 of culture to day 19 is presented in figure 4.23. Most of the samples have been thawed after freezing and seem to have survived this process. The long-term survival after thawing has not been assessed, because of time.

***Table 4.3: Result from optimization phase of method development**. 'Sample ID' indicates tumor tissue sample, 'weight' is indicated for each sample, 'number of spheroids' derived after digestion with 'Liberase DH' and 'Collagenase II', 'number of passages before freezing', 'number of gels before freezing', if sample has been 'frozen', 'thawed and survived' or 'discarded'.*

Sample ID	Weight (g)	Number of spheroids		Number of passages before freezing	Number of gels before freezing	Frozen or discarded	Thawed and survived
		Liberase DH	Collagenase II				
CRC-11	0.927	3700	1600	2	7	Frozen	Yes
CRC-12	0.126	-	-	-	-	No spheroids in sample	-
CRC-13	0.602	52000	84000	2	3	Frozen	Yes
CRC-14	0.446	8240	12240	2	4	Frozen	Yes
CRC-15	0.056	52	212	-	-	Discarded, no spheroids in gel	-
CRC-16	1.128	2400	>8000	1	12	Frozen	Yes
CRC-17	1.168	3630	22000	1	17	Frozen	Not thawed

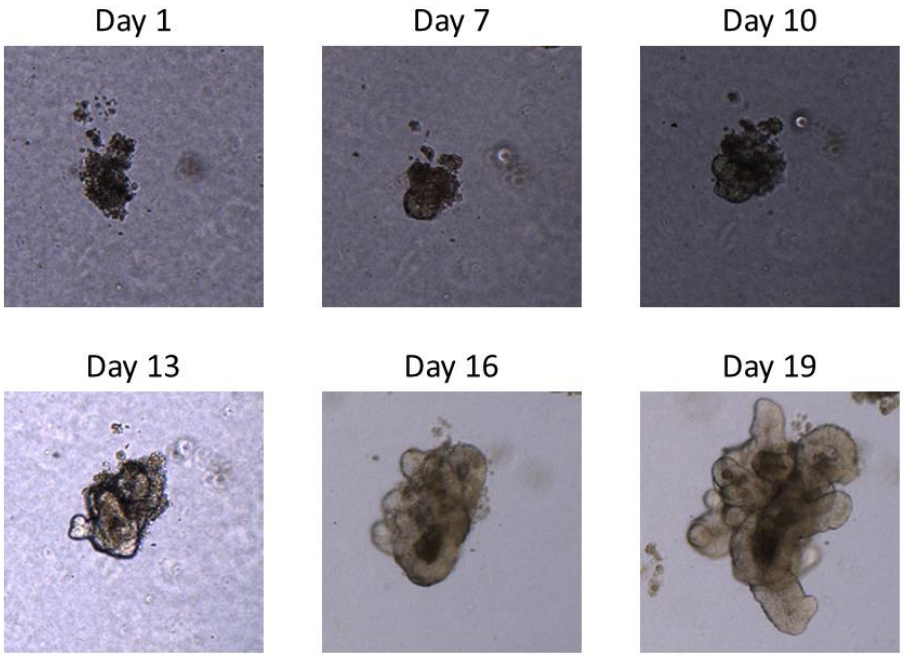

***Figure 4.23: CTOSs from tissue sample CRC-16, digested by collagenase II and seeded in Geltrex.** Presenting growth in spheroids from day 1 to day 19 in gel, creating spheroids with intestinal structure*

Jeppesen et al. (90) describes an incubation time of 20 min with the digestive enzyme collagenase II. The incubation time was prolonged to 2 h for CRC-11, the same incubation time as Liberase DH, but it is possible that this was too long, resulting in over-digestion of the sample and removal of a considerable number of spheroids during subsequent filtration steps. The incubation time was set to 20 min for subsequent samples. The digestive incubation step was changed to incubation in a water bath with a magnetic stirrer in the optimization phase, from the shaking water bath in the initial phase of method development. Overall, did digestion with Collagenase II give more spheroids than Liberase DH, as shown in figure 4.24. But it is observed that Liberase DH treated the spheroids more carefully.

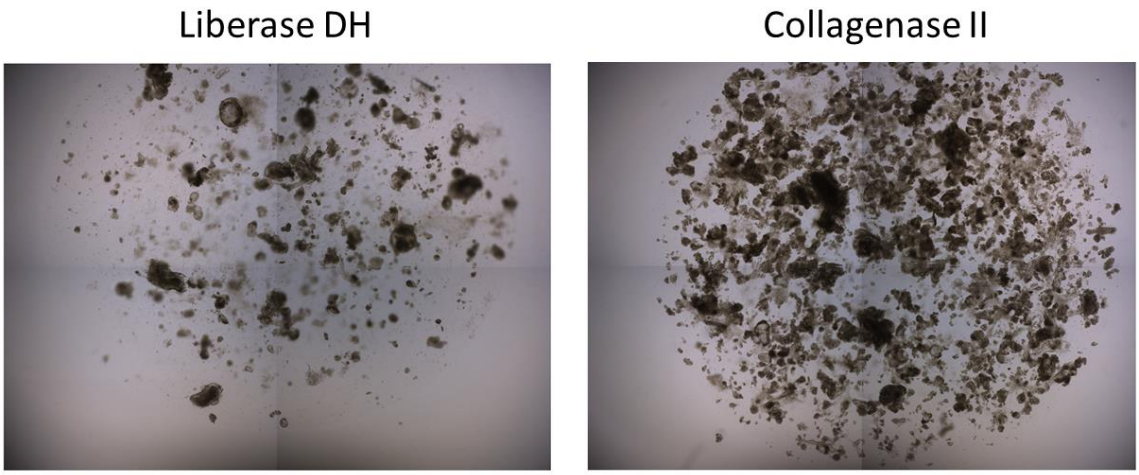

Figure 4.24: Spheroid outcome from digestion enzymes Liberase DH and Collagenase II*. Collagenase II gave more spheroids than Liberase DH, but also more single cells. Pictures are from sample CRC-16, first day of cultivation embedded in Geltrex. Figures are from four different fields of gel, joined to one figure.*

Geltrex, Matrigel and CellMatrix type I-A dissolved occasionally after addition of medium and incubation. This can be caused by several factors like seeding density of spheroids, gel composition, and manual fails. Both Matrigel and Geltrex gave good looking spheroids, and the gel was easy to work with. Cultrex gave very thin gels, and as a consequence the spheroids grew in 2D layer. Cellmatrix type I-A still solidified very easily. Average outcome of spheroid from gels is presented in figure 4.25.

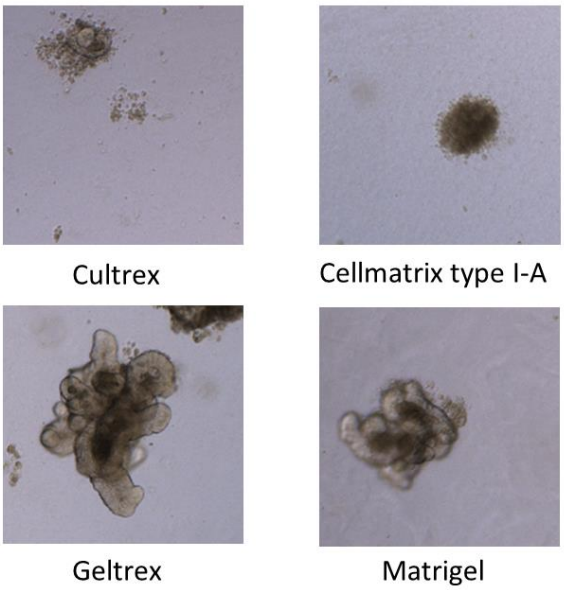

Figure 4.25: Spheroids from sample CRC-17 in four different gels, Cultrex, Cellmatrix type I-A, Geltrex and Matrigel after 19 days of incubation*. Cultrex and Cellmatrix type I-A gave low outcome of viable spheroids, often growing in 2D layer. Geltrex and Matrigel gave higher outcome of viable spheroid, with a stable 3D structure.*

For splitting procedure, was collagenase II used to split the spheroids. However, a considerable number of spheroids seemed to get lost, giving a low yield. Steps for filtering with 500 µm pluriStrainer were removed and the number of washing steps were reduced, giving a higher yield for spheroid outcome after splitting.

5 Discussion

The overall aim of this project was to discover and validate human target genes of EBV-miR-BART10-3p, gene expression changes and changes in migration and proliferative behavior of colon cancer cells in co-culture with *F. nucleatum,* in addition to establish a CRC patient derived spheroid model. Because of time and limited access to the lab in the at the end of the master period, several experiments have not been performed in biological triplicates. By this reason, we cannot conclude on the results from these experiments, however, we have evaluated the differences between technical replicates. This is also the case for full validation of the colorectal cancer tissue originated spheroid model, as the long-term survival of spheroids after thawing has not been evaluated.

Results shows that several genes were affected by co-culture with *F. nucleatum,* indicating that the cells gene expression is severely altered in the presence of remote bacteria. Several genes were also classified as downregulated by co-transfection of EBV-miR-BART10-3p, indicating that the miRNA have an effect on targeted human genes.

5.1 Co-culture of *F. nucleatum* and colorectal cancer cells

The fusobacteria take advantage of its several virulence factors to adhere to and invade epithelial cells. We have shown that *F. nucleatum* invades the CRC cell line DLD-1, increases the gene expression of pro-inflammatory cytokines *CXCL8* and *CSF2,* and cytokine secretion of CXCL8, both with increased concentration and incubation time of *F. nucleatum.* The persistent and increasing exposure to *F. nucleatum* leads to initiation of immune response, inflammatory processes and activation of several pathways leading to carcinogenesis.

Direct physical contact between microorganisms and surface of epithelial cells triggers the expression of a variety of immune response mediators from epithelial cells (126). The interaction of microorganisms with the intestinal epithelium initially involves recognition by Toll-like receptors (TLRs) (127), where the TLR-4 receptor is shown to be upregulated in CRC tissues. The fusobacterial lipopolysaccharide (LPS) engage TLR-4 and subsequently MYD88 in colon cancer cell lines, which have the key downstream effector NF-κB (23). Activation of NF-κB pathway, which is the main signaling pathway regulating inflammatory responses implicated in CRC tumorigenesis, facilitate tumor progressing through the

expression of pro-inflammatory chemokines like CXCL8 and CSF2 (127). The presence of *F. nucleatum* is also shown to initiate several other pathways in CRC, like the MAPK pathway and PI3K-AKT pathway (36, 128).

5.1.1 Cell migration and proliferation affected by *F. nucleatum*

F. nucleatum has been shown to promote cell migration and cell proliferation in CRC *in vitro* studies. Previously studies have showed significant differences in wound healing properties, contrary to our investigations, where the differences in wound healing between non-treated cells and cells co-cultured with *F. nucleatum* were marginal (figure 4.10). Significant wound healing and migration have been described in CRC cell line co-cultures with *F. nucleatum* at MOI 100 and 1000 (23, 129). We experienced that a MOI over 600 caused cell death and detachment from the well surface, making it unattainable to investigate wound healing, and a MOI of 300 was decided as the appropriate number of bacteria to be used.

Increased cell proliferation in co-culture with *F. nucleatum* (figure 4.11) have in this study been observed but is not fully investigated. The method chosen was too time consuming and laborious, so the experiment was chosen to not be performed in several biological replicates. More evidence has shown that *F. nucleatum* play a critical role in and promotes the proliferation of CRC (23, 98). Colorectal cancer cells invaded by *F. nucleatum* showed a distinct increase in IL-8, IL-6 and TNF-α mRNA levels, which are cytokines know to benefit the proliferation of tumor cells (21). Increased proliferation is also shown to be achieved by activating TLR-4 signaling to NF-κB by the LPS of *F. nucleatum* (23). Both CRC tumor cell migration and proliferation have been shown to be promoted by the upregulation of miR-21 (130).

5.1.2 Internalization of *F. nucleatum* in DLD-1 cells

We have proven that *F. nucleatum* invades the CRC cell line DLD-1 (figure 4.16 – 4.18) and can be found localized on both outside and inside of CRC cells, visualized by fluorescent staining and confocal microscopy.

The adhesion and invasion of *F. nucleatum* is shown to be dependent on the fusobacterial FadA-adhesin binding to E-cadherin on CRC cells (36). The binding FadA-E-cadherin alters the integrity of the cells, increasing permeabilization and invasion of *F. nucleatum* (131). The adherence to epithelial cells is important for colonization, and the invasion allows the bacteria to both evade the host immune surveillance and spread deeper into the tissue (126). The adhesion and invasion activates β-catenin signaling that leads to increased expression of *Wnt* genes, oncogenes, transcription factors, and inflammatory genes and promotes tumor cell proliferation (21, 36).

5.1.3 Upregulation of *CXCL8* and *CSF2* in bacteria infected cells

In this study, the gene expression of *CXCL8* and *CSF2*, and cytokine release of CXCL8, were shown to increase with both incubation time and increased concentration of *F. nucelatum* in co-culture with colorectal cancer cells. Direct physical contact between microorganisms and surface of epithelial cells triggers the expression of a variety of immune response mediators from the epithelial cells (126). The interaction of bacteria with the intestinal epithelium usually involves recognition by Toll-like receptors (TLRs) (127). Lipopolysaccharide (LPS), a gram-negative antigen, is shown to be involved in the progression of CRC and can cause significant systemic locational inflammation of colorectal tissue and systemic inflammation of the organism caused by cytokines (132). The expression and secretion of inflammatory cytokines is shown to play an important role in CRC development and progression (133).

The fusobacterial virulence factors, RadD and Fap2, contributes to the enrichment and abundance of *F. nucleatum* in CRC, by co-aggregation of bacteria and inhibition of tumor cell killing by immune cells. By this they generate a proinflammatory microenvironment contributing to colorectal carcinogenesis (41, 48, 53, 54). The fusobacterial lipopolysaccharide (LPS) is shown to engage TLR-4 and subsequently MYD88 in colon cancer cell lines, which have the key downstream effector NF-κB (23). NF-κB is the main signaling pathway regulating inflammatory responses implicated in CRC tumorigenesis, and activation of NF-κB facilitates tumor progression through the expression of pro-inflammatory chemokines like CXCL8 and CSF2 (127).

The gene expression of *CXCL8* and *CSF2* showed to increase with incubation time of *F. nucleatum* co-culture, aside from the drastic decrease in gene expression after 12 h of incubation, as shown in figure 4.12 and 4.13. The time-dependent effect on cytokine release is controlled by a degree of self-limiting release, decreasing the cytokine production to avoid an overreaction which can in worst case cause septic shock in the host. When the stimulation with *F. nucleatum* persists, the production of cytokines resumes, in addition to the cytokines autocrine effect on tumor cells, the cells create a greater upregulation of gene expression and release of cytokines in an attempt to stimulate immune cells to remove the unknown microbe. This explains the results for timeseries experiment of co-culture with *F. nucleatum.* The persistent secretion of CXCL8 protein in all timepoints is a delayed response to the increase in gene expression.

The release of pro-inflammatory mediators like IL-1, IL-6, IL-8, CSF2 and TNF-α from intestinal epithelial cell lines and macrophages has been shown to increase with increasing concentration of LPS (134-137). This correlates with the increase of *CXCL8* and *CSF2* we see after co-culture with increasing MOI of *F. nucleatum,* shown in figure 4.14 and 4.15. The persistence infection and increased number of bacteria gives higher expression and secretion of pro-inflammatory cytokines, in attempt to stimulate immune cells to remove the unknown microbe.

As discussed, the cytokines CSF2 and CXCL8 is released by epithelial cells as a response to unknown and potential harmful microbes, initiating events leading to acute inflammation. Figure 4.3 and 4.4 from The Protein Atlas show that the expression of *CSF2* and *CXCL8* in colon is very low for both genes and the expression is limited to a few cell types such as lung and some immune cells. The reason for the high expression in lung tissue is because of this organs role in protecting against external pathogens entering via the respiratory tract (138). CXCL8 and CSF2 enhances the respiratory defense against pathogens, stimulate pathogen killing and clearance of the alveoli by stimulating proliferation and activation of immune cells through extracellular signaling pathways (139-141).

The *CSF2* (colony stimulating factor-2, or granulocyte macrophage-colony stimulating factor) gene encodes a cytokine, functioning as a hematological cell growth factor that stimulates stem cells to produce immune cells like granulocytes and monocytes (142). The cytokine is

produced by a variety of cells, including epithelial cells and tumor cells, in response to inflammatory cytokines and innate immune activation (142, 143). In these cells, bacterial endotoxins, like LPS, and inflammatory cytokines, such as IL-1, IL-6 and TNF-α, are potent inducers of CSF2 (144). The regulation of gene expression is exerted at both transcriptional and post-transcriptional levels (144).

CSF2s role in tumor progression is contradictory, as it has been described to express both antitumor activity and stimulatory effects on tumor progression and migration (142, 143). CSF2 is also shown to have different roles in and be affected by the tumor microenvironment (145). CSF2 induces protective immunity by stimulating the recruitment, maturation, and functioning of dendritic cells, activating the immune system against specific antigens and exerting anti-tumor effects (145). Contrary, is CSF2 shown to play an important role in the polarization and activation of tumor-associated macrophages (TAMs), affecting the immune response and tumor microenvironment towards pro-tumorigenic environment (145). Most colorectal cancers exhibit a consistent production and secretion of CSF2, and highly increased CSF2 expression is found in more evolved cancers, indicating poor prognosis (142, 143, 145, 146). The increased levels of CSF2 may be a cause of demethylation of the *CSF2* gene in tumor tissue, promoting oncogene expression and chemotherapy resistance (145).

The expression of CSF2 is shown to be higher in CRC tumor tissue than in the adjacent normal tissue (142). CSF2 promotes growth and migration of tumor cells by enhancing the expression of Matrix metalloproteinases (MMPs), which induces keratinocyte growth and accelerates wound healing (143). CSF2 also promotes the motility of cancer cells, tumor growth and metastasis by activating MAPK/ERK signaling pathways, in response to intracellular and extracellular stimuli (142). The overexpression of CSF2 has been associated with STAT5 phosphorylation and STAT5 proteins play a pivotal part in the multistep process of tumorigenesis. CSF2 is also shown to activate the JAK2/STAT pathway and PI3K pathway (147).

CXCL8 (C-X-C motif chemokine ligand 8 or IL-8, interleukin 8) is a member of the C-X-C-chemokine family, and is a pro-inflammatory cytokine produced by neutrophils, macrophages, endothelial cells and cancer cells (148). CXCL8 is associated with tumor progression, angiogenesis, migration and metastasis (148). In addition to being associated with tumor size, tumor grading, depth of infiltration, liver metastasis and survival in CRC, high expression of CXCL8 correlates to poor CRC prognosis (149). The biological action of

CXCL8 is mediated through binding to its receptors CXCR1 and CXCR2, and can be regulated in an autocrine and paracrine matter (150).

The host inflammatory immune response contributes to the neoplastic progression of CRC through TLR2 and TLR4 activation of the pro-inflammatory cytokines IL-1B, IL-6 and IL-8 in a potentially miRNA-dependent process (127). The CXCL8/CXCR1/2 signaling plays a substantial role in the tumor microenvironment and is important for tumor progression and metastasis (151). CXCL8 and its receptors is known to induce the epithelial-mesenchymal transition (EMT) of CRC cells to help them escape from the hosts immunosurveillance and resist anokis (152). This promotes the formation of circulating tumor cells (CTCs) and the colonization of distant organs (152). Colorectal cancer and its liver metastasis are significantly associated with elevated CXCL8 signaling within the tumor environment (152).

CXCL8 activates multiple signaling pathways related to cancer progression, including PI3K/AKT, TP53 and Raf/MEK/ERK pathways (151). PI3K acts as a major downstream intracellular signal of CXCL8, where PI3K induces phosphorylation of its substrate, AKT, which plays a critical role in modulating cell survival, angiogenesis and migration (128). CXCL8 activates the MAPK pathway in cancer cells, classified as the classical Raf/MEK/ERK pathway, and is associated with modulation of invasion, cell survival and cell proliferation (128). The CXCL8-TP53 signaling pathway plays a role in promoting tumor progression and survival mechanisms of the CRC cells (152). TP53 is a mutated form of the known protein p53, originally a tumor suppressor protein (152). The activation of NF-κB also leads to increased expression of miR-21, a well-recognized miRNA in CRC associated with activation of the oncogenic cascade in CRC (23, 56).

5.2 Transfection of EBV-miR-BART10-3p

Epstein-Barr virus has been associated with several cancers and there have been shown a link between EBV infection and CRC (44, 46, 69, 80-83). The levels of EBV-miR-BART10-3p has been shown to be significantly upregulated in CRC tumor samples, but its role in CRC is mostly unknown (44). The miRNA has been found to directly target and regulate genes in nasopharyngeal cancer (NPC) and EBV-associated-gastric cancer (EBVaGC) (86, 153). By targeting the *BTRC* gene in NPC cells and *DDK* in EBVaCG, EBV-miR-BART10-3p promoted cell proliferation, invasion and migration capabilities of the cancer cells by

downstream expression of β-catenin and Snail and directly downregulating the *DKK* mRNA (85, 86, 153). The overexpression of EBV-miR-BART10-3p in CRC tissue can then indicate that upregulation of the miRNA could have a significantly impact on genes and cellular processes, which can lead to tumor development and progression (44).

Epstein-Barr virus infects and enter B lymphocytes in its initial infection and is found in its latent stage in naïve B-cells, activated B lymphocytes and dividing B cells (68, 69, 72, 75, 154). In an immune response reaction, EBV can accompany immune cells migrating to a place of infection or inflammation, and subsequently maneuver from the B cells to for example cells in the intestine or cancer cells (155). In its new site of infection, EBV can exert it latent genes, like EBV-miR-BARTs, and target genes for up- or downregulation, promoting oncogenic properties.

We have showed that the gene expression levels of *SAP18* and *CCND1* is significantly downregulated by EBV-miR-BART10-3p, figure 4.19 and 4.21. The EBV-miR-BART10-3p binds to the 3'UTR of the target genes *SAP18* and *CCND1,* suppressing the mRNA expression by inhibiting their translation or causing degradation of their transcript.

The gene *SAP18* encodes the Sin3A associated protein of 18 kDa and was first demonstrated to be a component of the Sin3 histone deacetylase (Sin3-HDAC) complex, which is found to be involved in deacetylation of histones and transcriptional repression (156-159). SAP18 exhibits a conserved ubiquitin-like β-grasp fold, a protein motif involved in protein-protein interactions and in the assembly of multiprotein complexes (156, 158, 160). The fold in SAP18 is also required for efficient splicing regulatory activity, as SAP18 together with RNPS1 and Acinus forms the apoptosis and splicing-associated protein (ASAP) complex (160). The ASAP complex is involved in the regulation of both RNA splicing and apoptosis (156, 160). In transcription, is RNPS1 involved in the prevention of R-loop formation, while Acinus and SAP18 suppresses the transcription with help from histone deacetylase (161). The downregulation of *SAP18* gene expression can then lead to suppression of the formation of the ASAP complex and increase the transcription of genes originally set for downregulation, which can cause oncogenic properties.

SAP18 is found to be highly expressed in immune cells, as shown in figure 4.7, mainly because of its role in the histone deacetylase complex (HDAC). HDACs are involved in the

epigenetic regulation of innate immune responses through TLRs and interferon (IFN) signaling (162). HDAC can affect the immune response from a cell in a positive and negative regulatory manner, both inducing and suppressing the production of inflammatory mediators and antiviral responses by histone modification (163). HDACs regulates genes via epigenetic regulation through chromatin DNA and histone modification by methylation and acetylation, among other mechanisms, which control innate immune cell expression (162). Deregulation of *SAP18* can cause silencing of the HDAC complex, suppressing the regulation of genes, in addition to repressing the immune response, the downregulation of SAP18 can allow for uncontrolled growth of cancer cells or virus.

The SAP18/ERK/STAT3 signaling regulates hematopoietic cell differentiation in the tumor microenvironment (157). Reduced SAP18 expression during tumor conditions, subsequently activates the ERK/STAT3 signaling pathway which promotes the differentiation of hematopoietic stem and progenitor cells (HSPCs) into monocytic myeloid-derived suppressor cells (mo-MDSCs), causing an accumulation of mo-MDSCs (157). Degradation or downregulation of SAP18 is also shown to result in activation of NF-κB pathway, promoting endothelial cell migration, invasion and angiogenesis (156).

Cyclin D1, encoded by *CCND1*, is a member of cell-cycle-associated nuclear proteins and induces G1 to S-phase cell cycle transition by binding cyclin dependent kinase 4 and 6 (CDK4/6) to phosphorylate and inactivate the RB protein (164, 165). *CCND1* is known as an oncogene, as it promotes cell proliferation and plays a major role in oncogenesis (164). The *CCND1* gene is disrupted in cancer cell genome usually by the process of gene amplification or chromosome translocation which may lead to cancer development (165). The overexpression of cyclin D1 has been shown in many tumors, i.e. endometrial, thyroid, urothelial bladder, breast, brain gliomas, esophageal and colorectal cancer (165, 166).

Literature report that *CCND1* is frequently upregulated in CRC and other malignancies, contrary in our study where EBV-miR-BART10-3p showed to downregulate *CCND1*. Several other miRNAs are shown to downregulate Cyclin D1 in CRC, and other cancers or tissues. MiR-446 is shown to significantly decrease the Cyclin D1 expression, implying that the overexpression of miR-446 could prevent the G1-S transition, leading to accumulation of cells in G0/G1 phase and attenuation of cell proliferating in CRC (167). MiR-9 downregulates the

expression of Cyclin D1 via directly targeting 3'UTR of Cyclin D1, inhibiting the proliferation, invasion, and metastasis of gastric cancer cell *in vitro* and *in vivo* (164). MiR-15b directly downregulates *CCND1* expression by targeting the 3'UTR of Cyclin D1 in glioma specimens and cell lines (168), and miR-365 inhibits cell cycle progression and promotes apoptosis of colon cancer cells by targeting Cyclin D1 (166). The miRNAs indicated show tumor suppressing effects partially through downregulation of C*CND1* (167). Since EBV-miR-BART10-3p also significantly decreases the *CCND1* expression, it indicates that it acts in the same manner as miR-446, miR-9, miR-15b and miR-365, hence as a tumor suppressing miRNA.

5.3 Colorectal cancer tissue-originated spheroids

The colorectal tissue-originated spheroids (CTOSs) method development showed many flaws, like difficulties with digestion of tumor tissue, gel solidifying, instability and dissolving and laborious splitting procedure.

Method improvements that have been carried out, consists of mainly digestive enzyme and seeding gels for the spheroids. The digestive enzymes main role is to dissociate the minced tumor pieces into smaller cell clumps, but to maintain the cell-to-cell contact, which is the main hypothesis in Kondo et al. (92) procedure for successful CTOSs preparation. The Liberase DH digestive enzymes consists of a mix of highly purified Collagenase I and II and the neutral protease Dispase® (169). The enzyme blend is meant to increase the quality of tissue dissociation and improve the viability and functionality of isolated cells, where the collagenase enzymes digest the intracellular matrix and the neutral protease act synergistically with the collagenases (169). Collagenase I and collagenase II, also incorporated in Liberase DH, are proteases that cleave the bond between a neutral amino acid (X) and glycine in the sequence Pro-X-Glyc-Pro, which is found with high frequency in collagen (170). The pure collagenase II gave a higher yield of spheroids, than the enzyme blend Liberase DH, indicating that the tumor tissue was better dissociated with the use of pure collagenase than an enzyme blend. The survival of spheroids dissociated with collagenase II was a bit lower than for those dissociated with Liberase DH, in addition to giving more single cells after digestion. Since the two collagenases work in the same way, it might be the protease that cleaves

fibronectin, collagen IV and to a lesser extent collagen I, in addition to other properties that makes it less effective in digesting and dissociating colorectal cancer tumors (171).

The Cellmatrix Type I-A, recommended by Kondo et al. (92), gave multiple complications in way of solidifying too rapidly, instability and dissolving when adding medium to the gel. Several improvements, like smaller gel drop, smaller volume of spheroids added to gel and adding spheroids to gel solution before seeding into plate were performed. A combination of these improvements gave more stable gels and a greater outcome of spheroids with use of the Cellmatrix Type I-A.

In addition to sorting out the right combination of volume of spheroids, gel, and medium for the CellMatrix Type I-A gel, were three other gels, Geltrex, Cultrex and Matrigel, included in the optimization phase protocol for preparation and culturing of CTOSs. The main purpose of the gels is to function as an extracellular matrix, which create a supportive environment for the spheroids in terms of stability and growth. The alternative gels only require resuspension with medium before seeding, while Cellmatrix type I-A also requires reconstitution buffer in addition to medium.

Many factors affect gel stability and spheroid survival and growth, like gel and medium composition, method for addition of spheroids, and spheroids condition before addition to the gel. Three of the gels, Geltrex, Matrigel and Cellmatrix type I-A, occasionally dissociated when serum-free stem cell medium was added and incubation for some time. Matrigel and Geltrex gave good looking spheroids, and the gels were easy to work with. Matrigel is one of the most commonly used gels in 3D culturing and show a high rate for giving viable spheroids, while Geltrex is not much investigated. Cultrex gave very thin gels and consequently the spheroids grew in 2D, giving a very low yield of successful spheroids. Cellmatrix type I-A still solidified very easily, giving the same challenges as indicated in the initial phase of methods development. The medium and gel composition can be further optimized, same can method for addition of spheroids and amount of spheroid added to the gels. The gels Cultrex and Matrigel gave the highest yield of viable spheroids with intestinal structure, as shown in figure 4.25.

The splitting procedure was changed from manual splitting of the spheroids with needles, to using Collagenase II to dissociate the spheroids, giving a less labor intense procedure, and making it easier to split more spheroids in shorter time. This gave more single cells in general,

but the viability of spheroids seemed to be good after splitting. However, a considerable number of spheroids got lost during the new splitting procedure, and therefore were the filter step with 500 µm pluriStrainer and several washing steps removed. This gave a higher yield and spheroids bigger than 500 µm in size but did not change the viability.

The freezing procedure was based on methods used for stem cell organoids, with addition of fetal calf serum (FCS) to provide for nutrients at thawing, and the cryoprotectant DMSO for preventing crystals in the medium at freezing. The cryovials were frozen in an isopropanol freezing box, which allows for a cooling of 1 °C per min. Overall, gave the freezing and thawing procedures viable spheroids as shown in table 4.3. Some spheroids require some time to grow in size, but the viability appear to be good. This indicates that the spheroids endure the process of being frozen and thawed, which provides promising opportunities for further experiments.

Overall, did the digestive enzyme collagenase II and centrifugation of spheroids give a greater outcome of spheroids before seeding into gels, which is good for experiments needing large quantities of spheroids. The different gels gave different yield of spheroids after cultivation, with Matrigel and Geltrex giving the highest yield of viable spheroids. Matrigel and Geltrex have been chosen to be used for further establishment and reseeding of CTOSs. Splitting procedure, with the use of Collagenase II for dissociation of spheroids give a less laborious and faster method of splitting spheroids. Freezing and thawing procedures give viable spheroids, indicating that the spheroid samples manage the stress of freezing and thawing, and the cell-cell contact was kept through the process and give viable spheroids.

As the definition of an established CTOSs culture is set to that the spheroids manage to be split, frozen and thawed, have in total six CTOSs cultures been established in this project.

6 Conclusion

F. nucleatum, E. coli and EBV-miR-BART10-3p affect several genes in colorectal cancer cell lines.

F. nucleatum were shown to internalize in CRC cells, as well as upregulate the genes *CXCL8* and *CSF2* which have a central role in the immune response and the initiation and progression of CRC. Further investigations would be to find out where in the CRC cell *F. nucleatum* localizes and which proteins it interacts with to promote carcinogenic effects, as well as validate more genes associated with *F. nucleatum* co-culture to identify *F. nucleatum's* role in CRC.

EBV-miR-BART10-3p were shown to downregulate the target genes *SAP18* and *CCND1*. *SAP18* can have cancer associated effects when downregulated. *CCND1* is shown to have tumor suppressing effects when downregulated and is considered an oncogene when upregulated. This shows that the EBV-miR-BART10-3p acts in a cancer suppressing manner, when targeting the *CCND1* 3'UTR.

The cancer tissue-originated spheroids (CTOSs) method is considered established, as the spheroids manage the process of being split, frozen and thawed. Further experiments are needed to conclude for digestion enzyme and seeding gel, but the method gives a high yield of spheroids outcome. The CTOSs will be further used in experiments screening for therapeutic agents, and experiments conducting the interaction with intestinal microbiota can be carried out.

7 References

1. Bray F, Ferlay J, Soerjomataram I, Siegel RL, Torre LA, Jemal A. Global cancer statistics 2018: GLOBOCAN estimates of incidence and mortality worldwide for 36 cancers in 185 countries. CA Cancer J Clin. 2018;68(6):394-424.

2. Arnold M, Sierra MS, Laversanne M, Soerjomataram I, Jemal A, Bray F. Global patterns and trends in colorectal cancer incidence and mortality. Gut. 2017;66(4):683-91.

3. Migliore L, Migheli F, Spisni R, Coppedè F. Genetics, cytogenetics, and epigenetics of colorectal cancer. J Biomed Biotechnol. 2011;2011:792362-.

4. Gustavsson B, Carlsson G, Machover D, Petrelli N, Roth A, Schmoll HJ, et al. A review of the evolution of systemic chemotherapy in the management of colorectal cancer. Clin Colorectal Cancer. 2015;14(1):1-10.

5. Fearon ER, Vogelstein B. A genetic model for colorectal tumorigenesis. Cell. 1990;61(5):759-67.

6. Simon K. Colorectal cancer development and advances in screening. Clin Interv Aging. 2016;11:967-76.

7. Vogelstein B, Fearon ER, Hamilton SR, Kern SE, Preisinger AC, Leppert M, et al. Genetic alterations during colorectal-tumor development. The New England journal of medicine. 1988;319(9):525-32.

8. Helsedirektoratet. Nasjonalt handlingsprogram med retningslinjer for diagnostikk, behandling og oppfølging av kreft i tykktarm og endetarm 2019 [cited 2020 Mar 24]. Available from: https://www.helsebiblioteket.no/retningslinjer/kreft-i-tykktarm-og-endetarm/innhold.

9. Kuipers EJ, Grady WM, Lieberman D, Seufferlein T, Sung JJ, Boelens PG, et al. Colorectal cancer. Nat Rev Dis Primers. 2015;1:15065-.

10. Compton CC, Greene FL. The staging of colorectal cancer: 2004 and beyond. CA Cancer J Clin. 2004;54(6):295-308.

11. Kreftregisteret. Nasjonalt kvalitetsregister for tykk- og endetarmskreft, Årsrapport 2018 [cited 2020 April 04].

12. Compton CC. Colorectal carcinoma: diagnostic, prognostic, and molecular features. Mod Pathol. 2003;16(4):376-88.

13. Siegel RL, Miller KD, Jemal A. Cancer statistics, 2019. CA Cancer J Clin. 2019;69(1):7-34.

14. Siegel RL, Miller KD, Goding Sauer A, Fedewa SA, Butterly LF, Anderson JC, et al. Colorectal cancer statistics, 2020. CA Cancer J Clin. 2020.

15. Ladabaum U, Dominitz JA, Kahi C, Schoen RE. Strategies for Colorectal Cancer Screening. Gastroenterology. 2020;158(2):418-32.

16. Schreuders EH, Ruco A, Rabeneck L, Schoen RE, Sung JJ, Young GP, et al. Colorectal cancer screening: a global overview of existing programmes. Gut. 2015;64(10):1637-49.

17. Tunsjo HS, Gundersen G, Rangnes F, Noone JC, Endres A, Bemanian V. Detection of Fusobacterium nucleatum in stool and colonic tissues from Norwegian colorectal cancer patients. Eur J Clin Microbiol Infect Dis. 2019;38(7):1367-76.

18. Sears CL. The who, where and how of fusobacteria and colon cancer. eLife. 2018;7.

19. Keku TO, McCoy AN, Azcarate-Peril AM. Fusobacterium spp. and colorectal cancer: cause or consequence? Trends Microbiol. 2013;21(10):506-8.

20. Kostic AD, Chun E, Robertson L, Glickman JN, Gallini CA, Michaud M, et al. Fusobacterium nucleatum potentiates intestinal tumorigenesis and modulates the tumor-immune microenvironment. Cell Host Microbe. 2013;14(2):207-15.

21. Rubinstein MR, Wang X, Liu W, Hao Y, Cai G, Han YW. Fusobacterium nucleatum promotes colorectal carcinogenesis by modulating E-cadherin/beta-catenin signaling via its FadA adhesin. Cell Host Microbe. 2013;14(2):195-206.

22. Louis P, Hold GL, Flint HJ. The gut microbiota, bacterial metabolites and colorectal cancer. Nature reviews Microbiology. 2014;12(10):661-72.

23. Yang Y, Weng W, Peng J, Hong L, Yang L, Toiyama Y, et al. Fusobacterium nucleatum Increases Proliferation of Colorectal Cancer Cells and Tumor Development in Mice by Activating Toll-Like Receptor 4 Signaling to Nuclear Factor-kappaB, and Up-regulating Expression of MicroRNA-21. Gastroenterology. 2017;152(4):851-66.e24.

24. Castellarin M, Warren RL, Freeman JD, Dreolini L, Krzywinski M, Strauss J, et al. Fusobacterium nucleatum infection is prevalent in human colorectal carcinoma. Genome research. 2012;22(2):299-306.

25. Wu J, Li Q, Fu X. Fusobacterium nucleatum Contributes to the Carcinogenesis of Colorectal Cancer by Inducing Inflammation and Suppressing Host Immunity. Transl Oncol. 2019;12(6):846-51.

26. Tsao S-W, Tsang CM, To K-F, Lo K-W. The role of Epstein-Barr virus in epithelial malignancies. The Journal of pathology. 2015;235(2):323-33.

27. Albanese M, Tagawa T, Bouvet M, Maliqi L, Lutter D, Hoser J, et al. Epstein-Barr virus microRNAs reduce immune surveillance by virus-specific CD8+ T cells. Proceedings of the National Academy of Sciences of the United States of America. 2016;113(42):E6467-E75.

28. Tagawa T, Albanese M, Bouvet M, Moosmann A, Mautner J, Heissmeyer V, et al. Epstein-Barr viral miRNAs inhibit antiviral CD4+ T cell responses targeting IL-12 and peptide processing. J Exp Med. 2016;213(10):2065-80.

29. Qiu J, Smith P, Leahy L, Thorley-Lawson DA. The Epstein-Barr virus encoded BART miRNAs potentiate tumor growth in vivo. PLoS Pathog. 2015;11(1):e1004561-e.

30. Vereide DT, Seto E, Chiu YF, Hayes M, Tagawa T, Grundhoff A, et al. Epstein-Barr virus maintains lymphomas via its miRNAs. Oncogene. 2014;33(10):1258-64.

31. Hannigan GD, Duhaime MB, Ruffin MTt, Koumpouras CC, Schloss PD. Diagnostic Potential and Interactive Dynamics of the Colorectal Cancer Virome. mBio. 2018;9(6):e02248-18.

32. Vojtechova Z, Tachezy R. The Role of miRNAs in Virus-Mediated Oncogenesis. International journal of molecular sciences. 2018;19(4):1217.

33. Gallo A, Miceli V, Bulati M, Iannolo G, Contino F, Conaldi PG. Viral miRNAs as Active Players and Participants in Tumorigenesis. Cancers (Basel). 2020;12(2):358.

34. Arthur JC, Gharaibeh RZ, Muhlbauer M, Perez-Chanona E, Uronis JM, McCafferty J, et al. Microbial genomic analysis reveals the essential role of inflammation in bacteria-induced colorectal cancer. Nat Commun. 2014;5:4724.

35. Saus E, Iraola-Guzmán S, Willis JR, Brunet-Vega A, Gabaldón T. Microbiome and colorectal cancer: Roles in carcinogenesis and clinical potential. Mol Aspects Med. 2019;69:93-106.

36. Shang FM, Liu HL. Fusobacterium nucleatum and colorectal cancer: A review. World journal of gastrointestinal oncology. 2018;10(3):71-81.

37. Zhang X, Zhu X, Cao Y, Fang J-Y, Hong J, Chen H. Fecal Fusobacterium nucleatum for the diagnosis of colorectal tumor: A systematic review and meta-analysis. Cancer Med. 2019;8(2):480-91.

38. Lamont RJ, Hajishengallis G. Polymicrobial synergy and dysbiosis in inflammatory disease. Trends Mol Med. 2015;21(3):172-83.

39. Maloy KJ, Powrie F. Intestinal homeostasis and its breakdown in inflammatory bowel disease. Nature. 2011;474(7351):298-306.

40. Tomkovich S, Dejea CM, Winglee K, Drewes JL, Chung L, Housseau F, et al. Human colon mucosal biofilms from healthy or colon cancer hosts are carcinogenic. The Journal of clinical investigation. 2019;130(4):1699-712.

41. Kaplan CW, Lux R, Haake SK, Shi W. The Fusobacterium nucleatum outer membrane protein RadD is an arginine-inhibitable adhesin required for inter-species adherence and the structured architecture of multispecies biofilm. Mol Microbiol. 2009;71(1):35-47.

42. Baxter NT, Zackular JP, Chen GY, Schloss PD. Structure of the gut microbiome following colonization with human feces determines colonic tumor burden. Microbiome. 2014;2:20.

43. Wong SH, Zhao L, Zhang X, Nakatsu G, Han J, Xu W, et al. Gavage of Fecal Samples From Patients With Colorectal Cancer Promotes Intestinal Carcinogenesis in Germ-Free and Conventional Mice. Gastroenterology. 2017;153(6):1621-33.e6.

44. Mjelle R, Sjursen W, Thommesen L, Sætrom P, Hofsli E. Small RNA expression from viruses, bacteria and human miRNAs in colon cancer tissue and its association with microsatellite instability and tumor location. BMC Cancer. 2019;19(1):161.

45. Yang Y-C, Liem A, Lambert PF, Sugden B. Dissecting the regulation of EBV's BART miRNAs in carcinomas. Virology. 2017;505:148-54.

46. Tafvizi F, Fard ZT, Assareh R. Epstein-Barr virus DNA in colorectal carcinoma in Iranian patients. Pol J Pathol. 2015;66(2):154-60.

47. Flanagan L, Schmid J, Ebert M, Soucek P, Kunicka T, Liska V, et al. Fusobacterium nucleatum associates with stages of colorectal neoplasia development, colorectal cancer and disease outcome. Eur J Clin Microbiol Infect Dis. 2014;33(8):1381-90.

48. Brennan CA, Garrett WS. Fusobacterium nucleatum - symbiont, opportunist and oncobacterium. Nature reviews Microbiology. 2019;17(3):156-66.

49. Rubinstein MR, Baik JE, Lagana SM, Han RP, Raab WJ, Sahoo D, et al. Fusobacterium nucleatum promotes colorectal cancer by inducing Wnt/beta-catenin modulator Annexin A1. EMBO Rep. 2019;20(4).

50. Kostic AD, Gevers D, Pedamallu CS, Michaud M, Duke F, Earl AM, et al. Genomic analysis identifies association of Fusobacterium with colorectal carcinoma. Genome research. 2012;22(2):292-8.

51. Mima K, Nishihara R, Qian ZR, Cao Y, Sukawa Y, Nowak JA, et al. Fusobacterium nucleatum in colorectal carcinoma tissue and patient prognosis. Gut. 2016;65(12):1973-80.

52. Yu T, Guo F, Yu Y, Sun T, Ma D, Han J, et al. Fusobacterium nucleatum Promotes Chemoresistance to Colorectal Cancer by Modulating Autophagy. Cell. 2017;170(3):548-63.e16.

53. Abed J, Emgard JE, Zamir G, Faroja M, Almogy G, Grenov A, et al. Fap2 Mediates Fusobacterium nucleatum Colorectal Adenocarcinoma Enrichment by Binding to Tumor-Expressed Gal-GalNAc. Cell Host Microbe. 2016;20(2):215-25.

54. Gur C, Ibrahim Y, Isaacson B, Yamin R, Abed J, Gamliel M, et al. Binding of the Fap2 protein of Fusobacterium nucleatum to human inhibitory receptor TIGIT protects tumors from immune cell attack. Immunity. 2015;42(2):344-55.

55. Témoin S, Wu KL, Wu V, Shoham M, Han YW. Signal peptide of FadA adhesin from Fusobacterium nucleatum plays a novel structural role by modulating the filament's length and width. FEBS Lett. 2012;586(1):1-6.

56. Holt RA, Cochrane K. Tumor Potentiating Mechanisms of Fusobacterium nucleatum, A Multifaceted Microbe. Gastroenterology. 2017;152(4):694-6.

57. Gottwein E, Cullen BR. Viral and cellular microRNAs as determinants of viral pathogenesis and immunity. Cell host & microbe. 2008;3(6):375-87.

58. Bartel DP. MicroRNAs: genomics, biogenesis, mechanism, and function. Cell. 2004;116(2):281-97.

59. Zhu Y, Haecker I, Yang Y, Gao S-J, Renne R. γ-Herpesvirus-encoded miRNAs and their roles in viral biology and pathogenesis. Current opinion in virology. 2013;3(3):266-75.

60. Yang H-J, Huang T-J, Yang C-F, Peng L-X, Liu R-Y, Yang G-D, et al. Comprehensive profiling of Epstein-Barr virus-encoded miRNA species associated with specific latency types in tumor cells. Virol J. 2013;10:314-.

61. Bartel DP. Metazoan MicroRNAs. Cell. 2018;173(1):20-51.

62. Lee RC, Feinbaum RL, Ambros V. The C. elegans heterochronic gene lin-4 encodes small RNAs with antisense complementarity to lin-14. Cell. 1993;75(5):843-54.

63. Reinhart BJ, Slack FJ, Basson M, Pasquinelli AE, Bettinger JC, Rougvie AE, et al. The 21-nucleotide let-7 RNA regulates developmental timing in Caenorhabditis elegans. Nature. 2000;403(6772):901-6.

64. Kang D, Skalsky RL, Cullen BR. EBV BART MicroRNAs Target Multiple Pro-apoptotic Cellular Genes to Promote Epithelial Cell Survival. PLoS Pathog. 2015;11(6):e1004979-e.

65. Grundhoff A, Sullivan CS. Virus-encoded microRNAs. Virology. 2011;411(2):325-43.

66. Cullen BR. Transcription and processing of human microRNA precursors. Mol Cell. 2004;16(6):861-5.

67. Bartel DP. MicroRNAs: target recognition and regulatory functions. Cell. 2009;136(2):215-33.

68. Thompson MP, Kurzrock R. Epstein-Barr virus and cancer. Clin Cancer Res. 2004;10(3):803-21.

69. Mui UN, Haley CT, Tyring SK. Viral Oncology: Molecular Biology and Pathogenesis. J Clin Med. 2017;6(12):111.

70. Flint J. Principles of virology. 4th ed. ed. Washington D.C: ASM Press; 2015.

71. Petrara MR, Giunco S, Serraino D, Dolcetti R, De Rossi A. Post-transplant lymphoproliferative disorders: from epidemiology to pathogenesis-driven treatment. Cancer Lett. 2015;369(1):37-44.

72. Young LS, Rickinson AB. Epstein-Barr virus: 40 years on. Nature reviews Cancer. 2004;4(10):757-68.

73. Jacome AA, Lima EM, Kazzi AI, Chaves GF, Mendonca DC, Maciel MM, et al. Epstein-Barr virus-positive gastric cancer: a distinct molecular subtype of the disease? Rev Soc Bras Med Trop. 2016;49(2):150-7.

74. Shannon-Lowe CD, Neuhierl B, Baldwin G, Rickinson AB, Delecluse HJ. Resting B cells as a transfer vehicle for Epstein-Barr virus infection of epithelial cells. Proceedings of the National Academy of Sciences of the United States of America. 2006;103(18):7065-70.

75. Hooykaas MJG, Kruse E, Wiertz EJHJ, Lebbink RJ. Comprehensive profiling of functional Epstein-Barr virus miRNA expression in human cell lines. BMC genomics. 2016;17:644-.

76. Wang M, Yu F, Wu W, Wang Y, Ding H, Qian L. Epstein-Barr virus-encoded microRNAs as regulators in host immune responses. International journal of biological sciences. 2018;14(5):565-76.

77. Shinozaki-Ushiku A, Kunita A, Isogai M, Hibiya T, Ushiku T, Takada K, et al. Profiling of Virus-Encoded MicroRNAs in Epstein-Barr Virus-Associated Gastric Carcinoma and Their Roles in Gastric Carcinogenesis. Journal of virology. 2015;89(10):5581-91.

78. Kanda T. EBV-Encoded Latent Genes. In: Kawaguchi Y, Mori Y, Kimura H, editors. Human Herpesviruses. Singapore: Springer Singapore; 2018. p. 377-94.

79. Epstein MA, Achong BG, Barr YM. VIRUS PARTICLES IN CULTURED LYMPHOBLASTS FROM BURKITT'S LYMPHOMA. Lancet. 1964;1(7335):702-3.

80. Tsurumi T, Fujita M, Kudoh A. Latent and lytic Epstein-Barr virus replication strategies. Rev Med Virol. 2005;15(1):3-15.

81. Mehrabani-Khasraghi S, Ameli M, Khalily F. Demonstration of Herpes Simplex Virus, Cytomegalovirus, and Epstein-Barr Virus in Colorectal Cancer. Iran Biomed J. 2016;20(5):302-6.

82. Al-Antary N, Farghaly H, Aboulkassim T, Yasmeen A, Akil N, Al Moustafa A-E. Epstein-Barr virus and its association with Fascin expression in colorectal cancers in the Syrian population: A tissue microarray study. Human vaccines & immunotherapeutics. 2017;13(7):1573-8.

83. Bedri S, Sultan AA, Alkhalaf M, Al Moustafa AE, Vranic S. Epstein-Barr virus (EBV) status in colorectal cancer: a mini review. Hum Vaccin Immunother. 2019;15(3):603-10.

84. Marquitz AR, Raab-Traub N. The role of miRNAs and EBV BARTs in NPC. Semin Cancer Biol. 2012;22(2):166-72.

85. Min K, Lee SK. EBV miR-BART10-3p Promotes Cell Proliferation and Migration by Targeting DKK1. Int J Biol Sci. 2019;15(3):657-67.

86. Yan Q, Zeng Z, Gong Z, Zhang W, Li X, He B, et al. EBV-miR-BART10-3p facilitates epithelial-mesenchymal transition and promotes metastasis of nasopharyngeal carcinoma by targeting BTRC. Oncotarget. 2015;6(39):41766-82.

87. Wang M, Gu B, Chen X, Wang Y, Li P, Wang K. The Function and Therapeutic Potential of Epstein-Barr Virus-Encoded MicroRNAs in Cancer. Mol Ther Nucleic Acids. 2019;17:657-68.

88. Iizasa H, Kim H, Kartika AV, Kanehiro Y, Yoshiyama H. Role of Viral and Host microRNAs in Immune Regulation of Epstein-Barr Virus-Associated Diseases. Front Immunol. 2020;11:367-.

89. Ishiguro T, Ohata H, Sato A, Yamawaki K, Enomoto T, Okamoto K. Tumor-derived spheroids: Relevance to cancer stem cells and clinical applications. Cancer science. 2017;108(3):283-9.

90. Jeppesen M, Hagel G, Glenthoj A, Vainer B, Ibsen P, Harling H, et al. Short-term spheroid culture of primary colorectal cancer cells as an in vitro model for personalizing cancer medicine. PloS one. 2017;12(9):e0183074.

91. Árnadóttir SS, Jeppesen M, Lamy P, Bramsen JB, Nordentoft I, Knudsen M, et al. Characterization of genetic intratumor heterogeneity in colorectal cancer and matching patient-derived spheroid cultures. Mol Oncol. 2018;12(1):132-47.

92. Kondo J, Endo H, Okuyama H, Ishikawa O, Iishi H, Tsujii M, et al. Retaining cell-cell contact enables preparation and culture of spheroids composed of pure primary cancer cells from colorectal cancer. Proc Natl Acad Sci U S A. 2011;108(15):6235-40.

93. Hirschhaeuser F, Menne H, Dittfeld C, West J, Mueller-Klieser W, Kunz-Schughart LA. Multicellular tumor spheroids: an underestimated tool is catching up again. J Biotechnol. 2010;148(1):3-15.

94. Schütte M, Risch T, Abdavi-Azar N, Boehnke K, Schumacher D, Keil M, et al. Molecular dissection of colorectal cancer in pre-clinical models identifies biomarkers predicting sensitivity to EGFR inhibitors. Nature communications. 2017;8:14262-.

95. Mitra A, Mishra L, Li S. Technologies for deriving primary tumor cells for use in personalized cancer therapy. Trends Biotechnol. 2013;31(6):347-54.

96. Kondo J, Inoue M. Application of Cancer Organoid Model for Drug Screening and Personalized Therapy. Cells. 2019;8(5).

97. Young M, Reed KR. Organoids as a Model for Colorectal Cancer. Curr Colorectal Cancer Rep. 2016;12(5):281-7.

98. Kasper SH, Morell-Perez C, Wyche TP, Sana TR, Lieberman LA, Hett EC. Colorectal cancer-associated anaerobic bacteria proliferate in tumor spheroids and alter the microenvironment. Scientific reports. 2020;10(1):5321-.

99. Brennan CA, Garrett WS. Gut Microbiota, Inflammation, and Colorectal Cancer. Annu Rev Microbiol. 2016;70:395-411.

100. Min S, Kim S, Cho S-W. Gastrointestinal tract modeling using organoids engineered with cellular and microbiota niches. Exp Mol Med. 2020;52(2):227-37.

101. Williamson IA, Arnold JW, Samsa LA, Gaynor L, DiSalvo M, Cocchiaro JL, et al. A High-Throughput Organoid Microinjection Platform to Study Gastrointestinal Microbiota and Luminal Physiology. Cell Mol Gastroenterol Hepatol. 2018;6(3):301-19.

102. Gilmore AP. Anoikis. Cell Death Differ. 2005;12 Suppl 2:1473-7.

103. mirVana™ miRNA Mimic, Negative Control #1: Thermo Fischer Scientific; 2020 [cited 2020 Apr 10]. Available from: https://www.thermofisher.com/order/catalog/product/4464058#/4464058.

104. Schneider CA, Rasband WS, Eliceiri KW. NIH Image to ImageJ: 25 years of image analysis. Nature Methods. 2012;9(7):671-5.

105. 25 Culture-Inserts 2 Well for self-insertion: Ibidi; 2020 [cited 2020 Apr 30]. Available from: https://ibidi.com/culture-inserts/25-25-culture-inserts-2-well-for-self-insertion.html.

106. µ-Slide 8 Well Grid-500: Ibidi; 2020 [cited 2020 May 15]. Available from: https://ibidi.com/gridded-dishes-slides/39--slide-8-well-grid-500.html.

107. Nagy A, Vitásková E, Černíková L, Křivda V, Jiřincová H, Sedlák K, et al. Evaluation of TaqMan qPCR System Integrating Two Identically Labelled Hydrolysis Probes in Single Assay. Scientific Reports. 2017;7(1):41392.

108. Applied Biosystems StepOne™ and StepOnePlus™ Real-Time PCR Systems Reagent Guide: Applied Biosystems 2010 [cited 2020 Mar 19]. Available from: http://tools.thermofisher.com/content/sfs/manuals/cms_046739.pdf.

109. siCHECK Vectors 2800 Woods Hollow Road, Madison, WI 53711-5399 USA Promega Corporation; 2016 [cited 2020 Mar 18]. Available from: https://no.promega.com/-/media/files/resources/msds/c8000/c8021.pdf?la=en-us.

110. Sherf BA, Navarro SL, Hannah RR, Wood KV. Dual-luciferase reporter assay: an advanced co-reporter technology integrating firefly and Renilla luciferase assays. Promega Notes. 1996;57(2):2-8.

111. LightSwitch Luciferase Assay System Overview: Switchgear Genomics; 2020 [cited 2020 May 01]. Available from: https://switchgeargenomics.com/resources/science-technology.

112. Quantikine ELISA Human IL-8/CXCL8 Immunoassay 614 McKinley Place NE, Minneapolis, MN 55413: R&D Systems; 2018 [cited 2020 Mar 18]. Available from: https://resources.rndsystems.com/pdfs/datasheets/d8000c.pdf.

113. ELISA Basic Guide Endeavour House, Langford Lane, Langford Business Park, Kidlington, OX5 1GE: Bio-Rad Laboratories, Inc; 2017 [cited 2020 May 16]. Available from: https://www.bio-rad-antibodies.com/static/2017/an-introduction-to-elisa/elisa-basics-guide.pdf.

114. MicroImaging CZ. LSM 510 META / LSM 510 META DuoScan. Germany2006.

115. Microscopy Techniques and Culture Surfaces: Find the Perfect Match, Confocal Microscopy: Ibidi; 2020 [cited 2020 May 16]. Available from: https://ibidi.com/content/216-confocal-microscopy.

116. Weston SA, Parish CR. New fluorescent dyes for lymphocyte migration studies. Analysis by flow cytometry and fluorescence microscopy. J Immunol Methods. 1990;133(1):87-97.

117. eBioscience™ CFSE: Thermo Fisher Scientific 2017 [cited 2020 Mar 19]. Available from: https://assets.thermofisher.com/TFS-Assets/LSG/manuals/65-0850.pdf.

118. Actin Staining Protocol Thermo Fisher Scientific; 2020 [cited 2020 Mar 19]. Available from: https://www.thermofisher.com/no/en/home/references/protocols/cell-and-tissue-analysis/microscopy-protocol/actin-staining-protocol.html.

119. DAPI stain: Thermo Fischer Scientific 2020 [cited 2020 Mar 27]. Available from: https://www.thermofisher.com/no/en/home/life-science/cell-analysis/fluorophores/dapi-stain.html.

120. Uhlen M, Fagerberg L, Hallstrom BM, Lindskog C, Oksvold P, Mardinoglu A, et al. Proteomics. Tissue-based map of the human proteome. Science (New York, NY). 2015;347(6220):1260419.

121. CSF2: Human Protein Atlas; 2020 [cited 2020 May 13]. Available from: https://www.proteinatlas.org/ENSG00000164400-CSF2/tissue.

122. CXCL8: Human Protein Atlas 2020 [cited 2020 May 13]. Available from: https://www.proteinatlas.org/ENSG00000169429-CXCL8/tissue.

123. Agarwal V, Bell GW, Nam JW, Bartel DP. Predicting effective microRNA target sites in mammalian mRNAs. eLife. 2015;4.

124. SAP18: Human Protein Atlas 2020 [cited 2020 May 13]. Available from: https://www.proteinatlas.org/ENSG00000150459-SAP18/tissue.

125. CCND1: Human Protein Atlas 2020 [cited 2020 May 13]. Available from: https://www.proteinatlas.org/ENSG00000110092-CCND1/tissue.

126. Han YW, Shi W, Huang GT, Kinder Haake S, Park NH, Kuramitsu H, et al. Interactions between periodontal bacteria and human oral epithelial cells: Fusobacterium nucleatum adheres to and invades epithelial cells. Infect Immun. 2000;68(6):3140-6.

127. Proença MA, Biselli JM, Succi M, Severino FE, Berardinelli GN, Caetano A, et al. Relationship between Fusobacterium nucleatum, inflammatory mediators and microRNAs in colorectal carcinogenesis. World J Gastroenterol. 2018;24(47):5351-65.

128. Liu Q, Li A, Tian Y, Wu JD, Liu Y, Li T, et al. The CXCL8-CXCR1/2 pathways in cancer. Cytokine Growth Factor Rev. 2016;31:61-71.

129. Chen Y, Chen Y, Zhang J, Cao P, Su W, Deng Y, et al. Fusobacterium nucleatum Promotes Metastasis in Colorectal Cancer by Activating Autophagy Signaling via the Upregulation of CARD3 Expression. Theranostics. 2020;10(1):323-39.

130. Li C, Zhao L, Chen Y, He T, Chen X, Mao J, et al. MicroRNA-21 promotes proliferation, migration, and invasion of colorectal cancer, and tumor growth associated with down-regulation of sec23a expression. BMC cancer. 2016;16:605-.

131. Fardini Y, Wang X, Témoin S, Nithianantham S, Lee D, Shoham M, et al. Fusobacterium nucleatum adhesin FadA binds vascular endothelial cadherin and alters endothelial integrity. Mol Microbiol. 2011;82(6):1468-80.

132. Zhu G, Huang Q, Zheng W, Huang Y, Hua J, Yang S, et al. LPS Upregulated VEGFR-3 Expression Promote Migration and Invasion in Colorectal Cancer via a Mechanism of Increased NF-kappaB Binding to the Promoter of VEGFR-3. Cell Physiol Biochem. 2016;39(5):1665-78.

133. Zhu G, Lin C, Cheng Z, Wang Q, Hoffman RM, Singh SR, et al. TRAF6-Mediated Inflammatory Cytokines Secretion in LPS-induced Colorectal Cancer Cells Is Regulated by miR-140. Cancer Genomics Proteomics. 2020;17(1):23-33.

134. Suzuki M, Hisamatsu T, Podolsky DK. Gamma interferon augments the intracellular pathway for lipopolysaccharide (LPS) recognition in human intestinal epithelial cells through coordinated up-regulation of LPS uptake and expression of the intracellular Toll-like receptor 4-MD-2 complex. Infect Immun. 2003;71(6):3503-11.

135. Eckmann L, Jung HC, Schurer-Maly C, Panja A, Morzycka-Wroblewska E, Kagnoff MF. Differential cytokine expression by human intestinal epithelial cell lines: regulated expression of interleukin 8. Gastroenterology. 1993;105(6):1689-97.

136. Meng F, Lowell CA. Lipopolysaccharide (LPS)-induced macrophage activation and signal transduction in the absence of Src-family kinases Hck, Fgr, and Lyn. J Exp Med. 1997;185(9):1661-70.

137. Wang Y, Han G, Wang K, Liu G, Wang R, Xiao H, et al. Tumor-derived GM-CSF promotes inflammatory colon carcinogenesis via stimulating epithelial release of VEGF. Cancer Res. 2014;74(3):716-26.

138. Branchett WJ, Lloyd CM. Regulatory cytokine function in the respiratory tract. Mucosal Immunology. 2019;12(3):589-600.

139. Shiomi A, Usui T. Pivotal roles of GM-CSF in autoimmunity and inflammation. Mediators Inflamm. 2015;2015:568543-.

140. Brown RL, Sequeira RP, Clarke TB. The microbiota protects against respiratory infection via GM-CSF signaling. Nature communications. 2017;8(1):1512-.

141. Reynolds CJ, Quigley K, Cheng X, Suresh A, Tahir S, Ahmed-Jushuf F, et al. Lung Defense through IL-8 Carries a Cost of Chronic Lung Remodeling and Impaired Function. Am J Respir Cell Mol Biol. 2018;59(5):557-71.

142. Chen Y, Zhao Z, Chen Y, Lv Z, Ding X, Wang R, et al. An epithelial-to-mesenchymal transition-inducing potential of granulocyte macrophage colony-stimulating factor in colon cancer. Scientific reports. 2017;7(1):8265-.

143. Hong I-S. Stimulatory versus suppressive effects of GM-CSF on tumor progression in multiple cancer types. Exp Mol Med. 2016;48(7):e242-e.

144. Shi Y, Liu CH, Roberts AI, Das J, Xu G, Ren G, et al. Granulocyte-macrophage colony-stimulating factor (GM-CSF) and T-cell responses: what we do and don't know. Cell Res. 2006;16(2):126-33.

145. Xu Z, Zhang Y, Xu M, Zheng X, Lin M, Pan J, et al. Demethylation and Overexpression of CSF2 are Involved in Immune Response, Chemotherapy Resistance, and Poor Prognosis in Colorectal Cancer. Onco Targets Ther. 2019;12:11255-69.

146. Urdinguio RG, Fernandez AF, Moncada-Pazos A, Huidobro C, Rodriguez RM, Ferrero C, et al. Immune-dependent and independent antitumor activity of GM-CSF aberrantly expressed by mouse and human colorectal tumors. Cancer Res. 2013;73(1):395-405.

147. Lee Y-Y, Wu W-J, Huang C-N, Li C-C, Li W-M, Yeh B-W, et al. CSF2 Overexpression Is Associated with STAT5 Phosphorylation and Poor Prognosis in Patients with Urothelial Carcinoma. J Cancer. 2016;7(6):711-21.

148. Li J, Liu Q, Huang X, Cai Y, Song L, Xie Q, et al. Transcriptional Profiling Reveals the Regulatory Role of CXCL8 in Promoting Colorectal Cancer. Front Genet. 2020;10:1360-.

149. Cheng XS, Li YF, Tan J, Sun B, Xiao YC, Fang XB, et al. CCL20 and CXCL8 synergize to promote progression and poor survival outcome in patients with colorectal cancer by collaborative induction of the epithelial-mesenchymal transition. Cancer Lett. 2014;348(1-2):77-87.

150. Ning Y, Manegold PC, Hong YK, Zhang W, Pohl A, Lurje G, et al. Interleukin-8 is associated with proliferation, migration, angiogenesis and chemosensitivity in vitro and in vivo in colon cancer cell line models. Int J Cancer. 2011;128(9):2038-49.

151. Xiao YC, Yang ZB, Cheng XS, Fang XB, Shen T, Xia CF, et al. CXCL8, overexpressed in colorectal cancer, enhances the resistance of colorectal cancer cells to anoikis. Cancer Lett. 2015;361(1):22-32.

152. Bie Y, Ge W, Yang Z, Cheng X, Zhao Z, Li S, et al. The Crucial Role of CXCL8 and Its Receptors in Colorectal Liver Metastasis. Dis Markers. 2019;2019:8023460-.

153. Ougolkov A, Zhang B, Yamashita K, Bilim V, Mai M, Fuchs SY, et al. Associations among beta-TrCP, an E3 ubiquitin ligase receptor, beta-catenin, and NF-kappaB in colorectal cancer. J Natl Cancer Inst. 2004;96(15):1161-70.

154. Elgui de Oliveira D, Müller-Coan BG, Pagano JS. Viral Carcinogenesis Beyond Malignant Transformation: EBV in the Progression of Human Cancers. Trends in microbiology. 2016;24(8):649-64.

155. Cain D, Kondo M, Chen H, Kelsoe G. Effects of acute and chronic inflammation on B-cell development and differentiation. J Invest Dermatol. 2009;129(2):266-77.

156. Ding X, Xu J, Wang C, Feng Q, Wang Q, Yang Y, et al. Suppression of the SAP18/HDAC1 complex by targeting TRIM56 and Nanog is essential for oncogenic viral FLICE-inhibitory protein-induced acetylation of p65/RelA, NF-kappaB activation, and promotion of cell invasion and angiogenesis. Cell Death Differ. 2019;26(10):1970-86.

157. Han X, Shi H, Sun Y, Shang C, Luan T, Wang D, et al. CXCR2 expression on granulocyte and macrophage progenitors under tumor conditions contributes to mo-MDSC generation via SAP18/ERK/STAT3. Cell Death Dis. 2019;10(8):598-.

158. Makishima S, Boonvisut S, Ishizuka Y, Watanabe K, Nakayama K, Iwamoto S. Sin3A-associated protein, 18 kDa, a novel binding partner of TRIB1, regulates MTTP expression. J Lipid Res. 2015;56(6):1145-52.

159. Zhang Y, Iratni R, Erdjument-Bromage H, Tempst P, Reinberg D. Histone deacetylases and SAP18, a novel polypeptide, are components of a human Sin3 complex. Cell. 1997;89(3):357-64.

160. Singh KK, Erkelenz S, Rattay S, Dehof AK, Hildebrandt A, Schulze-Osthoff K, et al. Human SAP18 mediates assembly of a splicing regulatory multiprotein complex via its ubiquitin-like fold. RNA. 2010;16(12):2442-54.

161. Deka B, Singh KK. Multifaceted Regulation of Gene Expression by the Apoptosis- and Splicing-Associated Protein Complex and Its Components. International journal of biological sciences. 2017;13(5):545-60.

162. Hu Y, Suliman BA. Roles of HDACs in the Responses of Innate Immune Cells and as Targets in Inflammatory Diseases. Advances in experimental medicine and biology. 2017;1024:91-110.

163. Shakespear MR, Halili MA, Irvine KM, Fairlie DP, Sweet MJ. Histone deacetylases as regulators of inflammation and immunity. Trends Immunol. 2011;32(7):335-43.

164. Zheng L, Qi T, Yang D, Qi M, Li D, Xiang X, et al. microRNA-9 suppresses the proliferation, invasion and metastasis of gastric cancer cells through targeting cyclin D1 and Ets1. PloS one. 2013;8(1):e55719-e.

165. Balcerczak E, Pasz-Walczak G, Kumor P, Panczyk M, Kordek R, Wierzbicki R, et al. Cyclin D1 protein and CCND1 gene expression in colorectal cancer. Eur J Surg Oncol. 2005;31(7):721-6.

166. Guo F, Xue J. MicroRNA-628-5p inhibits cell proliferation and induces apoptosis in colorectal cancer through downregulating CCND1 expression levels. Mol Med Rep. 2020;21(3):1481-90.

167. Tong F, Ying Y, Pan H, Zhao W, Li H, Zhan X. MicroRNA-466 (miR-466) functions as a tumor suppressor and prognostic factor in colorectal cancer (CRC). Bosn J Basic Med Sci. 2018;18(3):252-9.

168. Sun G, Shi L, Yan S, Wan Z, Jiang N, Fu L, et al. MiR-15b targets cyclin D1 to regulate proliferation and apoptosis in glioma cells. Biomed Res Int. 2014;2014:687826-.

169. Liberase DH Research Grade: Sigma-Aldrich; 2020 [cited 2020 May 02]. Available from: https://www.sigmaaldrich.com/catalog/product/roche/libdhro?lang=en&region=NO.

170. Collagenase, Type II, powder: Thermo Fisher Scientific; 2020 [cited 2020 May 02]. Available from: https://www.thermofisher.com/order/catalog/product/17101015#/17101015.

171. Dispase I: Sigma-Aldrich; 2020 [cited 2020 May 02]. Available from: https://www.sigmaaldrich.com/catalog/product/sigma/d4818?lang=en&region=NO.

172. Amin MB, American Joint Committee on C. AJCC cancer staging manual. 8th ed. ed. New York, N.Y: Springer; 2017.

173. Clinton J, McWilliams-Koeppen P. Initiation, Expansion, and Cryopreservation of Human Primary Tissue-Derived Normal and Diseased Organoids in Embedded Three-Dimensional Culture. Current Protocols in Cell Biology. 2019;82(1):e66.

Supplementary

A Supplementary tables

Table S1: AJCC (American Joint Committee on cancer) TNM staging system 8th edition*

T (tumor invasion)	Description
TX	Primary tumor cannot be assessed
T0	No evidence of a primary tumor
Tis	Carcinoma in situ or intramucosal carcinoma
T1	Tumor invades submucosa
T2	Tumor invades muscularis propria
T3	Tumor invades through muscularis propria into subserosa or into non-peritonealized pericolic or perirectal tissues
T4a	Tumor invades through wall of colon or rectum but does not invade other organs or structures.
T4b	Tumor directly invades other organs or structures and/or perforates visceral peritoneum
N (spread to regional lymph nodes)	
NX	Regional lymph nodes cannot be assessed
N0	No spread to nearby lymph nodes
N1	Metastasis in 1 to 3 regional lymph nodes
N1c	Metastasis in fat nearby regional lymph nodes
N2a	Metastasis in 4 to 6 regional lymph nodes
N2b	Metastasis in 7 or more regional lymph nodes
M (occurrence of distant metastasis)	
MX	Distant metastasis cannot be assessed
M0	No distant metastasis

M1a	Metastasis to 1 distant organ (such as liver/lung) or distant set of lymph nodes
M1b	Metastasis in more than 1 distant organ (such as liver/lung) or distant set of lymph nodes
M1c	Metastasis to the peritoneum. Maybe distant metastasis to distant organs or lymph nodes

Table S2: AJCC TNM Stage grouping 8th edition**

Stage group	Tumor invasion	Lymph node metastasis	Distant metastasis
Stage O	Tis	N0	M0
Stage I	T1-T2	N0	M0
Stage II	T3-T4a	N0	M0
Stage III	Any T	N1-N2	M0
Stage IV	Any T	Any N	Any M

*,**: Tables are modified from AJCC cancer staging manual 8th edition (172).

Table S3: Materials, instruments, and reagents used in this study

Product name	Art.nr/Catalogue nr.	Manufacturer
Commercial kits		
Sandwich Enzyme-linked Immunosorbent assay (ELISA) Human CXCL8/IL-8	D8000C	R&D Systems
Total RNA purification Kit	37500	Norgen biotek corp
High-Capacity RNA-to-cDNA kit	4387406	Applied Biosystems
QIAquick PCR purification Kit	28106	QIAGEN
Monarch DNA Gel Extraction Kit	T1020	New England Biolabs
Q5 High-Fidelity PCR kit	E0555	New England Biolabs
Sense mRNA-Seq Library Prep Kit V2	–	Lexogen
Wizard *Plus* Miniprep DNA Purification system	A1460	Promega
Dual-Luciferase® Reporter Assay System	E1910	Promega
LightSwitch Luciferase Assay System	LS010	SwitchGear Genomics
Technical equipment and instruments		
EVOS FL Auto Cell Imaging System	–	Invitrogen
Mastercycler® EP (Thermal cycler) + annen	–	Eppendorf, UK
NanoDrop ND-1000 Spectrophotometer	–	NanoDrop Technologies, Inc., US/Thermo Scientific
FLUOstar® Omega microplate reader	–	BMG Labtech, Germany
McFarland Densitometer	–	BioSan
Step One Plus Real-Time PCR system	–	Applied Biosystems

Zeiss LSM 510 META confocal microscope	–	Zeiss
Cell lines and products for cell culture maintenance		
DLD-1 cell line	–	In-house cell line
SW480 cell line	–	In-house cell line
SW620 cell line	–	In-house cell line
LS411N cell line	–	In-house cell line
RPMI-1640 Medium	R8758	Sigma-Aldrich
Dulbecco's Modified Eagle Medium (DMEM)	D5796	Sigma-Aldrich
Fetal Bovine serum	F7520	Sigma-Aldrich
Trypsin	T3924	Sigma-Aldrich
Penicillin-Streptomyocin	P0781	Sigma-Aldrich
L-glutamine	G7513	Sigma-Aldrich
Dulbecco's phosphate buffered saline (PBS)	–	Sigma-Aldrich
Other reagents		
Lipofectamine RNAiMAX	13778	Invitrogen
XhoI	R0146	New England Biolabs
NotI	R3189	New England Biolabs
CutSmart Buffer	B7204S	New England Biolabs
2x ligase buffer	B2200S	New England Biolabs
Quick Ligase	M2200S	New England Biolabs
DharmaFECT DUO Transfection Reagent	T-2010	Thermo Scientific
Opti-MEM® Reduced Serum Medium	11058-021	Gibco
TaqMan Universal Master Mix II, no UNG	4440040	Applied Biosystems

Tryptic Soy Broth	1.46432	Sigma-Aldrich
CFSE	65-0850-85	Invitrogen
DAPI	D1306	Invitrogen
Rhodamine Phalloidin	R415	Invitrogen
Equipment for cell culture experiments		
Fastidious Anaerobe Agar (F.A.A) with horse blood agar plates (FHB)	12957138/PB0225A	Thermo Fischer Scientific
Anaerobic jar	28029-1EA-F	Sigma-Aldrich
Anaerobic indicator test	59886	Sigma-Aldrich
Anaerobic atmosphere generation bags	68061	Sigma-Aldrich
Culture-Inserts 2 well for self-insertion	80209	Ibidi
µ-slide 8 well Grid-500	80826	Ibidi

Table S4: Difference between *F. nucleatum* and TSB-treated SW620 cells. Foldchange is log2 and shows the difference between *F. nucleatum* and TSB, average expression describes the average expression of gene across all samples and the adjusted p-values is Benjamin Hochberg-adjusted. The table is sorted by fold change. Genes that are further validated in the thesis are indicated in yellow. Shown is top 100 genes sorted by unadjusted P-value.

ENSEMBL	Gene Symbol	Fold change (log2)	Average Expression	P-Value	Adjusted P-Value
ENSG00000125730	C3	628996651	3.15775015	8.26E-09	1.59E-05
ENSG00000163739	CXCL1	4.84766721	4.47693324	7.58E-15	1.02E-10
ENSG00000008517	IL32	3.98729605	3.10981224	9.72E-12	3.27E-08
ENSG00000108691	CCL2	3.56881835	0.78285171	6.84E-06	0.00153852
ENSG00000163734	CXCL3	3.55068806	3.80875986	1.58E-13	1.07E-09
ENSG00000185215	TNFAIP2	3.12415221	4.44373028	5.09E-13	2.28E-09
ENSG00000163131	CTSS	3.10935289	2.42622412	0.00089477	0.01432373
ENSG00000115009	CCL20	3.08924447	3.08569832	1.69E-08	2.53E-05
ENSG00000169429	CXCL8	3.00762663	3.7529938	1.52E-11	4.08E-08
ENSG00000164400	CSF2	2.95449624	2.07260303	1.92E-06	0.00066921
ENSG00000215182	MUC5AC	2.49968011	2.56654004	5.60E-07	0.00034253
ENSG00000124875	CXCL6	2.47292373	4.47722324	2.20E-10	4.94E-07
ENSG00000168961	LGALS9	2.41968417	1.2148618	4.75E-05	0.00386951
ENSG00000100628	ASB2	2.39549387	0.29935329	0.00371007	0.03116131
ENSG00000081041	CXCL2	2.30861791	1.20113173	2.20E-06	0.00070487
ENSG00000134061	CD180	2.30724028	0.03248965	0.01326594	0.06484447
ENSG00000090339	ICAM1	2.25897384	1.12497748	3.86E-05	0.00361393
ENSG00000183044	ABAT	2.20329484	0.9522313	0.00047671	0.01046941
ENSG00000137673	MMP7	2.19724178	2.44605481	7.83E-08	8.77E-05
ENSG00000182179	UBA7	2.10795387	0.77199569	0.0003652	0.00962916

ENSG00000124762	CDKN1A	2.06478642	1.41633874	0.00279838	0.02675715
ENSG00000162148	PPP1R32	1.98687073	0.26855435	0.00415052	0.03317091
ENSG00000058085	LAMC2	1.96112257	3.34515944	2.05E-07	0.00017251
ENSG00000028277	POU2F2	1.92150426	2.36245373	1.78E-06	0.00066574
ENSG00000031081	ARHGAP31	1.91386632	0.12360313	0.00733317	0.04548395
ENSG00000198929	NOS1AP	1.91004623	0.01333793	0.02208238	0.08946723
ENSG00000205220	PSMB10	1.90009384	3.88301403	6.75E-08	8.25E-05
ENSG00000118503	TNFAIP3	1.83430775	3.30727367	4.33E-07	0.0003064
ENSG00000167680	SEMA6B	1.79421232	0.7337545	0.00419557	0.03330452
ENSG00000172602	RND1	1.77038964	0.90082562	0.00075019	0.01289994
ENSG00000215788	TNFRSF25	1.74851919	0.32025649	0.00426534	0.03367941
ENSG00000111012	CYP27B1	1.7410124	0.78648843	0.00048919	0.01056528
ENSG00000234745	HLA-B	1.71863726	4.52114672	1.56E-08	2.53E-05
ENSG00000187942	LDLRAD2	1.70964827	0.12744282	0.00330892	0.02920092
ENSG00000104936	DMPK	1.69748374	0.03393677	0.04128836	0.13168989
ENSG00000163735	CXCL5	1.61001795	0.03380359	0.03208444	0.11229553
ENSG00000007516	BAIAP3	1.60678858	0.66357676	0.00588034	0.04032697
ENSG00000006210	CX3CL1	1.60489107	3.56385042	1.98E-07	0.00017251
ENSG00000198915	RASGEF1A	1.59887469	0.80581298	0.00688081	0.04397273
ENSG00000151240	DIP2C	1.57486522	0.5028626	0.02608329	0.09899576
ENSG00000105516	DBP	1.55129877	0.1313299	0.01055367	0.0565399
ENSG00000069399	BCL3	1.54763438	2.44618429	3.27E-06	0.00095637
ENSG00000173264	GPR137	1.5439217	2.15951531	0.00280182	0.02675859
ENSG00000088881	EBF4	1.54157972	0.10878231	0.01254004	0.0626164
ENSG00000110944	IL23A	1.53682266	3.20831502	1.70E-06	0.00066152
ENSG00000122863	CHST3	1.52935326	0.07111393	0.0315536	0.11119005

ENSG00000167077	MEI1	1.51322126	0.8881249	0.01103242	0.05809781
ENSG00000161682	FAM171A2	1.51021455	0.48756405	0.00397756	0.03235712
ENSG00000123454	DBH	1.50767473	0.02378884	0.02987753	0.10771131
ENSG00000163874	ZC3H12A	1.49876937	3.25565828	2.89E-06	0.00088213
ENSG00000185479	KRT6B	1.48402052	1.25421538	0.00299268	0.02775348
ENSG00000184371	CSF1	1.45310666	1.38895832	0.00101303	0.01544472
ENSG00000196843	ARID5A	1.44893134	0.75182056	0.00795084	0.04759495
ENSG00000280670	CCDC163	1.44635345	1.53408785	0.00096741	0.01505832
ENSG00000056558	TRAF1	1.44248276	1.19691308	0.00088176	0.0142014
ENSG00000077463	SIRT6	1.43351823	1.33738617	0.00463017	0.03533594
ENSG00000187583	PLEKHN1	1.42706397	0.22161227	0.00791669	0.04756736
ENSG00000196155	PLEKHG4	1.42540062	1.42616277	0.00072311	0.01261167
ENSG00000146232	NFKBIE	1.41939796	1.71929168	0.00057961	0.01145218
ENSG00000240065	PSMB9	1.41599838	2.03725938	0.00128977	0.01741318
ENSG00000166311	SMPD1	1.40808512	2.39129717	4.96E-05	0.00393922
ENSG00000186352	ANKRD37	1.38838105	0.3950475	0.0109264	0.05770907
ENSG00000163545	NUAK2	1.38344007	2.84170685	0.00063332	0.01182819
ENSG00000104856	RELB	1.37009466	2.76894055	0.00035815	0.00962916
ENSG00000181284	TMEM102	1.36363931	1.2872485	0.00348582	0.02984334
ENSG00000170684	ZNF296	1.34839045	1.32601936	0.00495907	0.03657963
ENSG00000182985	CADM1	1.33874003	1.07303712	0.00731807	0.04547417
ENSG00000136490	LIMD2	1.33772735	0.47188309	0.0424685	0.13398664
ENSG00000138356	AOX1	1.32887122	0.1666057	0.01669449	0.0745569
ENSG00000171608	PIK3CD	1.32125975	2.7418602	0.00058718	0.01149326
ENSG00000222009	BTBD19	1.31442632	1.63250384	0.02539622	0.09734975
ENSG00000105298	CACTIN	1.30857703	1.158119	0.01692713	0.07524597

ENSG00000160993	ALKBH4	1.30714599	1.51097588	0.00336408	0.02937664
ENSG00000130766	SESN2	1.3045624	0.88055191	0.02301762	0.09165471
ENSG00000172478	MAB21L4	1.29922471	0.66127842	0.00712429	0.04487137
ENSG00000101342	TLDC2	1.28723701	1.53870465	0.00180595	0.02125283
ENSG00000168685	IL7R	1.27424974	2.6756304	0.00352823	0.03004695
ENSG00000132793	LPIN3	1.26765153	1.86147838	0.00855251	0.04993534
ENSG00000139880	CDH24	1.26157243	1.62355046	0.01091415	0.05766702
ENSG00000081277	PKP1	1.2612246	0.22278793	0.03286623	0.11415316
ENSG00000155961	RAB39B	1.2604386	0.75660136	0.01890737	0.0809594
ENSG00000105656	ELL	1.25125683	2.5504718	0.00048084	0.01051359
ENSG00000167676	PLIN4	1.25018379	0.56052296	0.01812521	0.07862248
ENSG00000134873	CLDN10	1.23433938	0.57509395	0.01248109	0.06248457
ENSG00000197536	C5orf56	1.2340247	1.86939206	0.0007076	0.01247063
ENSG00000107099	DOCK8	1.22850981	1.08258631	0.00916631	0.05198449
ENSG00000142173	COL6A2	1.22216785	1.27928873	0.02652882	0.10009068
ENSG00000142494	SLC47A1	1.22103778	0.0108646	0.04351364	0.13613097
ENSG00000114626	ABTB1	1.2114011	0.40778639	0.04424971	0.13761004
ENSG00000197249	SERPINA1	1.21062931	6.76220656	1.66E-07	0.0001593
ENSG00000135736	CCDC102A	1.20278578	1.77198605	0.00642417	0.04226256
ENSG00000100031	GGT1	1.2024202	1.03757898	0.00784707	0.04731691
ENSG00000126246	IGFLR1	1.20067656	0.39243031	0.01221401	0.06165231
ENSG00000137218	FRS3	1.19952105	1.37624672	0.00350147	0.0298758
ENSG00000185101	ANO9	1.19332571	4.73614134	5.03E-07	0.0003219
ENSG00000112561	TFEB	1.19300495	0.32920576	0.02483876	0.09600656
ENSG00000091073	DTX2	1.19110874	3.18024135	0.00014911	0.0062268
ENSG00000070371	CLTCL1	1.1879403	1.65010309	0.00297841	0.02773391

ENSG00000184378	ACTRT3	1.1869831	0.67683116	0.0164538	0.07412202
ENSG00000185507	IRF7	1.18374011	0.8847881	0.01475155	0.06886064

Table S5: Difference between *F. nucleatum* and TSB-treated DLD-1 cells. Foldchange is log2 and shows the difference between *F. nucleatum* and TSB, average expression describes the average expression of gene across all samples, the adjusted p-values is Benjamin Hochberg-adjusted. The table is sorted by fold change. Genes that are further validated in the thesis are indicated in yellow. Shown is the top 100 genes sorted by unadjusted P-value.

ENSEMBL	Gene Symbol	Fold change (log2)	Average Expression	P-Value	Adjusted P-Value
ENSG00000115009	CCL20	2.48952623	0.47204074	0.0004168	0.06143284
ENSG00000033122	LRRC7	2.36922519	-1.1843959	0.0118875	0.09514401
ENSG00000204311	PJVK	2.34458724	-0.8961379	0.0057782	0.07403445
ENSG00000153930	ANKFN1	2.33822029	-1.6005656	0.014793	0.10490645
ENSG00000163739	CXCL1	2.26859821	2.28454506	1.66E-07	0.00108293
ENSG00000198443	KRTAP4-1	2.14313818	-1.2483517	0.0088463	0.08492272
ENSG00000197013	ZNF429	2.11118541	0.41251202	0.010814	0.09159975
ENSG00000078579	FGF20	2.07983288	-0.7387513	0.0035678	0.06872402
ENSG00000049249	TNFRSF9	2.01282104	1.14391107	2.96E-05	0.06143284
ENSG00000260589	STAM-AS1	1.99995664	-1.4244587	0.0357478	0.15476479
ENSG00000183098	GPC6	1.99940475	-0.9136881	0.0046565	0.07208044
ENSG00000125869	LAMP5	1.97644806	0.70554478	0.0623187	0.20536375
ENSG00000173432	SAA1	1.9482172	-0.5346956	0.0068481	0.07752648
ENSG00000185686	PRAME	1.93190432	-0.7184032	0.054834	0.19195291
ENSG00000013725	CD6	1.91643031	-1.2483517	0.0187075	0.11505582
ENSG00000073737	DHRS9	1.89040841	-1.3165861	0.029686	0.14018499

ENSG00000258738	LOC112268124	1.88188032	-0.0092794	0.0135419	0.10089799
ENSG00000250305	TRMT9B	1.85180454	-0.2660721	0.0107034	0.09122358
ENSG00000163440	PDCL2	1.83612519	-0.589423	0.0065137	0.07652825
ENSG00000148346	LCN2	1.82358061	4.4938495	5.74E-08	0.00074878
ENSG00000179674	ARL14	1.8123259	0.12855452	0.005369	0.07363289
ENSG00000019505	SYT13	1.80341455	-1.234701	0.0507752	0.18384713
ENSG00000174827	PDZK1	1.80005246	0.0055707	0.035954	0.15508644
ENSG00000244184	LOC101559451	1.78055584	-1.0358588	0.0516212	0.18582765
ENSG00000128714	HOXD13	1.75409589	-1.2886373	0.0177644	0.11277719
ENSG00000206559	ZCWPW2	1.75182256	0.09930199	0.0073163	0.07938469
ENSG00000137265	IRF4	1.74065117	1.62187982	0.1356844	0.31819774
ENSG00000276345	LOC107987373	1.74064557	-1.4647443	0.0586686	0.19907231
ENSG00000255733	IFNG-AS1	1.73257244	-0.9634058	0.0952629	0.25959172
ENSG00000189325	C6orf222	1.65512935	-0.8435155	0.0187269	0.11505582
ENSG00000133135	RNF128	1.65500838	-0.7820854	0.043057	0.16861823
ENSG00000232284	GNG12-AS1	1.65436086	0.00567457	0.012278	0.09654474
ENSG00000137393	RNF144B	1.64394552	-0.6111919	0.0360108	0.15523421
ENSG00000272677	LOC101928963	1.63324892	0.43151708	0.0037114	0.06925482
ENSG00000186998	EMID1	1.61890668	-0.9811313	0.0494769	0.18130888
ENSG00000169429	CXCL8	1.59917232	3.96604142	4.33E-06	0.01883457
ENSG00000145569	OTULINL	1.58582362	-0.5842095	0.0518149	0.18616578
ENSG00000147065	MSN	1.56306412	1.488031	0.081935	0.23934687
ENSG00000135773	CAPN9	1.54448317	-1.0183085	0.0743582	0.22667794
ENSG00000149970	CNKSR2	1.54139072	-0.0409347	0.0310518	0.14367921
ENSG00000189375	TBC1D28	1.52221697	1.8192073	0.0242259	0.12792078
ENSG00000135077	HAVCR2	1.49032785	0.84085643	0.0026584	0.06388643

ENSG00000270362	HMGN3-AS1	1.48513289	-0.0119743	0.0296137	0.14015519
ENSG00000185519	FAM131C	1.47554774	-0.9364234	0.0449536	0.17253153
ENSG00000115008	IL1A	1.4661728	-0.7013704	0.0412139	0.16524003
ENSG00000164400	CSF2	1.45083657	-1.113113	0.1184866	0.29492796
ENSG00000169744	LDB2	1.43965277	-1.080363	0.0732385	0.22492064
ENSG00000231890	DARS-AS1	1.40811704	-0.4256529	0.0387273	0.16078462
ENSG00000155749	FLACC1	1.39762133	-0.1836517	0.0813538	0.23831752
ENSG00000129680	MAP7D3	1.39729471	-0.351653	0.0959158	0.2603429
ENSG00000069667	RORA	1.39292149	0.25545698	0.0728603	0.22478041
ENSG00000143603	KCNN3	1.38647676	-0.0634447	0.1392947	0.32341053
ENSG00000123388	HOXC11	1.37570779	-0.9702962	0.1110566	0.28502205
ENSG00000159905	ZNF221	1.37189003	-0.2536207	0.076946	0.2310422
ENSG00000166289	PLEKHF1	1.36014064	-0.4391597	0.0781776	0.23302242
ENSG00000184489	PTP4A3	1.34668898	-0.2861356	0.0805576	0.23688175
ENSG00000136535	TBR1	1.33596551	-1.2080662	0.1148481	0.29013204
ENSG00000153714	LURAP1L	1.32462227	-0.5075379	0.0676528	0.21550856
ENSG00000143297	FCRL5	1.32404737	0.50735759	0.1710059	0.36441079
ENSG00000172901	LVRN	1.32060279	-0.7200309	0.0870467	0.24609511
ENSG00000073849	ST6GAL1	1.31973075	1.45325423	0.0608495	0.20293016
ENSG00000164675	IQUB	1.31721893	-1.3520057	0.1148889	0.29017907
ENSG00000017483	SLC38A5	1.30599949	0.21525217	0.1730512	0.36738247
ENSG00000261335	LOC105274304	1.29164178	-0.9903597	0.0834971	0.24139838
ENSG00000100285	NEFH	1.29100481	-1.0183085	0.1166144	0.29233111
ENSG00000263006	ROCK1P1	1.27787315	0.85890094	0.011351	0.09356191
ENSG00000026025	VIM	1.27490807	1.92385876	0.1931671	0.39158414
ENSG00000134061	CD180	1.26941254	-0.1836517	0.1805579	0.37588868

ENSG00000234264	DEPDC1-AS1	1.26916386	0.35356594	0.0110238	0.09230538
ENSG00000254614	LOC728975	1.26335749	-1.1001936	0.1216451	0.29913969
ENSG00000140057	AK7	1.25897935	-1.1354694	0.159579	0.35039469
ENSG00000257815	LINC01481	1.25595321	0.53764439	0.0086139	0.08409973
ENSG00000171126	KCNG3	1.2472714	-0.7323677	0.0999663	0.2669517
ENSG00000182118	FAM89A	1.23501823	3.94725254	0.0001095	0.06143284
ENSG00000171310	CHST11	1.23402292	-0.0761107	0.0259952	0.13244159
ENSG00000170624	SGCD	1.23328982	-0.2162105	0.1302076	0.3112249
ENSG00000237499	LOC100130476	1.2215411	0.89615353	0.0134358	0.10056042
ENSG00000089101	CFAP61	1.22032111	-0.5198747	0.1001586	0.26724658
ENSG00000136167	LCP1	1.21995223	1.67036152	0.0894608	0.24999616
ENSG00000171873	ADRA1D	1.21695756	-0.1111988	0.0466541	0.17559315
ENSG00000265096	C1QTNF1-AS1	1.21383357	0.29822656	0.0382489	0.15980148
ENSG00000120820	GLT8D2	1.21048319	-0.330117	0.1155999	0.29090212
ENSG00000174428	GTF2IRD2B	1.20847668	-0.3127705	0.042529	0.16751105
ENSG00000197046	SIGLEC15	1.20566193	-1.3425736	0.1397118	0.32397549
ENSG00000188739	RBM34	1.18142167	-0.8824871	0.1099237	0.28317222
ENSG00000168685	IL7R	1.15723916	-0.5979201	0.1172206	0.29317922
ENSG00000258102	MAP1LC3B2	1.15482967	-0.1501106	0.0662602	0.21245268
ENSG00000197748	CFAP43	1.14893172	-0.178263	0.0520716	0.18653728
ENSG00000225265	TAF1A-AS1	1.14628755	0.60092948	0.0937489	0.25735109
ENSG00000267226	LOC101927322	1.14550797	-0.2658684	0.1236895	0.30155373
ENSG00000079101	CLUL1	1.13864116	0.55123811	0.0810955	0.23817206
ENSG00000168275	COA6	1.13839468	5.4335861	3.36E-05	0.06143284
ENSG00000187860	CCDC157	1.1349495	-0.9581923	0.154421	0.3429906
ENSG00000122188	LAX1	1.13406941	-1.0140898	0.2425315	0.44796438

ENSG00000221887	HMSD	1.12275391	-1.234701	0.1894631	0.3867181
ENSG00000133111	RFXAP	1.12194941	3.30917969	0.0018336	0.06297599
ENSG00000111913	RIPOR2	1.12000164	0.45638881	0.0259281	0.13223666
ENSG00000007062	PROM1	1.10866953	1.22366705	0.0135635	0.10093777
ENSG00000166596	CFAP52	1.10449689	-0.9084747	0.1389084	0.32288126
ENSG00000245573	BDNF-AS	1.10353619	0.52522124	0.0641834	0.20881998

Table S6: Difference *E. coli DH5α* and TSB-treated SW620 cells. Foldchange is log2 and shows the difference between *E. coli DH5α* and TSB, average expression describes the average expression of gene across all samples, the adjusted p-values is Benjamin Hochberg-adjusted. The table is sorted by fold change. Genes that are further validated in the thesis are indicated in yellow. Shown is the top 100 genes sorted by unadjusted P-value.

ENSEMBL	Gene Symbol	Fold change (log2)	Average Expression	P-value	Adjusted P-value
ENSG00000125730	C3	6.24323948	3.15775015	4.20E-09	7.06E-06
ENSG00000163739	CXCL1	4.95949187	4.47693324	2.52E-15	3.39E-11
ENSG00000108691	CCL2	3.87827569	0.78285171	1.06E-06	0.00083991
ENSG00000008517	IL32	3.80505654	3.10981224	8.85E-12	2.38E-08
ENSG00000163131	CTSS	3.51705989	2.42622412	0.00016229	0.03448346
ENSG00000163734	CXCL3	3.26391927	3.80875986	2.93E-13	1.97E-09
ENSG00000169429	CXCL8	3.21827163	3.7529938	2.30E-12	7.72E-09
ENSG00000115009	CCL20	3.13385226	3.08569832	6.20E-09	9.27E-06
ENSG00000185215	TNFAIP2	3.00581732	4.44373028	4.77E-13	2.14E-09
ENSG00000124875	CXCL6	2.62771408	4.47722324	4.26E-11	9.55E-08
ENSG00000137673	MMP7	2.55238647	2.44605481	3.68E-09	7.06E-06
ENSG00000081041	CXCL2	2.49678591	1.20113173	3.23E-07	0.0002899

ENSG00000164400	CSF2	2.40636294	2.07260303	1.22E-05	0.00629152
ENSG00000168961	LGALS9	2.17004087	1.2148618	7.72E-05	0.02251271
ENSG00000215182	MUC5AC	2.11556168	2.56654004	2.44E-06	0.001825
ENSG00000058085	LAMC2	2.05069633	3.34515944	5.26E-08	7.08E-05
ENSG00000100628	ASB2	2.04324821	0.29935329	0.00745677	0.23988326
ENSG00000224812	TMEM72-AS1	1.97481461	0.07217796	0.00190516	0.14884041
ENSG00000118503	TNFAIP3	1.90246323	3.30727367	1.28E-07	0.00015592
ENSG00000164342	TLR3	1.88540085	0.64269555	0.00020823	0.03859323
ENSG00000167077	MEI1	1.83955331	0.8881249	0.00179654	0.14671231
ENSG00000090339	ICAM1	1.83918259	1.12497748	0.00017593	0.0358452
ENSG00000213626	LBH	1.76355699	0.32774516	0.00743459	0.23988326
ENSG00000122863	CHST3	1.72401031	0.07111393	0.0124084	0.27748949
ENSG00000124762	CDKN1A	1.68946973	1.41633874	0.00733788	0.23891642
ENSG00000151240	DIP2C	1.66103124	0.5028626	0.01428336	0.27957863
ENSG00000205220	PSMB10	1.64367172	3.88301403	2.71E-07	0.00026054
ENSG00000183044	ABAT	1.62390532	0.9522313	0.00357936	0.18693546
ENSG00000063046	EIF4B	1.5425599	0.61959816	0.0380087	0.37117141
ENSG00000222009	BTBD19	1.52906312	1.63250384	0.00747603	0.23992894
ENSG00000196155	PLEKHG4	1.52635892	1.42616277	0.00020518	0.03859323
ENSG00000163354	DCST2	1.47188282	0.29123503	0.04119952	0.37945292
ENSG00000182179	UBA7	1.4613786	0.77199569	0.00459082	0.21106931
ENSG00000187942	LDLRAD2	1.45688273	0.12744282	0.00682764	0.23723848
ENSG00000246130	LOC286059	1.43490032	0.09817299	0.00942731	0.25818539
ENSG00000134873	CLDN10	1.42991071	0.57509395	0.00313158	0.17768077
ENSG00000234745	HLA-B	1.38834586	4.52114672	1.87E-07	0.00019339

ENSG00000105298	CACTIN	1.37068372	1.158119	0.00878385	0.25084742
ENSG00000184378	ACTRT3	1.35175173	0.67683116	0.00499332	0.21383814
ENSG00000123454	DBH	1.34640163	0.02378884	0.03886894	0.37365325
ENSG00000107099	DOCK8	1.31992915	1.08258631	0.00364153	0.18833702
ENSG00000110944	IL23A	1.30908943	3.20831502	6.77E-06	0.00379357
ENSG00000088881	EBF4	1.29141484	0.10878231	0.02423072	0.31633961
ENSG00000008382	MPND	1.29093408	0.62382087	0.0097579	0.26013064
ENSG00000105227	PRX	1.27663838	0.33624528	0.01949513	0.30074748
ENSG00000162148	PPP1R32	1.27003727	0.26855435	0.03892858	0.37365325
ENSG00000070371	CLTCL1	1.26948174	1.65010309	0.0010601	0.10811989
ENSG00000221990	EXOC3-AS1	1.26544685	0.01776026	0.01743102	0.29161386
ENSG00000196843	ARID5A	1.26358332	0.75182056	0.0126506	0.27748949
ENSG00000122694	GLIPR2	1.26066978	0.80543647	0.00392826	0.19710193
ENSG00000148143	ZNF462	1.2557301	0.86670816	0.00420187	0.19890376
ENSG00000198915	RASGEF1A	1.24068632	0.80581298	0.02133099	0.30743599
ENSG00000132793	LPIN3	1.22713212	1.86147838	0.00718333	0.23824568
ENSG00000233621	LINC01137	1.22189014	0.70711669	0.00475381	0.21134693
ENSG00000167680	SEMA6B	1.21549078	0.7337545	0.02948201	0.33803645
ENSG00000168685	IL7R	1.21348565	2.6756304	0.00336161	0.18217557
ENSG00000028277	POU2F2	1.21065044	2.36245373	0.00019916	0.03859323
ENSG00000088340	FER1L4	1.19289508	0.46356654	0.04205903	0.38284602
ENSG00000117226	GBP3	1.18922425	2.36713831	0.00158797	0.13531959
ENSG00000127463	EMC1	1.17257461	1.31147769	0.00126164	0.12032106
ENSG00000139880	CDH24	1.17005439	1.62355046	0.01181875	0.27554551
ENSG00000140459	CYP11A1	1.16740585	0.01354161	0.02525902	0.32379226
ENSG00000261183	SPINT1-AS1	1.16122506	0.34032007	0.02082958	0.30688226

ENSG00000163545	NUAK2	1.15782957	2.84170685	0.00182487	0.14753746
ENSG00000197536	C5orf56	1.15487799	1.86939206	0.00075229	0.08952231
ENSG00000134864	GGACT	1.14310203	0.17161546	0.04450209	0.39207422
ENSG00000172602	RND1	1.13707124	0.90082562	0.01238413	0.27748949
ENSG00000142677	IL22RA1	1.12913041	0.87447402	0.02192343	0.30999403
ENSG00000006210	CX3CL1	1.12496442	3.56385042	1.10E-05	0.00589537
ENSG00000126561	STAT5A	1.1205488	2.05165461	0.00775735	0.24452221
ENSG00000197249	SERPINA1	1.11229899	6.76220656	3.98E-07	0.00033457
ENSG00000101342	TLDC2	1.11193153	1.53870465	0.00344111	0.18217557
ENSG00000073910	FRY	1.11166438	0.94326204	0.03440719	0.35656428
ENSG00000115318	LOXL3	1.09311922	0.4719228	0.01522225	0.28155929
ENSG00000126231	PROZ	1.09059811	0.61599918	0.04356068	0.38689597
ENSG00000023445	BIRC3	1.08791539	4.67286654	6.23E-06	0.00378456
ENSG00000099822	HCN2	1.08070675	0.55790577	0.02076463	0.30688226
ENSG00000275410	HNF1B	1.07192083	0.2470877	0.03188109	0.34712957
ENSG00000234498	RPL13AP20	1.06655008	0.28498069	0.030143	0.33947478
ENSG00000048052	HDAC9	1.06271611	2.38074196	0.000221	0.04015871
ENSG00000148288	GBGT1	1.05826683	0.51820764	0.02174635	0.30927325
ENSG00000187720	THSD4	1.04228657	1.29173854	0.02980302	0.33803645
ENSG00000171608	PIK3CD	1.03811111	2.7418602	0.00279284	0.16747459
ENSG00000007516	BAIAP3	1.03296682	0.66357676	0.0465083	0.39783527
ENSG00000149573	MPZL2	1.02932607	5.19893078	1.82E-07	0.00019339
ENSG00000280670	CCDC163	1.02164088	1.53408785	0.00822822	0.24752779
ENSG00000135736	CCDC102A	1.00787989	1.77198605	0.01328928	0.27843587
ENSG00000163874	ZC3H12A	1.00609431	3.25565828	0.00016127	0.03448346
ENSG00000121075	TBX4	0.99898994	1.35415303	0.01172162	0.27554551

ENSG00000100228	RAB36	0.9743573	2.18934766	0.00469272	0.21134693
ENSG00000182600	SNORC	0.96825776	1.03950822	0.02687804	0.33037387
ENSG00000184584	TMEM173	0.96567354	2.24192102	0.00340941	0.18217557
ENSG00000149596	JPH2	0.96476066	1.20697663	0.01516339	0.28126847
ENSG00000240065	PSMB9	0.95897544	2.03725938	0.01344222	0.27843587
ENSG00000139567	ACVRL1	0.95494225	1.34004297	0.02304842	0.31160405
ENSG00000134940	ACRV1	0.95448821	0.8686409	0.02871406	0.33623376
ENSG00000187583	PLEKHN1	0.95152068	0.22161227	0.0488451	0.40162662
ENSG00000187800	PEAR1	0.95046595	0.85917439	0.0373627	0.36828456
ENSG00000144802	NFKBIZ	0.92768271	3.21843443	0.00015552	0.03448346
ENSG00000165424	ZCCHC24	0.92495858	1.66458179	0.01782443	0.29445343

Table S7: Difference *E. coli DH5α* and TSB-treated DLD-1 cells. Foldchange is log2 and shows the difference between *E. coli DH5α* and TSB, average expression describes the average expression of gene across all samples, the adjusted p-values is Benjamin Hochberg-adjusted. The table is sorted by fold change. Genes that are further validated in the thesis are indicated in yellow. Shown is the top 100 genes sorted by unadjusted P-value.

ENSEMBL	Gene symbol	Fold Change (log2)	Average expression	P-value	Ajusted p-value
ENSG00000197013	ZNF429	2.36767791	0.41251202	0.00581662	0.19303831
ENSG00000148346	LCN2	1.99329274	4.4938495	1.88E-08	0.00024538
ENSG00000049249	TNFRSF9	1.75903822	1.14391107	0.00015533	0.19303831
ENSG00000135077	HAVCR2	1.70274018	0.84085643	0.00105544	0.19303831
ENSG00000143341	HMCN1	1.51961897	0.00018198	0.0100284	0.1988948
ENSG00000257815	LINC01481	1.41073831	0.53764439	0.00447084	0.19303831
ENSG00000275896	PRSS2	1.39172344	0.79989922	0.01300643	0.20332093
ENSG00000179674	ARL14	1.3666396	0.12855452	0.03021059	0.23458589

ENSG00000206559	ZCWPW2	1.35329481	0.09930199	0.03351681	0.239199
ENSG00000245573	BDNF-AS	1.32649632	0.52522124	0.03194806	0.23690755
ENSG00000115009	CCL20	1.2585019	0.47204074	0.04435163	0.25974727
ENSG00000163739	CXCL1	1.24150933	2.28454506	0.00027566	0.19303831
ENSG00000140307	GTF2A2	1.19102275	1.70580955	0.00178788	0.19303831
ENSG00000134864	GGACT	1.16907375	0.94014561	0.01891703	0.2116364
ENSG00000008517	IL32	1.16878844	3.02168356	0.00058927	0.19303831
ENSG00000185565	LSAMP	1.16844612	1.22820892	0.02968222	0.23363373
ENSG00000176595	KBTBD11	1.14361231	0.89338968	0.01451164	0.20590964
ENSG00000196503	ARL9	1.11612631	1.18809252	0.01852467	0.2116364
ENSG00000247796	LOC257396	1.09855244	1.7337631	0.0034952	0.19303831
ENSG00000182118	FAM89A	1.08304723	3.94725254	0.00045544	0.19303831
ENSG00000274750	HIST1H3E	1.07593306	0.69025933	0.0236022	0.2219664
ENSG00000272677	LOC101928963	1.06543913	0.43151708	0.0458702	0.26186736
ENSG00000278811	LINC00624	1.05817343	0.34122913	0.048864	0.2656484
ENSG00000153956	CACNA2D1	1.05809919	1.28492858	0.00929059	0.19773093
ENSG00000263006	ROCK1P1	1.05254928	0.85890094	0.03476983	0.24369316
ENSG00000157601	MX1	1.0088779	1.00419547	0.02639068	0.22723649
ENSG00000007062	PROM1	1.00857999	1.22366705	0.02501043	0.22483553
ENSG00000168275	COA6	1.00795257	5.4335861	0.00013611	0.19303831
ENSG00000234264	DEPDC1-AS1	0.98323812	0.35356594	0.04435583	0.25974727
ENSG00000169429	CXCL8	0.96983392	3.96604142	0.00099665	0.19303831
ENSG00000104432	IL7	0.94611707	1.16083752	0.0365948	0.24609581
ENSG00000173535	TNFRSF10C	0.9236131	1.21387092	0.04761474	0.26374584
ENSG00000184786	TCTE3	0.90712135	0.84463196	0.04107807	0.25411945

ENSG00000005249	PRKAR2B	0.89821527	2.76236812	0.00659409	0.19773093
ENSG00000124102	PI3	0.87785149	2.23738752	0.00495599	0.19303831
ENSG00000169193	CCDC126	0.85404105	2.41050461	0.01106117	0.20071661
ENSG00000023445	BIRC3	0.85377108	4.39284597	0.00061273	0.19303831
ENSG00000135972	MRPS9	0.84073671	5.58096047	0.00010214	0.19303831
ENSG00000137628	DDX60	0.83033016	1.50886017	0.04550385	0.26131179
ENSG00000163584	RPL22L1	0.82940655	8.40020697	0.00540485	0.19303831
ENSG00000133111	RFXAP	0.82817117	3.30917969	0.01576833	0.20616249
ENSG00000204147	ASAH2B	0.81509762	2.88712237	0.01000005	0.19885119
ENSG00000180530	NRIP1	0.80907242	2.29915032	0.01095322	0.20071661
ENSG00000109472	CPE	0.79892248	1.66115729	0.04522246	0.26049813
ENSG00000100916	BRMS1L	0.79561084	4.61116584	0.00137231	0.19303831
ENSG00000164105	SAP30	0.79309873	3.91365814	0.00077239	0.19303831
ENSG00000146963	LUC7L2	0.78694113	4.07585101	0.00270367	0.19303831
ENSG00000125703	ATG4C	0.78481309	4.41414824	0.00075137	0.19303831
ENSG00000111802	TDP2	0.77741499	6.0056691	0.00094535	0.19303831
ENSG00000094841	UPRT	0.77614349	2.82405679	0.0024935	0.19303831
ENSG00000183784	DOCK8-AS1	0.77576811	2.30388588	0.00878317	0.19773093
ENSG00000109680	TBC1D19	0.77450199	3.08906408	0.01988823	0.21454636
ENSG00000164414	SLC35A1	0.7721856	2.71991832	0.00738958	0.19773093
ENSG00000147679	UTP23	0.754763	4.86351895	0.00333505	0.19303831
ENSG00000006625	GGCT	0.75189277	4.708498	0.00594923	0.19303831
ENSG00000132423	COQ3	0.75184172	4.21553827	0.00465918	0.19303831
ENSG00000138660	AP1AR	0.75118799	5.57016939	0.0033959	0.19303831
ENSG00000109270	LAMTOR3	0.74835426	6.05828017	0.00424016	0.19303831
ENSG00000122958	VPS26A	0.74350111	6.66873502	0.00221541	0.19303831

ENSG00000177640	CASC2	0.74037238	1.90178452	0.03794391	0.24901052
ENSG00000205707	ETFRF1	0.73931021	4.46951143	0.0170442	0.20801397
ENSG00000128609	NDUFA5	0.73078413	5.21213289	0.00339739	0.19303831
ENSG00000172071	EIF2AK3	0.72652918	2.71377515	0.01033289	0.20057119
ENSG00000176396	EID2	0.72294712	5.1693633	0.00160358	0.19303831
ENSG00000151413	NUBPL	0.71872914	3.34353088	0.0048443	0.19303831
ENSG00000237036	ZEB1-AS1	0.71640965	1.95566021	0.02337266	0.2219664
ENSG00000151287	TEX30	0.71528157	5.32427198	0.00400875	0.19303831
ENSG00000197780	TAF13	0.71507226	5.57910417	0.00795706	0.19773093
ENSG00000166130	IKBIP	0.71489895	4.59130901	0.00498062	0.19303831
ENSG00000123106	CCDC91	0.7119412	4.4783139	0.00417578	0.19303831
ENSG00000101132	PFDN4	0.70844905	5.80813693	0.00292499	0.19303831
ENSG00000214174	AMZ2P1	0.706454	3.23061593	0.00267861	0.19303831
ENSG00000172115	CYCS	0.70527146	8.61904328	0.0059087	0.19303831
ENSG00000156374	PCGF6	0.69925609	3.1962806	0.00634364	0.19773093
ENSG00000198039	ZNF273	0.6978364	3.34094608	0.00763841	0.19773093
ENSG00000137575	SDCBP	0.69719274	8.80943622	0.00061114	0.19303831
ENSG00000166260	COX11	0.69306363	6.44854701	0.00539558	0.19303831
ENSG00000104671	DCTN6	0.69241773	6.42821546	0.00590859	0.19303831
ENSG00000153140	CETN3	0.69164433	4.80638221	0.00309497	0.19303831
ENSG00000204344	STK19	0.68826828	1.88074419	0.03824621	0.24924006
ENSG00000133773	CCDC59	0.68743138	5.88211443	0.0046151	0.19303831
ENSG00000132541	RIDA	0.68701305	4.83069445	0.00598307	0.19303831
ENSG00000129128	SPCS3	0.68504399	8.16798708	0.00185209	0.19303831
ENSG00000197223	C1D	0.68402595	6.20203024	0.00403864	0.19303831
ENSG00000166797	CIAO2A	0.68364411	6.83319842	0.00262992	0.19303831

ENSG00000164603	BMT2	0.68051025	3.71396423	0.00368325	0.19303831
ENSG00000170417	TMEM182	0.67673882	3.64203898	0.00489769	0.19303831
ENSG00000145723	GIN1	0.67373305	3.70659312	0.02873914	0.23199255
ENSG00000118507	AKAP7	0.6726586	2.67537215	0.02129782	0.21894014
ENSG00000147669	POLR2K	0.67224385	6.38578214	0.00781617	0.19773093
ENSG00000180694	TMEM64	0.67181182	5.49512245	0.00992373	0.19885119
ENSG00000257167	TMPO-AS1	0.66954959	3.79949338	0.00331585	0.19303831
ENSG00000182093	WRB	0.66916337	6.16377291	0.00088516	0.19303831
ENSG00000120837	NFYB	0.66779169	5.22013939	0.00438895	0.19303831
ENSG00000149089	APIP	0.66248037	5.2179916	0.01399716	0.20590964
ENSG00000008952	SEC62	0.66208415	6.69850902	0.00237453	0.19303831
ENSG00000036054	TBC1D23	0.65986122	5.41942502	0.00936716	0.19773093
ENSG00000253738	OTUD6B-AS1	0.65904214	4.77624827	0.01009399	0.19898861
ENSG00000153130	SCOC	0.65867654	6.35360281	0.00604893	0.19447452
ENSG00000081087	OSTM1	0.65752795	4.63500975	0.00884549	0.19773093

Table S8: Difference between SW620 cells transfected with EBV-miR-BART10-3p mimic and non-targeting miRNA mimic. Foldchange is log2 and shows the difference between EBV-miR-BART10-3p mimic and non-targeting miRNA mimic, average expression describes the average expression of gene across all samples, the adjusted p-values is Benjamin Hochberg-adjusted. The table is sorted by fold change. Genes that are further validated in the thesis are indicated in yellow.

ENSEMBL	Gene Symbol	Fold Change (log2)	Average expression	P-value	Adjusted p-value
ENSG00000038274	MAT2B	-1.0060937	6.58733332	4.79E-06	0.00880318
ENSG00000071539	TRIP13	-0.6696718	6.96924596	9.89E-05	0.02228628
ENSG00000076248	UNG	-0.8524088	6.78638345	1.99E-05	0.0122929
ENSG00000101384	JAG1	0.89115786	7.58634209	1.09E-05	0.0122929
ENSG00000103275	UBE2I	-0.6924459	7.61034565	4.94E-05	0.017919
ENSG00000105976	MET	0.81942556	9.16477066	4.94E-06	0.00880318
ENSG00000110092	CCND1	-0.9484627	6.84467285	2.76E-05	0.0122929
ENSG00000113732	ATP6V0E1	-1.5729991	6.46642041	1.63E-07	0.00168589
ENSG00000119414	PPP6C	-0.8451959	6.5754235	3.72E-05	0.01484223
ENSG00000125356	NDUFA1	-0.9567633	5.05304449	5.14E-05	0.017919
ENSG00000126698	DNAJC8	-0.9025535	6.15993964	1.69E-05	0.0122929
ENSG00000135046	ANXA1	1.28993038	4.95898741	8.61E-05	0.02181368
ENSG00000137801	THBS1	-1.0270852	5.0697287	0.00023609	0.03554909
ENSG00000138434	ITPRID2	0.79679174	7.99388595	1.44E-05	0.0122929
ENSG00000150459	SAP18	-0.823255	8.51827949	2.18E-05	0.0122929
ENSG00000152102	FAM168B	-0.6333221	6.21135589	0.0003036	0.0376474

Table S9: Difference between LS411N cells transfected with EBV-miR-BART103p mimic and non-targeting miRNA mimic. Foldchange is log2 and shows the difference between EBV-miR-BART10-3p mimic and non-targeting miRNA mimic, average expression describes the average expression of gene across all samples, the adjusted p-values is Benjamin Hochberg-adjusted. The table is sorted by fold change. Genes that are further validated in the thesis are indicated in yellow.

ENSEMBL	Gene Symbol	Fold change (log2)	Average expression	P-value	Adjusted p-value
ENSG00000038274	MAT2B	-1.3845748	5.94842653	6.12E-05	0.02178192
ENSG00000071539	TRIP13	-1.1785189	7.08141224	5.17E-07	0.0019227
ENSG00000076248	UNG	-1.009413	6.40855526	9.53E-06	0.0081756
ENSG00000101384	JAG1	0.82480339	7.26350954	2.14E-05	0.012102
ENSG00000103275	UBE2I	-0.5462309	8.17004127	0.00029876	0.04578428
ENSG00000105976	MET	1.05110473	8.31654956	9.52E-07	0.00215199
ENSG00000110092	CCND1	-0.8128811	7.62025268	2.84E-05	0.01320123
ENSG00000113732	ATP6V0E1	-1.6533706	6.0021066	3.42E-07	0.00190389
ENSG00000119414	PPP6C	-1.0810811	6.88188617	6.73E-06	0.00625624
ENSG00000125356	NDUFA1	-1.0089886	5.02024442	6.25E-05	0.02178192
ENSG00000126698	DNAJC8	-1.2304552	6.60778669	9.65E-07	0.00215199
ENSG00000135046	ANXA1	1.07251192	6.99851715	2.43E-06	0.00424194
ENSG00000137801	THBS1	-0.9513426	4.69877543	3.74E-05	0.01544635
ENSG00000138434	ITPRID2	0.62440193	8.70986536	0.00019788	0.04026293
ENSG00000150459	SAP18	-1.0675806	7.11333808	4.94E-06	0.00501203
ENSG00000152102	FAM168B	-0.6801675	6.02484901	0.00023062	0.04065447

Table S10: Equipment, reagents, and gels for CTOSs culturing

Product name	Art.nr. / Catalogue nr.	Manufacturer
Equipment		
Stainless steel wire mesh, hole size 500 µm	Z289922-1EA	Sigma-Aldrich
40-µm cell strainer	421750	Corning
pluriStrainer 500 µm	43-50500-50	pluriSelect
Mr. Frosty™ Freezing Container, Isopropanol box	5100-0001	Thermo Fischer Scientific
Gels		
Cellmatrix Type I -A (Collagen, Type I, 3 mg/mL, pH 3.0)	631-00651	Nitta Gelatin Inc
Geltrex LDEV-Free hESC-qualified Reduced Growth Factor Basement Membrane Matrix	A1413302	Gibco
Cultrex Reduced Growth Factor Basement Membrane Extract, type 2	3533-005-02	R&D Systems
Corning ® Matrigel® Matrix, phenol red-free	734-0272	Corning Life Science
Supplemented DMEM		
DMEM	D6429-500ML	Sigma-Aldrich
100 units/mL penicillin	15140-112	Gibco
100 µg/mL streptomycin	15140-112	Gibco
Digestive enzymes		
Collagenase type II	17101015	Gibco
0,2 mg/ml collagenase type 4	LS004186	Worthington
0,28 units/ml Liberase DH	5401054001	Roche
Supplemented serum-free stem cell medium		
DMEM/F12 + Glutamax™-I	10565-018	Gibco
StemPro® hESC Supplement	A10006-01	Gibco

BSA 1,88%	A10008-01	Gibco
8 ng/mL bFGF	13256-029	Gibco
0,1 mM 2-mercaptoethanol	21985-023	Thermo Fischer Scientific
100 units/mL penicillin	15140-112	Gibco
100 µg/mL streptomycin	15140-112	Gibco
25 µg/ml amphotericin B	A2942-100ML	Sigma-Aldrich
Collagen solution		
Cellmatrix type I-A	631-00651	Nitta Gelatin Inc
DMEM	D6429-500ML	Sigma-Aldrich
Reconstitution buffer - 50 mM NaOH - 260 mM NaHCO3 - 200 mM Hepes	–	–
Other reagents		
PBS	–	Sigma-Aldrich
HBSS, calcium, magnesium, no phenol red	14025-050	Gibco
FCS – fetal calf serum	10-082-139	Gibco
DMSO	D8418	Sigma-Aldrich
1% BSA, Bovine Serum Albumin	B9000S	New England biolabs

B Supplementary figures

Figure S1: Human *SAP18* 3'UTR from TargetScan, showing binding sites for EBV-miR-BART10-3p conserved over species. White outline shows where the EBV-miR-BART10-3p binds to the 3'UTR of the human *SAP18* gene, and how the 3'UTR binding site for EBV-miR-BART10-3p is conserved over species.

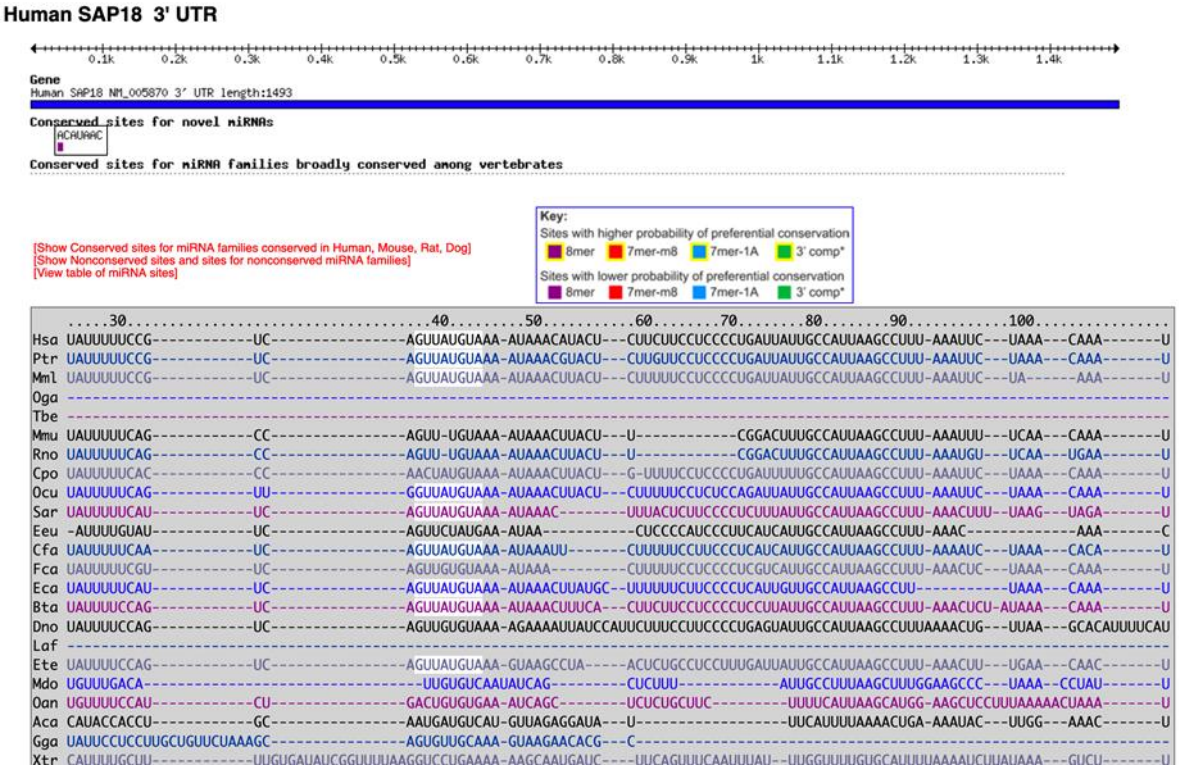

Figure S2: Human *CCND1* 3'UTR from TargetScan. Orange dot describes 6-mer binding site, and red dot describes 8-mer 1a binding site for EBV-miR-BART10-3p.

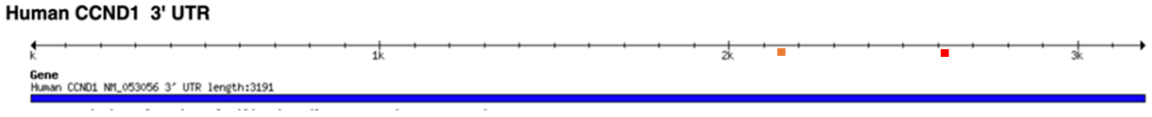

Figure S3: Sanger sequence of psiCHECK™-2 vector and *CCND1* insert. Yellow indicating *CCND1* forward primer, green+yellow indicating *CCND1* insert, pink indicating NotI cutting site and blue indicating XhoI cutting site. Unspecific ends are cut off.

>90FJ24_00164252_00164252
GGCGAGATCATTTAGATCCTCACACAAAAAACCAACACACAGATGTAATGAAAATAAAGATATTTTA
TTGCGGCCAGCGGCC||GCCAGAACACTAGTACATAACAGATTAAACATACCCAAAACCTCGA||GC
GATCGCCTAGAATTACTGCTCGTTCTTCAGCACGCGCTCCACGAAGCTCTTGATGTACTTACCCATTTC
ATCTGGAGCGTCCTCCTGGCTGAAGTGGAGGCCCTTCACCTTCACGAACTCGGTGTTAGGGAACTTC
TTAGCTCCCTCGACAATAGCGTTGGAAAAGAACCCAGGGTCGGACTCGATGAACATCTTAGGCAGAT
CGTCGCTGGCCCGAAGGTAGGCGTTGTAGTTGCGGACAATCTGGACGACGTCGGGCTTGCCTCCCTT
AACGAGAGGGATCTCGCGAGGCCAGGAGAGGGTAGGCCGTCTAACCTCGCCCTTCTCCTTGAATGG
CTCCAGGTAGGCAGCGAACTCCTCAGGCTCCAGTTTCCGCATGATCTTGCTTGGGAGCATGGTCTCG
ACGAAGAAGTTATTCTCAAGCACCATTTTCTCGCCCTCTTCGCTCTTGATCAGGGCGATATCCTCCTCG
ATGTCAGGCCACTCGTCCCAGGACTCGATCACGTCCACGACACTCTCAGCATGGACGATGGCCTTGA
TCTTGTCTTGGTGCTCGTAGGAGTAGTGAAAGGCCAGACAAGCCCCCCAGTCGTGGCCCACAAAGAT
GATTTTCTTTGGAAGGTTCAGCAGCTCGAACCAAGCGGTGAGGTACTTGTAGTGATCCAGGAGGCG
ATATGAGCCATTCCCGCTCTTGCCGGACTTACCCATTCCGATCAGATCAGGGATGATGCATCTAGCCA
CGGGCTCGATGTGAGGCACGACGTGCCTCCACAGGTAGCTGGAGGCAGCGTTACCATGCAGAAAAA
TCACGGCGTTCTCGGCGTGCTTCTCGGAATCATAGTAGTTGATGAAGGAGTCCAGCACGTTCATTTGC
TTGCAGCGAGCCCACCACTGAGGCCCAGTGATCATGCGTTTGCGTTGCTCGGGGTCGTACACCTTGG
AAGCCATGGTGGCTAGCCTATAGTGAGTCGTATTAAGTACTCTAGCCTTAAGAGCTGTAATTGAACT
GGGGAGTGG

Figure S4: Sanger sequence of psiCHECK™-2 and *CCND1* insert. Yellow box indicates *CCND1* 3'UTR 8-mer insert. Unspecific ends are cut off.

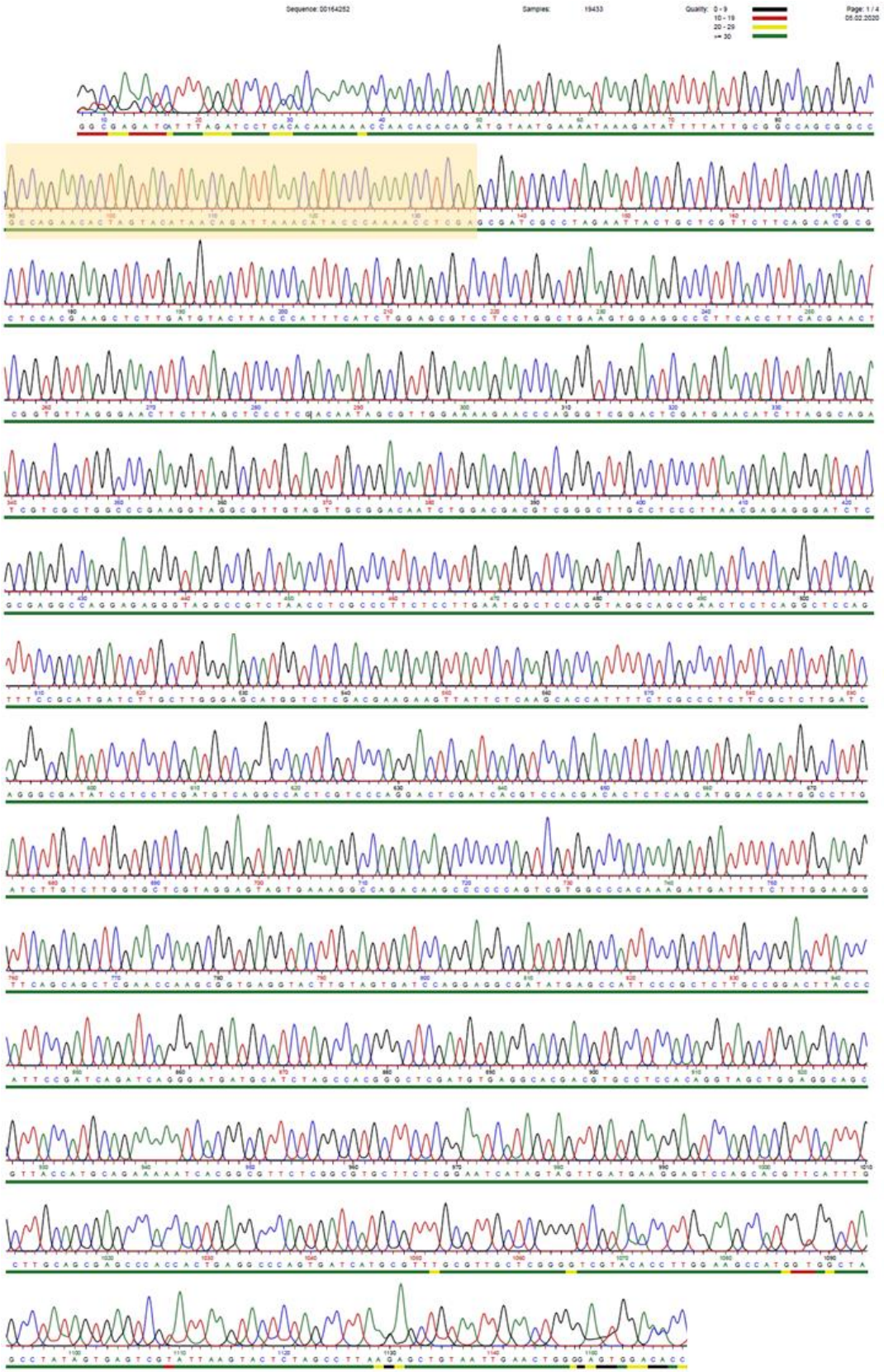

Figure S5: ELISA CXCL8 Standard curves for calculation of concentrations (pg/ml)

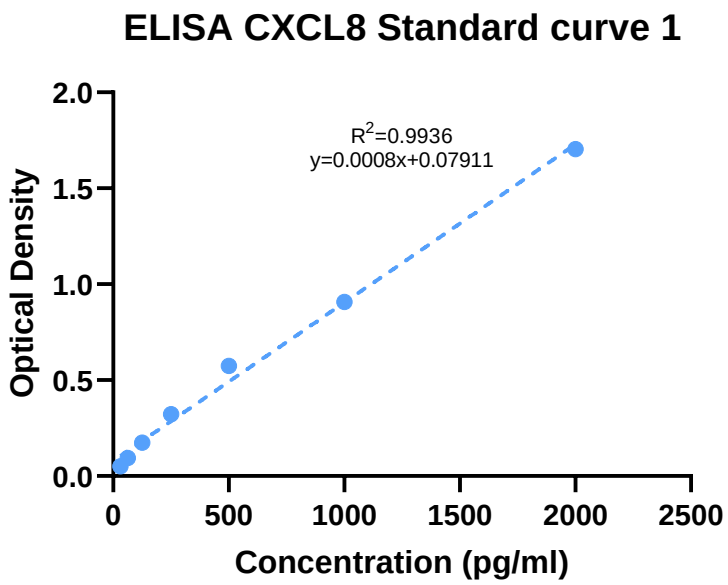

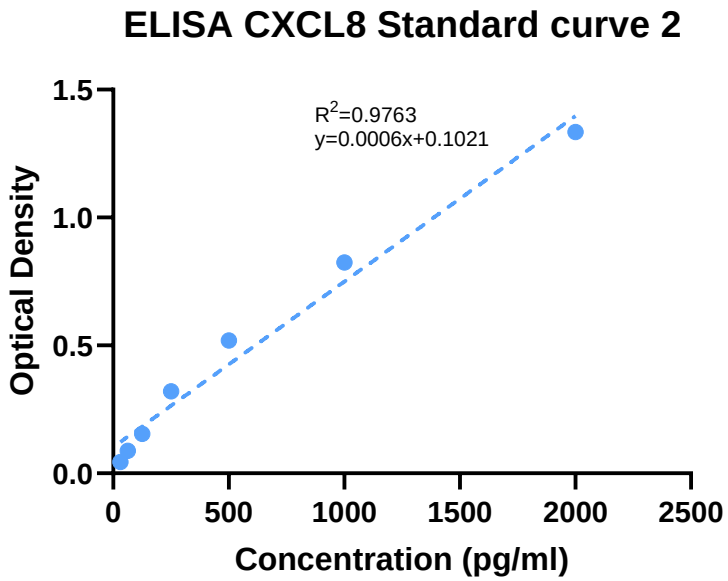

Figure S6: PCA plots showing the difference between treatment and cell line in four different cell lines, DLD-1, LS411N, SW480 and SW620. The plots indicate that there is a greater difference in expression between cell lines, than treatment. Left) Show grouping of cell lines. Right) Show different treatment. FUSO = *F. nucleatum*, TSB = non-treated sample, DH5 = *E. coli DH5α*

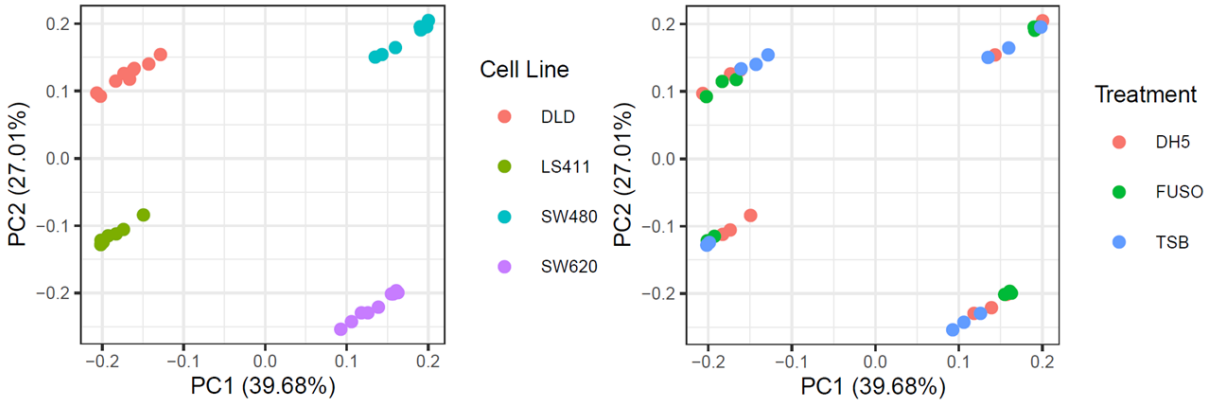

Figure S7: PCA plots for four cell lines, showing grouping for different treatment. Indicating that cell lines DLD and SW620 having the best grouping. A) DLD-1, B) LS411N, C) SW480, D) SW620. FUSO = *F. nucleatum*, TSB = non-treated sample, DH5 = *E. coli* DH5α

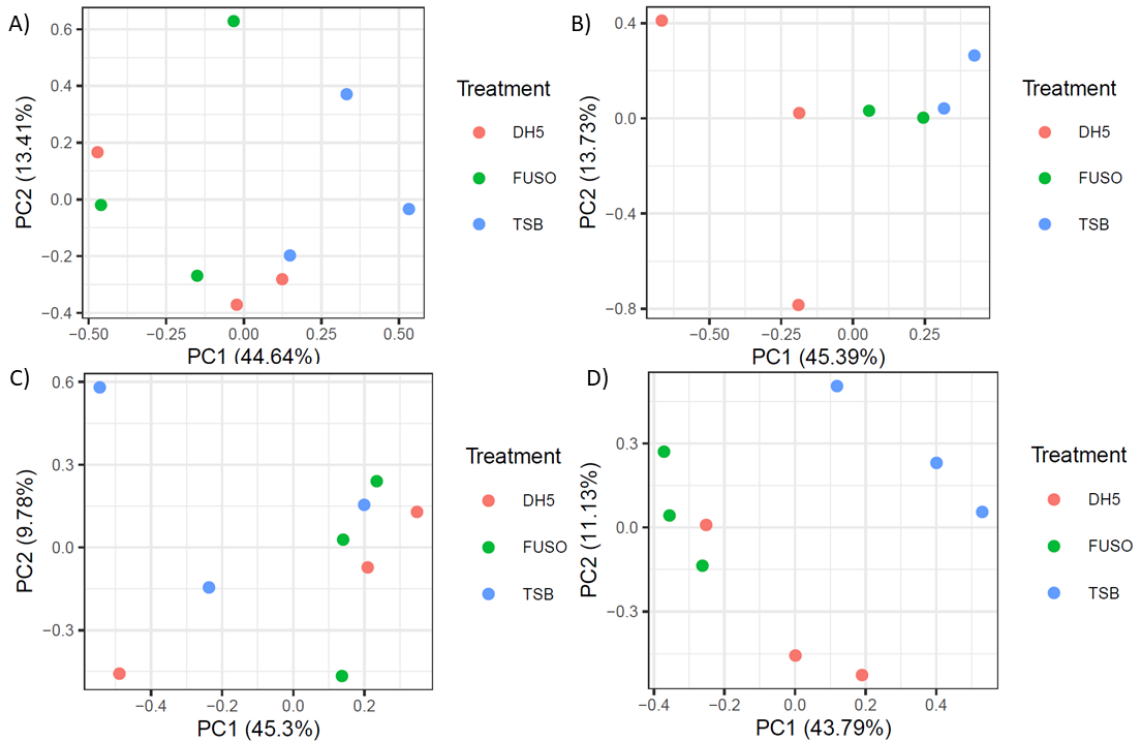

Figure S8: PCA plots showing the difference in mRNA expression between EBV-miR-BART10-3p mimic transfection and non-targeting miRNA mimic transfection in cell lines SW620 and LS411N. A) Transfection in cell line SW620 indicates that all groups treated with BART express the same mRNAs, while neg is more random. B) Transfection in cell line LS411N indicates that BART and NEG is grouped somehow together, as BART show downregulation. BART= EBV-miR-BART10-3p mimic, NEG=Non-targeting miRNA mimic.

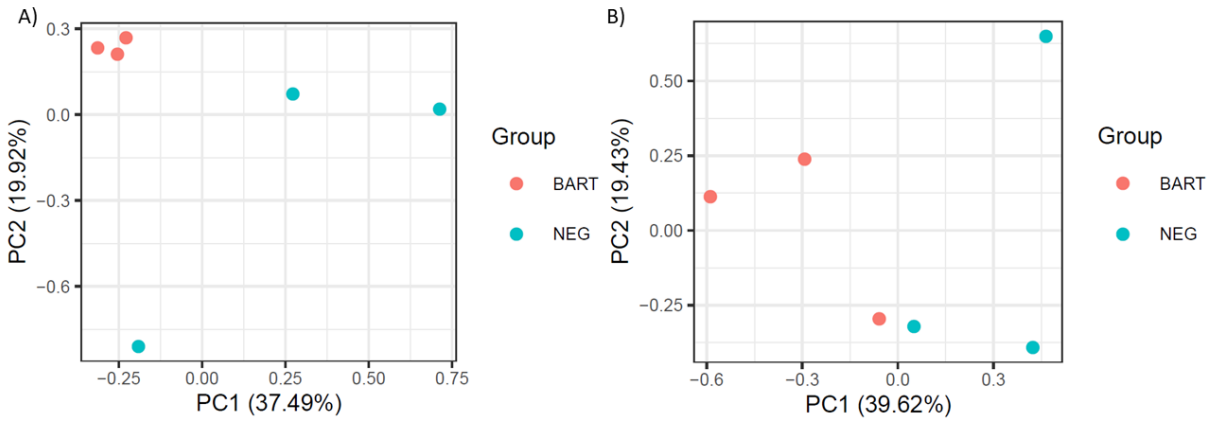

C Supplementary protocols

Protocol S1: Protocol for transformation by heat shock

Day 1

1. Ligation reaction product and control (empty) vector is added to respectively tubes of competent DH5α cells.
2. Incubate the mix of competent DH5α and ligation product on ice for 15-20 min.
3. Transfer tube to a 42 °C water bath and incubate for 50 sec.
4. Incubate on ice for 2 min.
5. Add 900 µl of SOC medium and incubate cells in a shaking incubator at 37 °C for 60-90 min.
6. Spin cells at max speed for 1 min, discard most of the supernatant, and resuspend cells in remaining SOC medium.
7. Spread resuspended cells to a prewarmed Amp-LB dish and incubate overnight at 37 °C, agar up.

Day 2

1. Inspect the Amp-LB dishes. Ideally there should be more colonies present on the dish containing vector with insert and fewer on the control dish.
2. Pick colonies from the insert dish and transfer to Amp-LB medium. Incubate in a shaking incubator at 37 °C.

Day 3

1. Make bacterial stock of clones, one part bacteria – four parts glycerol
2. Bacteria was lysed by boiling to access the vector DNA for PCR-screening.
3. Verification of insert.

Protocol S2: Initial phase protocol for CTOSs preparation and culture

1. Place the tissue sample in 20 ml of supplemented DMEM in a 50-ml centrifuge tube on ice immediately after tumor resection.
2. Store the specimen at 4 °C until ready to proceed. It is critical to start the following steps as soon as possible.
3. Discard the storage medium.
4. Wash the samples with 20 ml HBSS by inverting the tube.
5. Discard the HBSS solution.
6. Add 20 ml HBSS.
7. Transfer the medium and the samples to a 10-cm tissue culture dish.
8. Remove necrotic tissue using forceps or razor blades.
9. Transfer the samples to 30 ml HBSS in a new 10-cm tissue culture dish.
10. Mince the tissue forceps or razor blades into small (1-2 mm) pieces.
11. Transfer the medium and the minced tissue to a 50-ml centrifuge tube.
12. Centrifuge at 1000 rpm (200xg) at 4 ℃ for 5 min.
13. Discard the medium.
14. Wash the samples with 20 ml HBSS by inverting the tube.
15. Repeat steps 12-14.
16. Centrifuge at 1000 rpm (200xg) at 4 ℃ for 5 min.
17. Discard the HBSS wash solution.
18. Resuspend the pellets in 20 ml supplemented DMEM + Liberase DH.
19. Transfer the digestion mixture to a 100-ml sterile conical flask.
20. Digest the samples for 2 h in a 37 °C water bath on shaking.
21. Transfer the digestion medium to a 50 ml centrifuge tube.
22. Centrifuge at 1000 rpm (200xg) at 4 ℃ for 5 min.
23. Discard the medium.
24. Wash the samples with 20 ml HBSS by inverting the tube.
25. Filter the samples with a stainless-steel wire mesh (hole size 500 μm).
26. Transfer the filtrate to a 50 ml centrifuge tube.
27. Filter the samples with a 40 μm cell strainer.
28. Dip the bottom of the cell strainer in 30 ml HBSS in a 10 cm tissue culture dish; swirl it gently to remove the debris, the single cells, and the cell clumps with diameters < 40 μm.
29. Transfer the cell strainer to a new 10 cm tissue culture dish containing 30 ml HBSS.
30. Collect the spheroids that remain in the cell strainer using a 1 ml pipette.
31. Centrifuge at 1000 rpm (200xg) at 4 ℃ for 5 min.
32. Discard the HBSS wash solution.
33. wash the samples with 20 ml HBSS by inverting the tube.
34. Centrifuge at 1000 rpm (200xg) at 4 ℃ for 5 min.
35. Discard the HBSS wash solution.
36. Add 4 ml supplemented serum-free stem cell medium.
37. Transfer the spheroids and medium to a 6 cm non-treated dish.
38. Incubate in a 5% CO2-humified chamber at 37 °C for 24 h.
39. View under a microscope; CTOSs appear as bright, smooth spheres.

Protocol S3: Cellmatrix type I-A reconstitution and seeding protocol

1. Prepare a collagen solution by mixing the following in ratio A:B:C = 7:2:1
    A. Cell matrix type I-A (Nitta Gelation)
    B. DMEM (Gibco)
    C. Reconstitution buffer (50mM NaOH, 260 mM NaHCO3, 200 mM Hepes

    After mixing A and B well, add C and again mix well. Keep the reconstituted collagen solution on ice to prevent gel formation.
2. Add 100 µl reconstituted collagen solution onto a 3.5 cm non-treated dish to create a gel base.
3. Allow the gel to solidify at 37 °C for 30 min.
4. After gel formation, place the dish on ice.
5. Transfer the spheroids from the culture dish to a 50 ml tube, and centrifuge at 1000 rpm (200xg) at 4 °C for 5 min.
6. Put the CTOSs in the gel layer, pipetting gently to disperse the CTOSs evenly.
7. Add 3 mL supplemented serum-free stem cell medium.
8. Incubate in a 5% CO2-humified chamber at 37 °C for 2-3 weeks until the diameter of the CTOSs are ca 250 µm. change the medium every 3 days.

Protocol S4: Initial phase protocol for CTOSs splitting

1. Digest the gels in 3 ml DMEM + collagenase type IV at 37°C for 1 h.
2. Release the CTOSs from the digested gel by pipetting up and down
3. Transfer the CTOS suspension to a 15 ml centrifuge tube.
4. Add 10 ml PBS and mix gently.
5. Centrifuge at 1000 rpm (200 x g) for 2 min.
6. Discard the supernatant.
7. Add 5 ml HBSS containing 1% BSA and resuspend the CTOSs by pipetting; transfer them to a 6 cm non-treated culture dish.
8. Using microscopic observation, tear CTOSs using two sterile 23 G needles. One needle (held with the nondominant hand) holds the CTOS steady while a needle in the dominant hand tears the CTOS. Tear each CTOS into two to four pieces.
9. Add 3 ml serum-free stem cell medium to a new 3.5 cm nontreated dish.
10. Pick up the CTOS fragments with a pipette and transfer them to the dish prepared in step 9.
11. Incubate in a 5% CO2-humified chamber at 37 °C overnight.
12. Use a microscope the CTOSs, which appears as bright, smooth spheres.
13. Seed the split CTOS as described in “gel protocol”

Protocol S5: Optimization phase protocol for CTOS preparation and culture

1. Transfer 20 ml of supplemented DMEM to a 50 ml centrifuge tube and weigh tube with medium.
2. Place the tissue sample in 20 ml of supplemented DMEM in a 50 ml centrifuge tube on ice immediately after tumor resection or biopsy. Store the specimen at 4 °C until ready to proceed. It is critical to start the following steps as soon as possible and weigh the sample.
3. Discard the storage medium.
4. Wash the samples with 20 ml HBSS by inverting the tube and discard the HBSS wash solution.
5. Add 20 ml HBSS to the sample.
6. Add 20 ml HBSS to two 50 ml tubes labeled “L” for Liberase DH and “C” for Collagenase II, respectively, and weigh the two tubes.
7. Transfer the medium and the sample from step 5. to a 10 cm tissue culture dish.
8. Remove necrotic tissue using razor blades. Then cut sample in half and transfer on half to the “L” tube and the other to the “C” tube.
9. Weigh the two sample tubes and calculate the weight of the samples.
10. Transfer the samples to 30 ml HBSS in two separate 10 cm tissue culture dishes labelled “L” and “C”.
11. Mince the tissue with razor blades into small (1-2 mm) pieces.
12. Transfer the medium and the minced tissue to two separate 50 ml centrifuge tubes labeled “L” and “C”.
13. Centrifuge at 400xg at 4 °C for 5 min and discard the medium.
14. Wash the samples with 20 ml HBSS by inverting the tubes.
15. Repeat step 13 and 14.
16. Centrifuge at 400xg at 4 °C for 5 min and discard the wash solution.
17. Resuspend the pellet in the “L” tube in 20 ml supplemented DMEM + Liberase DH, and transfer to a 100 ml sterile conical flask with a magnet bar.
18. Digest the “L” sample for 2 h in 37 °C water bath with constant stirring.
19. Resuspend the pellet in “C” tube in 20 ml supplemented DMEM + collagenase type II, and transfer to a 100 ml sterile conical flask with a magnet bar.
20. Digest the “C” sample for 20 min in a 37°C water bath with constant stirring

The following steps below is separate for “L” and “C”.

21. Transfer the digestion medium to 50 ml centrifuge tube and centrifuge at 400xg at 4 °C for 5 min.
22. Discard the medium and wash the samples with 20 ml HBSS by inverting the tube.
23. Filter the samples with a 500 µm pluriStrainer into a new 50 ml tube.
24. Filter the samples with a 40 µm cell strainer into a new 50 ml tube.
25. Dip the bottom of the cell strainer in 30 ml HBSS in a 10 cm tissue culture dish, to remove the debris, single cells, and the cell clumps with diameters < 40 µm.
26. Transfer the cell strainer to a new 10 cm tissue culture dish containing 30 ml HBSS.
27. Collect the spheroids that remain in the cell strainer using a 1 ml pipette.
28. Centrifuge at 400xg at 4 °C for 5 min and discard the HBSS wash solution.
29. Resuspend the spheroids in 0.4 ml HBSS.
30. Add 10 µl to a glass slide and count the number of spheroids.

Seed the spheroids in the four types of gels.

31. Label Eppendorf tubes accordingly and aliquot the spheroids into Eppendorf tubes.
32. Centrifuge at 200xg at 4 °C for 5 min and discard the HBSS wash solution.
33. Resuspend spheroids in gel and medium according to the volumes in table below and seed into a pre-warmed 24-well plate. Gels are Cultrex (LC, CC), Geltrex (LG, CG), Matrigel (LM, CM), CellMatrix type I-A (LK, CK). RB - reconstitution buffer.

Gel composition				
	LC, CC	LG, CG	LM, CM	LK, CK
Medium	25 µl	33 µl	50 µl	20 µl
Gel	50 µl	67 µl	50 µl	70 µl
RB	-	-	-	10 µl

35. Incubate the plate for 30 min at 37 °C
36. Add 0.5 ml of supplemented serum-free stem cell medium to each well and incubate overnight at 37 °C
37. Change medium following overnight incubation and then change medium every third day.
38. Monitor the spheroids with imaging every third day for 14 days.

Protocol S6: Optimization phase protocol for CTOS splitting and freezing

1. Prewarm a 24-well plate at 37 °C.
2. Discard medium.
3. Digest gels with 0.5 ml DMEM + collagenase type IV at 37 °C for 1 h.
4. Release the CTOSs from the digested gel by pipetting up and down.
5. Transfer the CTOS suspension to a 50-ml centrifuge tube.
6. Add double volume of PBS to well and scrape the remaining gel or CTOS from the plate.
7. Centrifuge at 400xg for 2 min and discard the supernatant.
8. Resuspend the pellet in 20 ml supplemented DMEM + collagenase type II, and transfer to a 100 ml Erlenmeyer flask.
9. Digest sample for 20 min in a 37 °C water bath with constant stirring.
10. Transfer the digestion medium to a 50 ml centrifuge tube and wash the flask with 20 ml DMEM.
11. Centrifuge at 400xg at 4 °C for 5 min and discard the medium.
12. Wash the samples with 20 ml HBSS by inverting the tube.
13. Filter the samples with a 500 µm pluriStrainer filter. Optional: further digestion of 500 µm retentate, followed by another round of filtration. Keep track of digestion time and number of runs.
14. Transfer the filtrate to a 50-ml centrifuge tube.
15. Filter the samples with a 40 µm cell strainer.

16. Dip the bottom of the cell strainer in 30 ml HBSS in a 10-cm tissue culture dish; swirl it gently to remove debris, the single cells, and the cell clumps with diameter < 40 µm.
17. Transfer the cell strainer to a new 10-cm tissue culture dish containing 30 ml HBSS.
18. Collect the organoids that remain in the cell strainer using a 1 ml pipette.
19. Centrifuge at 400xg at 4 °C for 5 min and discard the medium.
20. Wash the samples with 30 ml HBSS by inverting the tube.
21. Centrifuge at 400xg at 4 °C for 5 min. Centrifuge twice if spheroids still are floating in the medium.
22. Discard the HBSS wash solution.
23. Resuspend spheroids in 0.4 ml of HBSS.
24. Add a small volume to a glass slide and count number of spheroids.
25. Separate the sample into two separate tubes labelled “Split” and “Freeze”

Split

Use frozen tips and keep Eppendorf tubes on ice the whole time.

i. Centrifuge at 400xg at 4 °C for 5 min.
ii. Discard the HBSS solution.
iii. Resuspend in the medium volume appropriate for the number of cells you want to seed out (20 % of total volume).
iv. Add CellMatrix type I-A (70 % of total volume) and reconstitution buffer (10 % of total volume).
v. Add 50 µl per well to a prewarmed 24-well plate.
vi. Incubate at 37 °C for 30 min and add 0.5 ml serum-free stem cell medium to each well.
vii. Incubate overnight at 37 °C.
viii. Change medium following overnight incubation, and then change medium every third.

Freeze

i. Centrifuge at 400xg at 4 °C for 5 min and discard the HBSS wash solution.
ii. Resuspend in the FCS (fetal calf serum) volume appropriate for achieving a spheroid density of 210 spheroids/ml (based on count in step 24).
iii. Add concentration 5 % DMSO of final volume.
iv. Immediately put the vials in an isopropanol box and store at -80°C until use.

Protocol S7: Protocol for thawing of CTOSs

Based on ATCC protocol for thawing of cryopreserved human organoids (173).

1. Prewarm a 24-well culture plate at 37 °C for at least 1 h.
2. Transfer the cryovial from LN_2 storage and immediately place in a 37 °C water bath and thaw rapidly. Be careful not to submerge the neck of the vial. This process should take less than 2 min.
3. Decontaminate the vial with 70 % ethanol and aseptically transfer to a biosafety cabinet (BSC).
4. Transfer the contents of the vial drop-wise to a 15 ml conical tube containing 6 ml of complete growth medium (serum-free stem cell medium).
5. Wash the cryovial three times with complete growth medium (1 ml/wash) and transfer to the 15 ml tube – i.e. should be 10 ml in the tube afterwards.
6. Centrifuge the conical tube at 400xg for 5 min at 4 °C.
7. Carefully aspirate the supernatant without disturbing the pellet while removing as much liquid as possible.
8. Remove the pre-warmed 24-well culture plate from the incubator and place in BSC.
9. Resuspend the pellet in 70 µl of Nitta Gelatin Cell Matrix I-A.
10. Add 20 µl of complete growth medium and mix properly.
11. Add 10 µl of reconstitution buffer and mix properly.
12. Quickly plate out two 50 µl gel drops in two of the wells in the 24-well plate.
13. Incubate at 37 °C for 30 min.
14. Add 0.5 ml of complete growth medium to the well.
15. Incubate at 37 °C overnight and change medium.
16. Monitor the spheroids (imaging) daily following thawing. Change medium every third day.

Julie Tro Jerud

The role of *Fusobacterium nucleatum* and the Epstein-Barr virus encoded EBV-miR-BART10-3p in colorectal cancer

NTNU
Kunnskap for en bedre verden